TOWARDS AN ACCESS ECONOMY MODEL FOR INDUSTRIAL PROCESS CONTROL

by

Luke Lambertus Rokebrand

Submitted in partial fulfillment of the requirements for the degree
Master of Engineering (Electrical Engineering)

in the

Department of Electrical, Electronic and Computer Engineering
Faculty of Engineering, Built Environment and Information Technology

UNIVERSITY OF PRETORIA

February 2020

SUMMARY

TOWARDS AN ACCESS ECONOMY MODEL FOR INDUSTRIAL PROCESS CONTROL

by

Luke Lambertus Rokebrand

Supervisor(s):	Prof. I.K. Craig
Department:	Electrical, Electronic and Computer Engineering
University:	University of Pretoria
Degree:	Master of Engineering (Electrical Engineering)
Keywords:	Competing controllers, Industry 4.0, Feedback control, Model Predictive Control (MPC), Surge tank control, Switching controllers, Input-output controllability.

With the ongoing trend in moving the upper levels of the automation hierarchy to the cloud, there has been investigation into supplying industrial automation as a cloud based service. There are many practical considerations which pose limitations on the feasibility of the idea. This research investigates some of the requirements which would be needed to implement a platform which would facilitate competition between different controllers which would compete to control a process in real-time. This work considers only the issues relating to implementation of the philosophy from a control theoretic perspective, issues relating to hardware/communications infrastructure and cyber security are beyond the scope of this work.

A platform is formulated and all the relevant control requirements of the system are discussed. It is found that in order for such a platform to determine the behaviour of a controller, it would need to simulate the controller on a model of the process over an extended period of time. This would require a measure of the disturbance to be available, or at least an estimate thereof. This therefore increases the complexity of the platform. The practicality of implementing such a platform is discussed in terms of system identification and model/controller maintenance.

A model of the surge tank from SibanyeStillwater's Platinum bulk tailings treatment (BTT) plant, the aim of which is to keep the density of the tank outflow constant while maintaining a steady tank level, was derived, linearised and an input-output controllability analysis performed on the model. Six controllers were developed for the process, including four conventional feedback controllers (decentralised PI, inverse, modified inverse and $\mathcal{H}_\infty$) and two Model Predictive Controllers (MPC) (one linear and another nonlinear). It was shown that both the inverse based and $\mathcal{H}_\infty$ controllers fail to control the tank level to set-point in the event of an unmeasured disturbance. The competing concept was successfully illustrated on this process with the linear MPC controller being the most often selected controller, and the overall performance of the plant substantially improved by having access to more advanced control techniques, which is facilitated by the proposed platform.

A first appendix presents an investigation into a previously proposed switching philosophy [15] in terms of its ability to determine the best controller, as well as the stability of the switching scheme. It is found that this philosophy cannot provide an accurate measure of controller performance owing to the use of one step ahead predictions to analyse controller behaviour. Owing to this, the philosophy can select an unstable controller when there is a stable, well tuned controller competing to control the process.

A second appendix shows that there are cases where overall system performance can be improved through the use of the proposed platform. In the presence of constraints on the rate of change of the inputs, a more aggressive controller is shown to be selected so long as the disturbance or reference changes do not cause the controller to violate these input constraints. This means that switching back to a less aggressive controller is necessary in the event that the controller attempts to violate these constraints. This is demonstrated on a simple first order plant as well as the surge tank process.

Overall it is concluded that, while there are practical issues surrounding plant and system identification and model/controller maintenance, it would be possible to implement such a platform which would allow a given plant access to advanced process control solutions without the need for procuring the services of a large vendor.

LIST OF ABBREVIATIONS

APC	Advanced process controller
CV	Controlled variable
DCS	Distributed control system
IoT	Internet of Things
LMPC	Linear model predictive control
LQT	Linear quadratic tracking
LTI	Linear time invariant
MIMO	Multiple-input multiple-output
MPC	Model predictive control
MV	Manipulated variable
NMPC	Nonlinear model predictive control
PI(D)	Proportional, integral (and derivative)
PLC	Programmable logic controller
RGA	Relative gain array
SIMC	Simple internal model control
SISO	Single input single output
SSE	Sum of the squares of the error
VM	Virtual machine

TABLE OF CONTENTS

CHAPTER 1 INTRODUCTION

1.1 CHAPTER OVERVIEW

This chapter presents a summary of the research presented in this work. Section 1.2 puts the problem into context and describes the research gap, Section 1.3 lists the objectives and research question addressed in this work, Section 1.4 lists the hypotheses relevant to this study as well as the approach used. The research goals and the contributions are detailed in Sections 1.5 and 1.6 respectively. An overview of the study is presented in Section 1.7 which highlights the focus area of each Chapter.

1.2 PROBLEM STATEMENT

1.2.1 Context of the problem

With the advent of platform based businesses such as Uber and Airbnb which facilitate the provision of services between customers and suppliers, there has been increasing interest in expanding the concept into different sectors and industries [1] - [4]. With this general trend to an access economy based model, it would not be far fetched to conceive a similar shift in the field of industrial automation [5]. This is made possible by the advent of the Internet of Things (IoT) where it is becoming feasible for many industrial automation products and services to be moved to cloud based software services. This has given rise to what has been termed Industry 4.0 where more and more devices are becoming interconnected with data being stored and processed in the cloud [7].

For most plants, levels 1 and 2 (L1 and L2 in Fig. 1.1) in the automation hierarchy exist locally on site, with the control being performed by dedicated Programmable Logic Controllers (PLCs) or Distributed Control Systems (DCS) in level 1, while Supervisory Control and Data Acquisition (PLC+SCADA) is performed at level 2. These controllers have been developed specifically to provide better stability,

reliability and a real-time operating system necessary for control applications [6]. What has also been noted, is the fact that cloud and network service providers are judged by their reliability and up-time, the same characteristics required of automation infrastructure [6]. In fact, there are already commercially available SCADA systems which are fully cloud based [8].

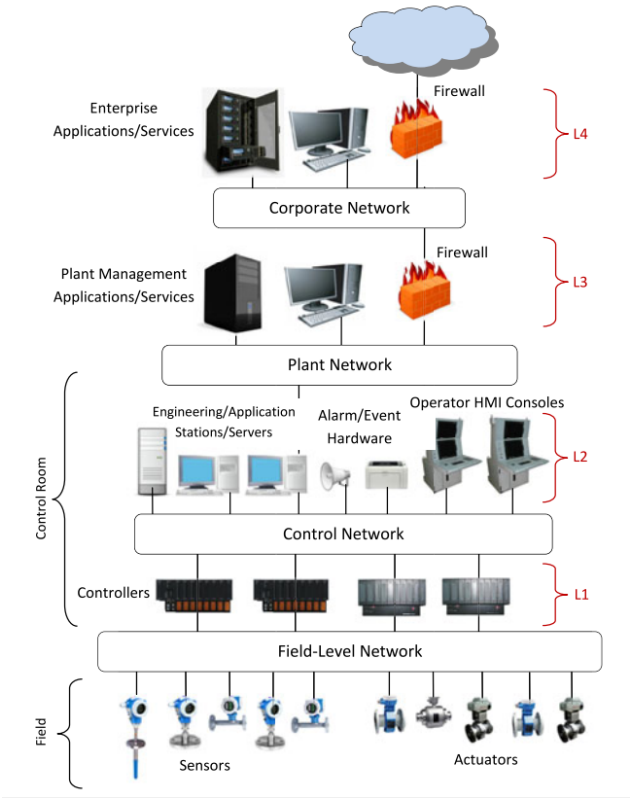

Figure 1.1. Automation hierarchy (taken from [11], © 2011 IEEE)

1.2.2 Research gap

With industrial automation relying on and adopting these advancements in technology, the possibility of supplying automation and control as a remote cloud based service has been investigated [9] - [14]. The common idea behind this research is the viability of moving all levels of the automation hierarchy in Fig. 1.1 to the cloud, except the base level of sensors and actuators which will now become smart devices.

Studies have been done which analyse the reliability and speed of cloud infrastructure by investigating the performance of a simple remote I/O switching procedure on some type of fieldbus network, performed by a virtual or cloud based controller compared with a local controller [9], [10]. It has also been shown that there are inherent advantages to moving control away from the process and towards a service-based approach in the cloud. A major advantage is the reduction in upfront hardware costs,

signal wiring, hardware maintenance as well as on-site commissioning time for skilled personnel [11].

Another advantage of the service based approach which has been highlighted is that of multiple redundancy and the possibility of the plant being able to choose the best controller, with various philosophies being proposed for implementing such multiple redundancy approaches [11] - [14]. Research has been done which proposes a predefined hierarchy of controllers with the process automatically selecting the highest available one in the hierarchy, falling to the next one should communication with the more desirable controller fail [11], [12]. This philosophy provides good redundancy, taking advantage of the ability to have multiple back-up controllers located on different cloud and internet services providers. This means that the best controller is predetermined and only the switching between them takes place in real-time. Other works have focused on switching between controllers based on network quality and computing resources, where a dedicated supervisory node selects willing controllers based on these performance measures [13], [14].

In the researched mentioned, it is assumed in all cases that the controllers are known to the plant, with focus placed on the advantages of moving the upper levels of the automation hierarchy to the cloud while addressing reliability issues. Thus the amount of work done in developing a method to select different cloud controllers based on some type of performance measure related to the process appears to be limited, particularly for the case where the controllers are unknown to the plant. It does not appear that the idea of a service-based approach to control has been investigated which evaluates and switches between competing suppliers in real-time.

1.3 RESEARCH OBJECTIVE AND QUESTIONS

The main objectives of this research are to:

- Formulate a control platform which allows for a number of different controllers to supply control inputs to a process, with the plant selecting the best controller to implement based on some performance measure, with no knowledge of how the control moves of each controller are generated. This idea is based on a philosophy previously presented in [15].

- Present a detailed derivation and analysis of the surge tank of Sibanye-Stillwater's Platinum tailings treatment plant and develop a number of control strategies for this plant.
- Simulate the proposed platform with the developed controllers competing to control the surge tank process.

The resulting research questions are:

- Is the switching method and performance measure based on one step ahead predictions as proposed in [15] a sufficient means of determining controller performance?
- How much information about the plant or process needs to be shared with the prospective controllers for controller development and implementation?
- Can the overall stability of a process be guaranteed, provided there is at least one stable controller competing to control the process?
- Can system performance possibly be improved in comparison with a single controller acting alone?
- What should happen in the event that a selected controller presents undesirable control moves (either on purpose or due to a technical fault)?
- Would the philosophy be viable from a practical point of view with regards to the implementation of advanced control solutions across such a platform (issues such as communication infrastructure and cyber security are outside the scope of this work)?

1.4 HYPOTHESIS AND APPROACH

The hypotheses of this study are as follows:

- The competing controllers will need to be supplied the same amount of information regarding the plant as a control vendor would need to develop a control solution. The necessary information would need to be stipulated by the platform. The competing controllers will also need to be trusted by the plant and prove their performance by simulation of their control solution on a model of the plant.

- A system stability guarantee will require that at least one of the individual controllers must be stable and that the interval between switching be longer than the slowest closed-loop dynamic response.
- It will be necessary for a controller to be installed locally at the plant to serve as a fallback strategy in the case of any technical faults.
- While there may be practical issues surrounding system identification and model/controller maintenance, such a platform would provide plants with access to advanced control solutions without the need for procuring the services of a large vendor.
- The performance measure based on one step ahead predictions as proposed in [15] can not give an accurate measure of controller performance and may be susceptible to instabilities.
- There may be instances where switching between controllers can improve overall performance in comparison with a single controller acting alone.

The approach followed is:

1. The recent trends in the migration of the automation hierarchy to the cloud and the practical limitations are presented.
2. An overview of advanced process control philosophies which may be employed by the competing control suppliers is presented.
3. A detailed analysis of the required structure of the platform to facilitate the competition between controllers as well as the information required by the controllers and the platform is presented.
4. A detailed model and input-output controllability analysis of the surge tank of Sibanye-Stillwater's Platinum tailings treatment plant is presented.
5. Six control philosophies for the surge tank process are presented including four conventional feedback and two MPC controllers.
6. A simulation of the proposed platform philosophy is presented with the six different controllers competing to control the surge tank process.
7. An analysis of the philosophy based on one step ahead predictions as proposed in [15] is presented.
8. A scenario where the proposed platform can facilitate the overall improvement of system performance is presented.

1.5 RESEARCH GOALS

The goals of this research are:

- To formulate the operating philosophy of the evaluating platform.
- To present a detailed model derivation and analysis, as well as a number of controllers for the surge tank process.
- To apply the competing controller philosophy to the surge tank process.
- To analyse the switching philosophy presented in [15].

1.6 RESEARCH CONTRIBUTION

A novel approach to the supply and procurement of advanced process control solutions was presented in the form of a platform which will facilitate competition between different controllers and award control of the process to the one found to be optimal according to some performance index. The practical aspects of implementing such a platform were investigated and a simulation presented using the surge tank process of Sibanye-Stillwater's Platinum tailings treatment plant.

The following articles were produced from this work:

- L.L Rokebrand, J.J. Burchell, L.E. Olivier, I.K. Craig, "Towards an Access Economy Model for Industrial Process Control: A Bulk Tailings Treatment Plant Case Study", submitted to 21st IFAC World Congress, Berlin, Germany, 12-17 Jul. 2020.
- L.L Rokebrand, J.J. Burchell, L.E. Olivier, I.K. Craig, "A Proposed Access Economy Model for Industrial Process Control", submitted to: Journal of Process Control, December 2019.

1.7 OVERVIEW OF STUDY

The structure of the dissertation is as follows:

- Chapter 2 provides a literature review of trends in migrating the lower levels of the automation hierarchy to the cloud, as well as a review of advanced process control philosophies and techniques.
- Chapter 3 presents the requirements and formulation of the proposed platform.
- Chapter 4 presents a detailed model derivation and analysis of the surge tank system.
- Chapter 5 presents the derivation of four conventional feedback and two MPC controllers for the surge tank process.
- Chapter 6 presents a simulation of the proposed platform with the six developed controllers competing to control the plant.
- Appendix A presents an analysis of the switching method proposed in [15].
- Appendix B presents a scenario where the proposed platform can facilitate an improvement in overall system performance.
- Appendix C presents a robust stability analysis of the four conventional feedback controllers presented in Chapter 5.

CHAPTER 2 LITERATURE STUDY

2.1 CHAPTER OBJECTIVES

This Chapter presents an overview of trends and findings with regards to migrating the lower levels of the automation hierarchy (Fig. 1.1) to the cloud is Section 2.2. A summary of control theories is presented is Section 2.3, namely conventional feedback control (including PI and $\mathcal{H}_\infty$ control) and MPC (including state estimation and output feedback as well as linear quadratic optimal control).

2.2 TRENDS IN MIGRATION TO THE CLOUD

A number of works have been published which propose different philosophies of how control could be provided as a service [11], [13], [14]. One approach [13], [14] focuses on awarding control of the plant based on network performance between the proposed controller and the plant, as well as computing capacity of the cloud-based controller. A local supervisory controller/node exists as a fall-back strategy which also serves as a plant start-up controller. This node will broadcast the plant model, plant IP address, prescribed control algorithm and estimated computational requirement on the network. All nodes willing to control the plant will send the estimated time delay and network dropout statistics between itself and the plant to the supervisory node. The supervisory node then ranks the willing controller nodes according to this information and sends it to the plant. Once this list of top willing controllers is sent to the plant, the plant begins sending state and current manipulated variables to all the controllers. The controllers calculate control moves/manipulated variables in a predictive control manner and send these to the plant in packets, and the plant implements the most current one (timestamp wise) at each control interval. The control philosophy is prescribed to the controllers by the node, which is a Network Predictive Control strategy [16]. All controllers thus employ the same control technique. Each controller periodically sends feedback to the supervisory node and if

no feedback is received from a controller, it is removed from the list and this information is relayed to the plant, which will then stop sending feedback measurements to this controller. The controller will be added back to the list if it begins to communicate again. This scheme does not discuss the willing controllers as vendors competing to control the plant, in this case the best controllers from an infrastructure performance point of view (network and computing ability) are chosen with the control method prescribed by the supervisory node.

Another approach [11] looks at the benefits of moving control to the cloud from a redundancy point of view. It is proposed that PID controllers are ranked in an ordered hierarchy. The plant stores the last implemented control move and the time elapsed since each controller implemented a control move. This information is sent to all controllers. The controllers each have an increasing time threshold, with the primary controller having the lowest threshold, and the rest increasing with position in the hierarchy. If no controller with a lower threshold has acted for a time equal to this threshold, that particular controller will engage as the active controller. This implements the hierarchy of controllers and allows for multiple redundancy to be achieved. The need for a smooth handover strategy between controllers was also noted. The strategy proposed is to adjust the initial value of the integrator term of the PID controller [17]. A cost benefit analysis also stated that costs could be reduced by between 45 and 55 % by using controllers on cloud virtual machines (VMs) as opposed to hardware controllers, which would mainly be due to the huge saving in hardware.

One issue mentioned in these works is the issue of variable time delays over the internet which can range from a few milliseconds to a few hundred milliseconds [11], [18]. For the Network Predictive Control scheme proposed, ([13], [14]) the predictive nature of this method is taken advantage of, as well as the assumption that a sequence of control predictions can be sent over the network in packets. The plant then selects the most recent (timestamp wise) control move of the series, discarding the older moves [16]. The other study based on redundancy [6] investigated control over the cloud using discrete time PID control. In order to mitigate delays, an adapted version of the Smith Predictor was used [11]. The Smith Predictor is used to control systems with dead time [19] by adjusting the controller to achieve a total closed-loop response which is a time delayed version of the closed-loop system without any time delay, i.e.

$$\bar{H}(z) = z^{-k}H(z) \tag{2.1}$$

where $\bar{H}$ is the desired closed-loop response, and H is the closed-loop response designed for with the

time delay ignored. In this instance the dead time is taken to be the varying time delay for data to be transmitted over the network/Internet. The value of the delay is taken as an exponentially weighted average of the measured network delays.

Discrete time control is classically done by sampling the feedback signal and generating the control signal at a fixed sampling period. When network delays of a few hundred milliseconds are added to the feedback and feedforward paths, and they are variable in length, it poses a problem to controller design. This however is not so much the case when the sampling period is very large, i.e. much larger than the maximum delay time, which is the case for some processes. The general rule is given that $0.2 < \omega h < 0.6$ where h is the sampling period and ω is the highest natural frequency of the closed-loop system [20].

A simple case-study, published in 2014, outlines this problem in supplying control as a service, namely inherent time delays over the network and in virtualised platforms [9]. Cloud services are typically run on a virtual platform, and to investigate this, a soft PLC (controller using normal PC as hardware) was installed on a virtual machine to emulate a cloud service. The test was conducted by connecting this virtual PLC through a Profinet network to a single remote I/O unit. The input was connected to a signal generator which turns an input on and off at a certain frequency. Once received, the PLC would invert the signal and write it to an output, which was then recorded on an oscilloscope. The combination of the Profinet network, PLC scan cycle time and the communication between the physical and virtual network results in a delay between the input and the output response. This is shown in Fig. 2.1. The delay ΔT as shown in Fig. 2.1 was sampled 1000 times and an average taken. This was done on the virtualised PLC and a hardware PLC in order to draw a comparison between the two. The results of this experiment are shown in the graph of Fig. 2.2 where the average $\overline{\Delta T}$ is plotted against the interval length T_I. The inferior performance of the virtualised system can be clearly seen from this figure. The performance deteriorates quite substantially with increased switching frequency of the input for both the virtualised and hardware PLC. This is due to increased traffic on the Profinet network between the I/O module and the PLC, with added delay for the virtualized case which is due to resource sharing between the host and the virtual machine [9]. In this experiment the Profinet network did not communicate to the virtual PLC via the internet, which would have further deteriorated the performance of the virtualized system, but it does show that if the sampling rate of the system is low, the virtualisation of the controller is a feasible proposition.

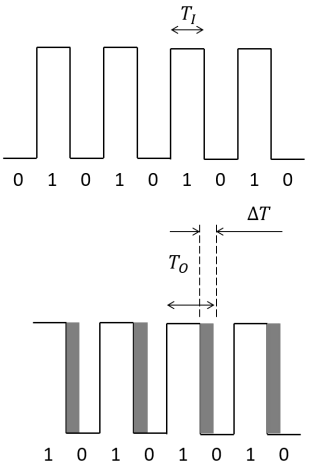

Figure 2.1. Output delay (adapted from [9], © 2011 IEEE).

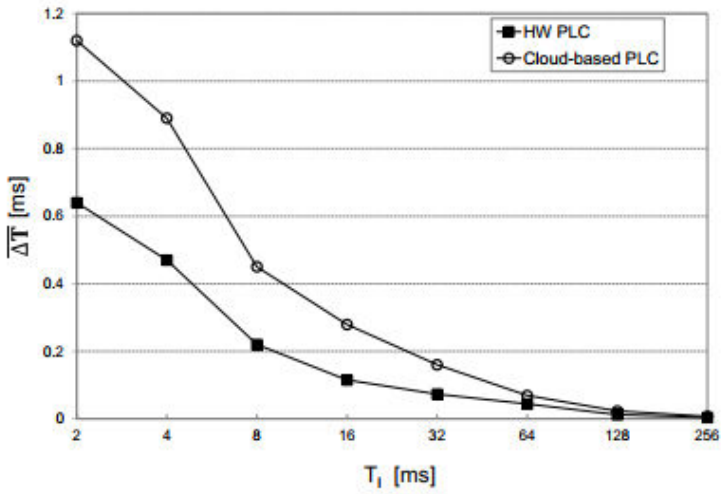

Figure 2.2. Hardware PLC vs virtual PLC (taken from [9], © 2011 IEEE) .

A similar experiment focused on the architecture of the virtual PLC in terms of dynamically scaling the controller in order to utilise resources more efficiently [10]. An experiment was conducted in which the automated switching of lights in a building was simulated and controlled by the remote PLC installed on a cloud server in a separate country. Again, their performance measure was the roundtrip delay from the time a measurement signal was sent to the controller to the time a corresponding control move was received. An average round-trip time delay of 377.65 ms was measured, with 99.72 % of them below 1000 ms, which is the maximum sample time limit specified for the BACNet protocol as stated by the authors.

It can thus be concluded that controlling processes which are soft real-time or have large sampling times is feasible from a virtual cloud platform. Soft real-time implies that if the data on the network is not received within a certain time frame, system performance degrades but it will not result in system failure. Network protocols such as CAN, Profibus and Profinet have been specifically developed to meet the requirements for time critical/hard real-time applications (e.g. ABS braking in automobiles, boiler control) [21]. The same holds for dedicated computers such as PLC's which run on real-time operating systems to meet strict timing requirements [22]. Thus, as soon as these real-time control focused networks/controllers are interfaced with the Internet and cloud services, the ability to guarantee control of hard real-time systems is lost.

The main factor to contend with from a control perspective when signals are sent over the Internet and non-real-time communication networks is the variation in the time delay which depends on issues such as network traffic and how the specific protocol such as Internet Protocol (IP) manages this [10], [22]. This is a problem which has been analysed within the field of Network Control Systems where different techniques to cope with network delays have been developed [21]. A common approach involves the determination of network delay statistics which are then incorporated as uncertainty in the controller design using techniques such as LQG [23] or robust control theory [24]. A different kind of approach includes the Network Predictive Control strategies where predictive control techniques are used to generate a sequence of control moves which are time-stamped, with the plant implementing the latest control move in the sequence [16]. Fig. 2.3 shows a good representation of the problem where τ_k^{ca} represents the delay between the controller and the actuator and τ_k^{sc} represents the delay between the sensor and the controller.

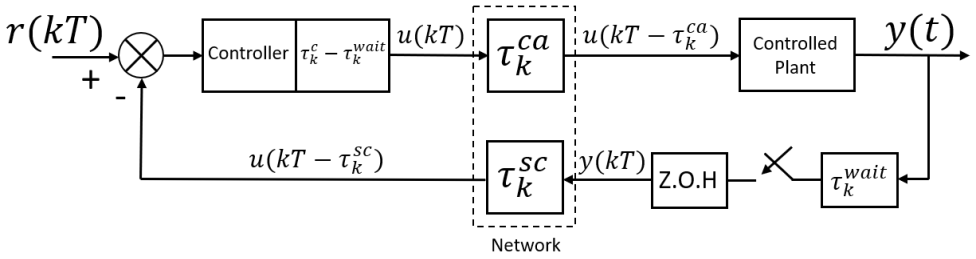

Figure 2.3. Networked control system with time delays (taken from [21], © 2011 IEEE) .

2.3 CONTROL PHILOSOPHIES

2.3.1 Conventional Feedback Control

Classical control techniques use feedback as the fundamental mechanism in generating control actions for the plant [25]. Fig. 2.4 shows the classical one degree-of-freedom feedback loop in which a feedback controller $\mathbf{G}_c$ is employed to control the output **y** of a plant which is influenced by the control inputs **u** via some dynamics denoted by $\mathbf{G}_p$. The aim of the controller is to manipulate the inputs **u** in order to keep the output **y** as close as possible to the reference **r** in the presence of measurement noise **n** and external disturbances **d** which influence the output **y** via some dynamics denoted by $\mathbf{G}_d$. This applies to the case where the models G_p and G_d are single-input single-output (SISO) in which case the signals y, u, r, d, n and e are scalar values, as well as the multiple-input multiple-output (MIMO) case (represented by bold $\mathbf{G}_p$ and $\mathbf{G}_d$) where signals **y**, **u**, **r**, **d**, **n** and **e** are column vectors. When using classical control techniques, $\mathbf{G}_p$ and $\mathbf{G}_d$ are usually taken to be linear time-invariant (LTI) models of the process given in transfer function matrix form (for the MIMO case) and thus the controller $\mathbf{G}_c$ is also a transfer function matrix relating the control action **u** to the error **e**. For the

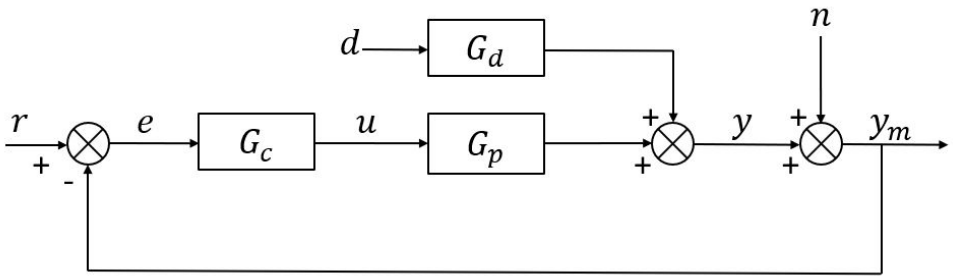

Figure 2.4. Classical feedback loop.

typical feedback loop shown in Fig. 2.4, the output **y** can be written in term of the reference **r**, the disturbance **d** and the noise **n** as:

$$\mathbf{y} = (\mathbf{I}+\mathbf{G}_p\mathbf{G}_c)^{-1}\mathbf{G}_p\mathbf{G}_c\mathbf{r} + (\mathbf{I}+\mathbf{G}_p\mathbf{G}_c)^{-1}\mathbf{G}_d\mathbf{d} + (\mathbf{I}+\mathbf{G}_p\mathbf{G}_c)^{-1}\mathbf{G}_p\mathbf{G}_c\mathbf{n} \tag{2.2}$$

The loop transfer function **L** defined as:

$$\mathbf{L} = \mathbf{G}_p\mathbf{G}_c \tag{2.3}$$

is used to provide a quantitative measure of the stability and performance of a feedback controller [26], [27]. Two other transfer functions which are of use in performance specification of feedback

controllers are the sensitivity transfer function **S** and complementary sensitivity transfer function **T** which are defined as:

$$\mathbf{S} = (\mathbf{I} + \mathbf{G}_p\mathbf{G}_c)^{-1} = (\mathbf{I} + \mathbf{L})^{-1} \tag{2.4}$$

$$\mathbf{T} = (\mathbf{I} + \mathbf{G}_p\mathbf{G}_c)^{-1}\mathbf{G}_p\mathbf{G}_c = \mathbf{SL} \tag{2.5}$$

From (2.4) and (2.5) it follows that:

$$\mathbf{S} + \mathbf{T} = (\mathbf{I} + \mathbf{L})^{-1} + (\mathbf{I} + \mathbf{L})^{-1}\mathbf{L} = (\mathbf{I} + \mathbf{L})^{-1}(\mathbf{I} + \mathbf{L}) = \mathbf{I} \tag{2.6}$$

It should be noted that the complementary sensitivity function **T** gives the relationship between the output **y** and both the reference **r** and noise signal **n**, while the sensitivity transfer function **S** is the factor by which the output, due to disturbances of the uncontrolled plant ($\mathbf{G}_d\mathbf{d}$), is multiplied by as a result of introducing feedback control. The sensitivity transfer function **S** also denotes the relationship between the error signal **e** and the reference signal **r**, that is:

$$\mathbf{e} = (\mathbf{I} + \mathbf{G}_p\mathbf{G}_c)^{-1}\mathbf{r} = \mathbf{Sr} \tag{2.7}$$

From (2.2) and (2.7) it is evident that the sensitivity transfer function **S** should be as close to zero as possible in order to suppress the error signal **e** as well as the effect of disturbances ($\mathbf{G}_d\mathbf{d}$) on the output **y**. A small sensitivity transfer function **S** requires a large loop transfer function **L**, i.e it is required that $\underline{\sigma}(\mathbf{L}) \gg 1$ for the MIMO case where $\underline{\sigma}$ denotes the minimum singular value, and $L \gg 1$ for the SISO case. A similar argument can be made for reference tracking as $\underline{\sigma}(\mathbf{L}) \gg 1$ would imply from (2.4) that $\bar{\sigma}(\mathbf{S}) \approx 0$ and $\underline{\sigma}(\mathbf{T}) \approx \bar{\sigma}(\mathbf{T}) \approx 1$ from (2.5), which would yield good reference tracking. On the other hand, a value for $\underline{\sigma}(\mathbf{T})$ as close as possible to 0 is desired to mitigate any response to sensor noise **n** in the output **y** as can be seen from (2.2); this requires that $\bar{\sigma}(\mathbf{L}) \ll 1$. It is thus evident that there is a conflict in design objectives of the one degree-of-freedom feedback loop. The effects of this trade-off is mitigated however because the requirement that $\bar{\sigma}(\mathbf{L}) \ll 1$ is applicable mainly to high frequencies where sensor noise **n** typically occurs, while the requirement that $\bar{\sigma}(\mathbf{L}) \gg 1$ is applicable to lower frequencies which the reference signal **r** and disturbance **d** would fall into [27], [28].

Provided that a -20 dB/dec roll-off is sufficient, the ideal loop transfer function matrix **L** is defined to be of the form:

$$\mathbf{L}^* = \frac{k}{s}\mathbf{I} \tag{2.8}$$

where $\mathbf{I}$ is the identity matrix and k is a constant gain factor [27]. This is achieved if and only if:

$$\mathbf{G}_c^* = \frac{k}{s}\mathbf{G}_p^{-1} \tag{2.9}$$

This ideal controller $\mathbf{G}_c^*$ yields the ideal sensitivity and complementary sensitivity transfer functions $\mathbf{S}^*$ and $\mathbf{T}^*$ of the form:

$$\mathbf{S}^* = \frac{s}{s+k}\mathbf{I} \tag{2.10}$$

$$\mathbf{T}^* = \frac{k}{s+k}\mathbf{I} \tag{2.11}$$

Fig 2.5 shows the Bode magnitude plots for the ideal transfer functions $\mathbf{L}^*$, $\mathbf{S}^*$ and $\mathbf{T}^*$ with a constant gain factor k of 1 for a SISO system. It can be seen that, as desired, the complementary sensitivity transfer function $\mathbf{T}^*$ is equal to one at low frequencies while it rolls off at -20 dB/dec at frequencies above 1 rad/sec. This frequency corresponds with the bandwidth of the controller and for ideal control corresponds with the gain factor k, thus increasing k will increase the bandwidth and thus the speed of response of the system [27]. This corresponds to the large magnitude of $\mathbf{L}^*$ at low frequencies and low magnitude at high frequencies. It should be noted that in a case where the system is MIMO, the singular values of the transfer function matrices are considered. For the case of ideal control, all singular values will be equal.

Unfortunately, ideal control is not always possible to achieve as it requires the inverse of the plant model $\mathbf{G}_p$. This is not possible in instances where the plant has zeros in the right half plane, time delays or a pole zero difference greater than two as this would lead to unstable, non-causal or un-realisable controllers respectively [27]. Plant models are also at best approximations of the real plant behaviour and thus perfect inversion in real life is not possible. Even though this is the case, the framework of the ideal control scenario provides a good reference for what is ideally possible and achievable for a given plant.

2.3.1.1 PI(D) control

Proportional, Integral and Derivative (PID) control is by far the most commonly used feedback control technique in the process automation industry [29]. The control move u generated by a PID controller

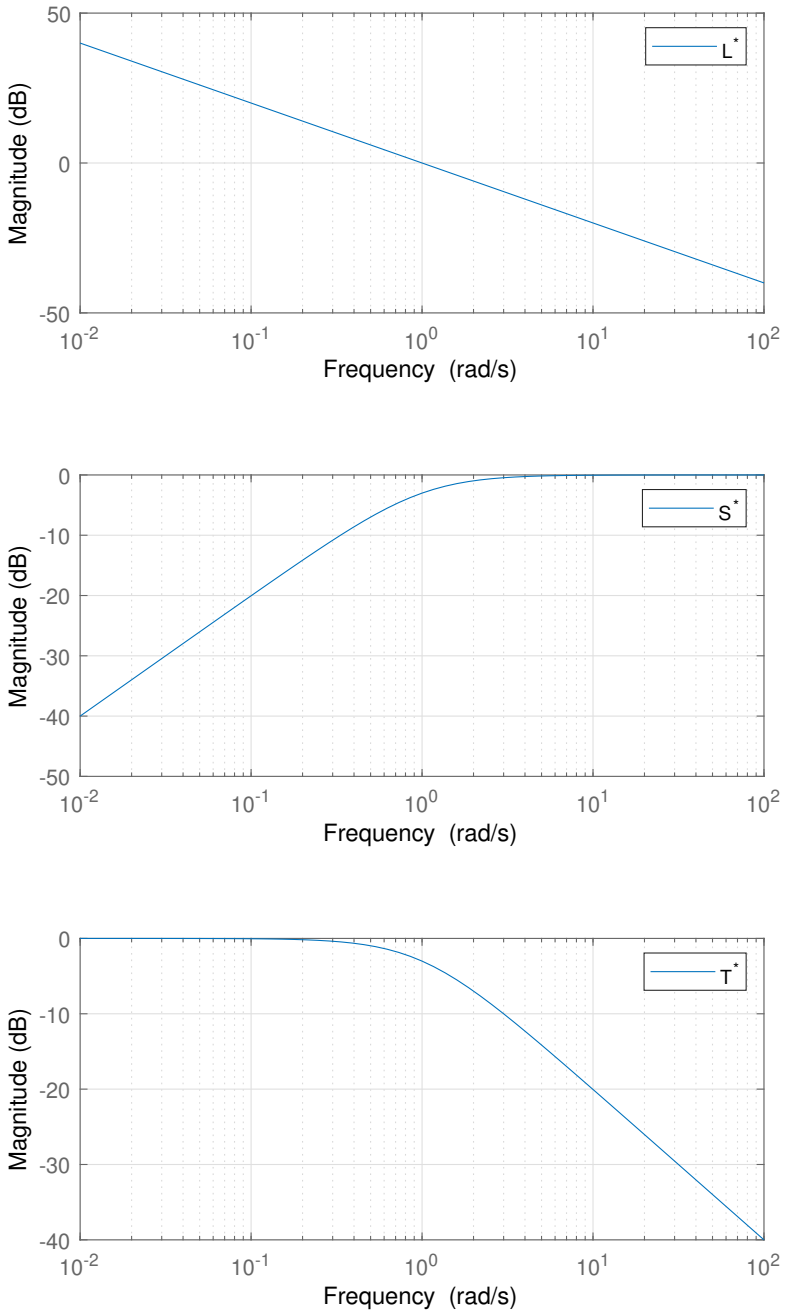

Figure 2.5. Frequency response characteristics of ideal control.

is given as:

$$u(t) = K_c\Big[e(t) + \frac{1}{\tau_I}\int_0^t e(t^*)dt^* + \tau_D\frac{de(t)}{dt}\Big] \tag{2.12}$$

where e is the error signal, which is the difference between the desired set-point or reference value r and the measured output of the system y which is expressed as [26]:

$$e(t) = r(t) - y(t). \tag{2.13}$$

Equation (2.12) can be expressed in transfer function form as:

$$\frac{U(s)}{E(s)} = K_c\Big[1 + \frac{1}{\tau_I s} + \tau_D s\Big] \tag{2.14}$$

Many approaches have been developed to calculate suitable values for the tuning parameters K_c, τ_I and τ_D based on the system response. Many industrial controllers use one of the methods along with some kind of automatic system identification procedure to generate values for these tuning parameters [26]. One approach is to close the feedback loop and use a bang-bang control strategy where the manipulated variable is switched between two values depending on the value of the process output. The period and amplitude of the output oscillations are then used to calculate tuning parameters which will yield certain pre-specified gain and phase margins [30]. This procedure is commonly referred to as relay auto-tuning [26].

It is worth noting that there are a number of practical considerations and drawbacks regarding the theoretical form of the PID controller given in (2.12) and (2.14) such as noise sensitivity in the derivative term, derivative and proportional kick and integral wind-up [20], [25], [26].

2.3.1.2 Noise filtering

Noise can pose a practical problem to the derivative term, and thus a filtered value of the derivative is used in practice instead of a direct approximation. A similar issue with the derivative term can be seen in (2.14) as this yields a non-realisable transfer function of the form:

$$\frac{U(s)}{E(s)} = K_c\Big[\frac{\tau_I\tau_D s^2 + \tau_I s + 1}{\tau_I s}\Big]. \tag{2.15}$$

Thus it is common to augment (2.14) by the addition of a derivative filter:

$$\frac{U(s)}{E(s)} = K_c\left[1 + \frac{1}{\tau_I s} + \frac{\tau_D s}{\alpha s + 1}\right] \tag{2.16}$$

where α is usually set to a small value in the range of 0.05 - 0.5. Another alternative is to use the ideal controller in (2.12)/(2.14) and filter the measured signal y which gives:

$$\frac{U(s)}{E(s)} = K_c\left[1 + \frac{1}{\tau_I s} + \tau_D s\right] \cdot \frac{1}{(sT_f)^2/2 + T_f s + 1} \tag{2.17}$$

for a second order filter [25]. This method is advantageous as filtering of the measured signal is often necessary [20].

2.3.1.3 Derivative and proportional kick

If step changes are made in the set-point, the derivative of the error signal will theoretically be infinite at the moment the change occurs. This phenomenon is referred to as derivative kick [25], [26]. Therefore, in cases were derivative action is used, it is common to apply the derivative action to the measured signal only. Similarly, the large error generated by a step change in the set-point r results in a large control action from the proportional term. A weighting term is sometimes applied to the set-point for the proportional term to eliminate this problem [25], [26]. These two adjustments give a controller of the following form:

$$u(t) = K_c\left[(\beta r(t) - y(t)) + \frac{1}{\tau_I}\int_0^t (r(t^*) - y(t^*))dt^* - \tau_D \frac{dy(t)}{dt}\right]. \tag{2.18}$$

2.3.1.4 Integral wind-up

In practice, a major issue to contend with in any control problem is the magnitude of the control actions which the actuator can provide. Let this actual actuator control action be denoted as v. In the ideal scenario, the actuator would output the control action provided by the controller (u) directly without delay and thus

$$v = u. \tag{2.19}$$

In practice however, if actuator dynamics are ignored, there is still an upper and lower limit on the value which can be realised in v. If this occurs and the required input needed to reject a disturbance or reach a given set-point is unachievable, the output will generally settle to some steady-state off-set from the

set-point. If this occurs, the integral term and thus the controller output u will increase indefinitely over time while the actuator output v remains constant. This phenomenon is termed integral wind-up.

If the disturbance or unreachable set-point which caused the controller to generate this control move is removed, this large integral term which has built up will start to decrease, which can take a significant amount of time, which is very undesirable behaviour. To overcome this, many anti-wind-up techniques have been developed, the simplest being to stop integrating the error when the process output saturates. This is relatively easy to achieve on a digital platform. There are a number of other methods which have been well documented [25], [26].

2.3.1.5 Digital implementation

The vast majority of PI(D) controllers in use today are implemented on a digital platform. In order to achieve this, it is necessary to discretise the integral and derivative terms in (2.12)/(2.14). The most common method is to simply approximate the integral and derivative terms as follows:

$$\int_0^t e(t^*)dt^* \approx \sum_{i=1}^{k} e_i \Delta t \tag{2.20}$$

$$\frac{dy}{dt} \approx \frac{y_k - y_{k-1}}{\Delta t} \tag{2.21}$$

where y_k and e_k denote the values of y and e at the k^{th} sampling interval and Δt denotes the time between samples [26]. The form of the integral approximation in (2.20) represents a forward Euler approximation of the integral, which is the simplest form. Other approximations such as the trapezoidal and Tustin approximation can be used which have slightly improved accuracy and stability properties [20].

The sampling interval Δt is an important aspect and needs to be short enough to capture the plant dynamics. The general rule of thumb is given as follows:

$$0.1 < \omega \cdot \Delta t < 0.6 \tag{2.22}$$

where ω is the frequency of the fastest dynamic expected in the closed-loop system [20].

In a digital platform, representation of a system in discrete state-space difference equations of the form:

$$\mathbf{x}(k+1) = \mathbf{\Phi}\mathbf{x}(k) + \mathbf{\Gamma}\mathbf{u}(k) \tag{2.23}$$

$$\mathbf{y}(k) = \mathbf{C}\mathbf{x}(k) + \mathbf{D}\mathbf{u}(k) \tag{2.24}$$

is very useful in terms of traceability and computational efficiency. If (2.16) is rewritten as:

$$\frac{U(s)}{E(s)} = \left[K_p + \frac{K_i}{s} + \frac{K_d s}{\alpha s + 1}\right] \tag{2.25}$$

where

$$\begin{aligned} K_p &= K_c \\ K_i &= \frac{K_c}{\tau_i} \quad , \\ K_d &= K_c \tau_d \end{aligned}$$

(2.25) can be written in continuous time state-space form as:

$$\begin{bmatrix} \dot{x}_{c1} \\ \dot{x}_{c2} \end{bmatrix} = \begin{bmatrix} 0 & 1 \\ 0 & -\frac{1}{\alpha} \end{bmatrix} \begin{bmatrix} x_{c1} \\ x_{c2} \end{bmatrix} + \begin{bmatrix} 0 \\ \frac{1}{\alpha} \end{bmatrix} e \tag{2.26}$$

$$u = \begin{bmatrix} K_i & (\alpha K_i - \frac{K_d}{\alpha}) \end{bmatrix} \begin{bmatrix} x_{c1} \\ x_{c2} \end{bmatrix} + \left[K_p + \frac{K_d}{\alpha}\right] e \tag{2.27}$$

This is then a standard LTI state-space system of the form:

$$\dot{\mathbf{x}}_c(t) = \mathbf{A}_c\mathbf{x}_c(t) + \mathbf{B}_c\mathbf{e}(t) \tag{2.28}$$

$$\mathbf{u}(t) = \mathbf{C}_c\mathbf{x}_c(t) + \mathbf{D}_c\mathbf{e}(t) \tag{2.29}$$

which can be converted into the equivalent discrete difference equation formulation of (2.23) and (2.24) through the following transformations [20]:

$$\mathbf{\Phi}_c = e^{\mathbf{A}_c \Delta t} \tag{2.30}$$

$$\mathbf{\Gamma}_c = \int_0^{\Delta t} e^{\mathbf{A}_c s} ds \cdot \mathbf{B}_c = \mathbf{A}_c^{-1} \cdot [e^{\mathbf{A}_c \Delta t} - \mathbf{I}] \cdot \mathbf{B}_c \tag{2.31}$$

where

$$\mathbf{x}_c(k+h) = \mathbf{\Phi}_c\mathbf{x}_c(k) + \mathbf{\Gamma}_c\mathbf{e}(k) \tag{2.32}$$

$$\mathbf{u}(k) = \mathbf{C}_c\mathbf{x}_c(k) + \mathbf{D}_c\mathbf{e}(k) \tag{2.33}$$

Applying this transformation to (2.26) yields:

$$\begin{bmatrix} x_{c1}(k+1) \\ x_{c2}(k+1) \end{bmatrix} = \begin{bmatrix} 1 & \alpha(1-e^{-\frac{\Delta t}{\alpha}}) \\ 0 & e^{-\frac{\Delta t}{\alpha}} \end{bmatrix} \begin{bmatrix} x_{c1}(k) \\ x_{c2}(k) \end{bmatrix} + \begin{bmatrix} \Delta t + \alpha(e^{-\frac{\Delta t}{\alpha}} - 1) \\ 1 - e^{-\frac{\Delta t}{\alpha}} \end{bmatrix} e(k) \tag{2.34}$$

with the output equation identical to that of (2.27). This is the digital form used in this work as well as the following simplified form for a PI only controller:

$$x_c(k+1) = x_c(k) + \Delta t e(k) \tag{2.35}$$

$$u(k) = K_i x_c(k) + K_p e(k) \tag{2.36}$$

which is equivalent to the Euler forward approximation of the integral.

2.3.1.6 Tuning and performance

The tuning of PI(D) controllers is a well developed topic with many different methods available which guarantee specified degrees of performance, such as the Ziegler-Nichols, Cohen-Coon and SIMC to name a few [25], [26]. These tuning rules are often used in practice and often form part of some auto-tuning capability [30]. These auto-tuning features are useful and well used in the process control industries due to the large number of control loops that need to be tuned. It has however been observed that the performance of these auto-tuning functions can be significantly improved [31].

One such set of rules which is widely used and provides good results is the SIMC tuning method. These rules are summarised for both first order and integrator plus time delay models which give the gain (K_c) and integral time constant (τ_i) for a PI controller of the form in (2.14) with no derivative action (i.e. $\tau_D = 0$). The parameter τ_c is used as a tuning parameter with smaller values yielding more aggressive behaviour. If the plant is a first order system with no time delay, the SIMC rules yield ideal control as previously discussed with the tuning parameter τ_c determining the bandwidth, with smaller values yielding a higher bandwidth.

PI(D) controllers form the basis of process control due to their simplicity and capability of handling uncertainty. The nature of PI(D) control is however inherently SISO. This presents a drawback for more complex MIMO processes, unless there is no interaction between the inputs and outputs and

Table 2.1. SIMC Tuning Rules [32]

Model	**G**(s)	K_c	τ_i
First order	$k\frac{e^{-\theta s}}{\tau s+1}$	$\frac{1}{k}\frac{\tau_i}{\tau_c+\theta}$	$\min[\tau, 4(\tau_c+\theta)]$
Integrator	$k\frac{e^{-\theta s}}{s}$	$\frac{1}{k}\frac{\tau_i}{\tau_c+\theta}$	$4(\tau_c+\theta)$

pairing can be done such that a single controller can be used for each pair. When this is not the case, more advanced control strategies such as model predictive control (MPC) are often used.

2.3.1.7 Mixed sensitivity $\mathcal{H}_\infty$ loop shaping control

Mixed sensitivity $\mathcal{H}_\infty$ loop shaping control is an advanced feedback control technique which aims to e.g. shape the sensitivity and complementary sensitivity transfer functions [27], [33], [34]. This technique requires that the feedback loop be represented in the generalised form shown in Fig. 2.6. The outputs $\mathbf{z}_1$, $\mathbf{z}_2$, $\mathbf{z}_3$ and $\mathbf{e}$ of the $\mathbf{P}$ structure in this form are given in terms of the inputs $\mathbf{r}$ and $\mathbf{u}$ as:

$$\begin{bmatrix}\mathbf{z}_1\\ \mathbf{z}_2\\ \mathbf{z}_3\\ \mathbf{e}\end{bmatrix} = \mathbf{P}(s)\begin{bmatrix}\mathbf{r}\\ \mathbf{u}\end{bmatrix} = \begin{bmatrix}\mathbf{W}_p & -\mathbf{W}_p\mathbf{G}_p\\ \mathbf{0} & \mathbf{W}_u\\ \mathbf{0} & \mathbf{W}_T\mathbf{G}_p\\ \mathbf{I} & -\mathbf{G}_p\end{bmatrix}\begin{bmatrix}\mathbf{r}\\ \mathbf{u}\end{bmatrix} \tag{2.37}$$

If the the feedback loop is closed via the controller $\mathbf{G}_c$, the reduced system is given as:

$$\begin{bmatrix}\mathbf{z}_1\\ \mathbf{z}_2\\ \mathbf{z}_3\end{bmatrix} = \begin{bmatrix}\mathbf{W}_p\mathbf{S}\\ \mathbf{W}_u\mathbf{G}_c\mathbf{S}\\ \mathbf{W}_T\mathbf{T}\end{bmatrix}\begin{bmatrix}\mathbf{r}\end{bmatrix} \tag{2.38}$$

where $\mathbf{S}$ and $\mathbf{T}$ are the sensitivity and complementary sensitivity transfer functions given in (2.4) and (2.5) respectively.

The terms $\mathbf{W}_p$, $\mathbf{W}_u$, $\mathbf{W}_T$ are weighting terms of appropriate dimension which define the desired shape of the singular values of the $\mathbf{S}$, $\mathbf{G}_c\mathbf{S}$ and $\mathbf{T}$ transfer function matrices respectively. $\mathbf{W}_p$ and $\mathbf{W}_T$ typically take the form:

$$\mathbf{W}_p = \frac{s+\omega_B}{s+\omega_B A}\mathbf{I} \tag{2.39}$$

$$\mathbf{W}_T = \frac{s+\omega_B}{As+\omega_B}\mathbf{I} \tag{2.40}$$

where ω_B is the desired controller bandwidth and A is a constant such that $A \ll 1$ [27]. It follows that

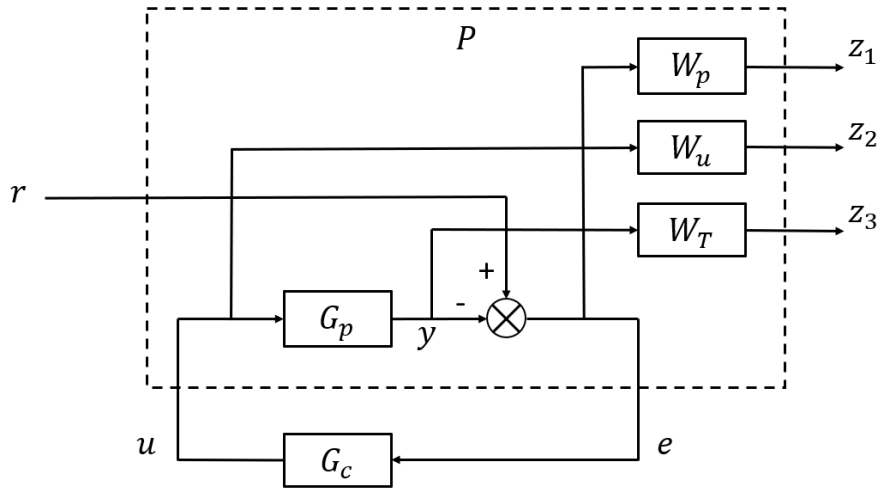

Figure 2.6. Generalised feedback control structure.

with $A = 0$, the singular values of $\mathbf{W}_p^{-1}$ and $\mathbf{W}_T^{-1}$ take the ideal forms shown in Fig. 2.5. The weight $\mathbf{W}_u$ typically takes the form of the identity matrix, given that the plant is scaled in such a way that the scaled inputs take on values between 0 and 1.

In deriving the controller $\mathbf{G}_c$, the $\mathcal{H}_\infty$ norm of the transfer function matrix in (2.38) (or some variant thereof) is minimised. The $\mathcal{H}_\infty$ norm of a matrix $\mathbf{H}$ is defined as:

$$\left\|\mathbf{H}\right\|_\infty = \max_{\omega} \quad \bar{\sigma}[\mathbf{H}(j\omega)] \tag{2.41}$$

which is the maximum value of the maximum singular value as a function of frequency [27]. This means that the controller synthesis procedure aims at achieving singular values for the sensitivity and complementary sensitivity transfer functions $\mathbf{S}$ and $\mathbf{T}$ which are less than some desired values specified by the weighting transfer function matrices $\mathbf{W}_p$ and $\mathbf{W}_T$ over all frequencies, while keeping the magnitude of the input $\mathbf{u}$ below the maximum allowed value as defined in $\mathbf{W}_u$.

2.3.2 Model Predictive Control (MPC)

Model predictive control is an advanced control technique which has been put to use extensively in the process control industry [35], and has also received much attention from the academic community [36] - [39]. The concept of MPC involves the optimisation of some performance function subject to the plant dynamics as well as constraints on the input and output variables which is solved at each sampling period. This can be expressed in mathematical terms as follows.

$$\min_{\mathbf{u},\delta} \quad V(\mathbf{x},\mathbf{u},\boldsymbol{\delta},\mathbf{y}_{ref}(\mathbf{k})) \tag{2.42}$$

subject to

$$\mathbf{x}(j+k+1|k) = \mathbf{f}(\mathbf{x}(j+k|k),\mathbf{u}(i+k|k)) \tag{2.43}$$

$$\mathbf{y}(j+k|k) = \mathbf{g}(\mathbf{x}(j+k|k),\mathbf{u}(i+k|k)) \tag{2.44}$$

$$\mathbf{x}(k|k) = \mathbf{x}_0 \tag{2.45}$$

$$\mathbf{u}_{min} \leq \mathbf{u}(i+k|k) \leq \mathbf{u}_{max} \tag{2.46}$$

$$\mathbf{y}_{min} - \boldsymbol{\delta}(k) \leq \mathbf{y}(j+k|k) \leq \mathbf{y}_{max} + \boldsymbol{\delta}(k) \tag{2.47}$$

$$j = 0,1,...,N_p - 1 \tag{2.48}$$

$$i = 0,1,...,N_c - 1 \tag{2.49}$$

$$N_p \geq N_c \times N_b \tag{2.50}$$

where $\mathbf{x} \in \Re^{N_x \times N_p}$, $\mathbf{u} \in \Re^{N_u \times N_c}$, $\mathbf{y} \in \Re^{N_y \times N_p}$, $\boldsymbol{\delta} \in \Re^{N_y}$, k is the present sampling instant, N_x is the number of states, N_u is the number of control inputs, N_y is the number of outputs, N_p is the number of predictions, N_c is the number of control moves, N_b is the number of time steps control vector is kept constant and $\mathbf{x}_0$ is the value of state at present sampling point.

The typical performance index V takes on a quadratic form such as:

$$\begin{aligned} V(\mathbf{u},\mathbf{x},\boldsymbol{\delta}) = &\sum_{j=1}^{N_p} (\mathbf{y}_{ref}(k+j|k) - \hat{\mathbf{y}}(k+j|k))^T \mathbf{Q} (\mathbf{y}_{ref}(k+j|k) - \hat{\mathbf{y}}(k+j|k)) \\ &+ \sum_{i=1}^{N_c} \Delta\mathbf{u}(i+k|k)^T \mathbf{R} \Delta\mathbf{u}(i+k|k) + \boldsymbol{\delta}(k)^T \boldsymbol{\Psi} \boldsymbol{\delta}(k) \end{aligned} \tag{2.51}$$

where $\mathbf{y}_{ref} \in \Re^{N_y}$, $\mathbf{Q} \in \Re^{N_y \times N_y}$, $\mathbf{R} \in \Re^{N_u \times N_u}$, $\boldsymbol{\Psi} \in \Re^{N_y \times N_y}$. The matrices $\mathbf{Q}$, $\mathbf{R}$ and $\boldsymbol{\Psi}$ are diagonal matrices used to weight the importance of the different input, output and slack variables which in turn adjusts the behaviour of the controller. $\hat{\mathbf{y}}$ indicates the predicted values of the process output and:

$$\Delta\mathbf{u}(i) = \mathbf{u}(i+k|k) - \mathbf{u}(i+k-1|k) \tag{2.52}$$

At each sampling instant a measurement of the system state $\mathbf{x}_0$ is taken. The measured state is then used as an initial condition for model predictions to be performed as part of the optimisation procedure. The specified number N_c of control vectors as well as the vector of slack variables $\boldsymbol{\delta}$ are the decision variables in the optimisation procedure.

The input column vectors of $\mathbf{u}$ are used to simulate the model with N_b denoting the number of subsequent time steps the input vector is kept constant. In the event that

$$N_p > N_c \times N_b, \tag{2.53}$$

the control vector is kept constant at the last move in the sequence, i.e. $\mathbf{u}(N_c)$, for the remainder of the prediction horizon N_p. The lower and upper constrains on the input denoted by $\mathbf{u}_{min}$ and $\mathbf{u}_{max}$ are taken into account explicitly by the optimisation algorithm and are never allowed to be violated. They are thus termed hard constraints.

The vector of slack variables $\boldsymbol{\delta}$ is used as a decision variable in the optimisation with the purpose of implementing soft constraints on the output variables. This allows the output to violate the constraints at times with the slack variables used to drive the outputs back slowly to within the constraints. Hence the elements in the weighting matrix $\boldsymbol{\Psi}$ are typically large.

The solution produces N_c control vectors which can be denoted as $\mathbf{u}^*$. The first vector in $\mathbf{u}^*$, that is $\mathbf{u}^*(0)$ is implemented on the plant at the beginning of the next time step. At the same time a new measurement of the state is taken and the optimisation process is repeated. For simple cases, particularly where there are no constraints on the inputs and outputs, analytical solutions to this optimisation problem can be found, otherwise some kind of numerical optimisation algorithm is used [36], [38]. In the latter case, it is obvious that solving this optimisation problem algorithmically would be time consuming, especially for complex models. This factor limits the sampling rate which can be achieved and is a major factor in the popularity of MPC in the field of process control where process dynamics are slow and longer sampling intervals are achievable.

As is the case with PI(D) control, there are a number of practical considerations which warrant mention.

2.3.2.1 Model types and state estimation

In most theoretical frameworks, the state-space formulation, similar to the one given above is used [37] - [39]. In contrast however, most commercial MPC algorithms use either impulse response, step response or discrete time transfer function models [35], [36]. Impulse response models pose a draw back in that they do not allow for the representation of unstable models or integrators [26].

A major complication in the state-space formulation is the fact that the full state $\mathbf{x}$ of the system often

cannot be measured, with only the output $\mathbf{y}$ being measurable. This problem is typically solved by the use of a Kalman filter to estimate the states [38]. The Kalman filter is a type of observer which uses the measured output of the system $\mathbf{y}_m$ along with a model of the system to determine an estimate of the state of the actual system as follows:

$$\hat{\mathbf{x}}(k) = \hat{\mathbf{x}}^*(k) + \mathbf{L}(\mathbf{y}_m(k) - \mathbf{C}\hat{\mathbf{x}}^*(k)) \tag{2.54}$$

$$\hat{\mathbf{x}}^*(k+1) = \mathbf{A}\hat{\mathbf{x}}(k) + \mathbf{B}\mathbf{u}(k) \tag{2.55}$$

For an LTI system $\hat{\mathbf{x}}$ denotes the estimated state and $\mathbf{y}_m$ denotes the measured output of the system. The Kalman filter uses co-variance information regarding uncertainty in the measurement $\mathbf{y}_m$ and the process to calculate the observer gain $\mathbf{L}$ which yields the best statistical estimate. It is assumed that the plant and measurement noise is Gaussian and effects the process as follows:

$$\mathbf{x}(k+1) = \mathbf{A}\mathbf{x}(k) + \mathbf{B}\mathbf{u}(k) + \mathbf{E}\mathbf{w}(k) \tag{2.56}$$

$$\mathbf{y}_m(k) = \mathbf{C}\mathbf{x}(k) + \mathbf{D}\mathbf{u}(k) + \mathbf{n}(k) \tag{2.57}$$

where $\mathbf{E}$ is a parameter of the process and $\mathbf{w}$ and $\mathbf{n}$ are the process and measurement noise which have covariance matrices $\mathbf{Q}_w$ and $\mathbf{R}_n$ respectively. The observer gain $\mathbf{L}$ is calculated as:

$$\mathbf{L} = \mathbf{P}(k)\mathbf{C}^T(\mathbf{C}\mathbf{P}(k)\mathbf{C}^T + \mathbf{R}_n)^{-1} \tag{2.58}$$

where

$$\mathbf{P}(k+1) = \mathbf{A}\mathbf{P}_f\mathbf{A}^T + \mathbf{G}\mathbf{Q}_w\mathbf{E}^T \tag{2.59}$$

$$\mathbf{P}_f = \mathbf{P}(k) - \mathbf{P}(k)\mathbf{C}^T(\mathbf{C}\mathbf{P}(k)\mathbf{C} + \mathbf{R}_n)^{-1}\mathbf{C}\mathbf{P}(k) \tag{2.60}$$

For nonlinear models, the state estimation becomes more complicated as nonlinear observers such as the Extended Kalman filters or Particle filters have to be used [38], [40].

It should be noted though that an equivalent concept to state estimation does not exist in other formulations of the MPC problem which do not use state-space models, such as Dynamic Matrix Control or Generalised Predictive Control, however they still make use of the measured output $\mathbf{y}_m$ [36]. The measured output is used differently in these formulations and forms part of a type of feedback discussed next.

2.3.2.2 Output feedback and off-set free MPC

In the state-space formulation as described above, if there is any mismatch between the plant and the model, or there are any unmeasured disturbances which effect the plant, the MPC controller will not be able to maintain the output at the reference value $\mathbf{y}_{ref}$ regardless of whether full state feedback is available or an observer is used to estimate the state. There are however a number of ways to overcome this.

A common approach for LTI systems is to augment the state-space model with the disturbance parameters **w** and **n** which can then be estimated by an observer. This method assumes a disturbance model of the form:

$$\mathbf{w}(k+1) = \mathbf{A}_w\mathbf{w}(k) \tag{2.61}$$

$$\mathbf{d}(k) = \mathbf{E}\mathbf{w}(k) \tag{2.62}$$

$$\mathbf{n}(k+1) = \mathbf{A}_n\mathbf{n}(k) \tag{2.63}$$

where **d** is the disturbance term affecting the system state dynamics, which is the third term in (2.56), while **n** directly affect the output. The system can then be augmented as follows:

$$\begin{bmatrix}\mathbf{x}(k+1)\\ \mathbf{w}(k+1)\\ \mathbf{n}(k+1)\end{bmatrix} = \begin{bmatrix}\mathbf{A} & \mathbf{E} & \mathbf{0}\\ \mathbf{0} & \mathbf{A}_w & \mathbf{0}\\ \mathbf{0} & \mathbf{0} & \mathbf{A}_n\end{bmatrix}\begin{bmatrix}\mathbf{x}(k)\\ \mathbf{w}(k)\\ \mathbf{n}(k)\end{bmatrix} + \begin{bmatrix}\mathbf{B}\\ \mathbf{0}\\ \mathbf{0}\end{bmatrix}\mathbf{u}(k) \tag{2.64}$$

$$\mathbf{y}(k) = \begin{bmatrix}\mathbf{C} & \mathbf{0} & \mathbf{I}\end{bmatrix}\begin{bmatrix}\mathbf{x}(k)\\ \mathbf{w}(k)\\ \mathbf{n}(k)\end{bmatrix} + \mathbf{D}\mathbf{u}(k) \tag{2.65}$$

An observer can then be used to estimate the states **x** and disturbances **w** and **n**. These disturbance estimates are then passed to the MPC controller where they are incorporated in the predictions done in the optimisation process. These disturbance estimates will enable the controller to achieve zero offset from the reference signal. This approach is well documented from an MPC perspective in [38] and in conjunction with state feedback control in [20] where it is shown that this approach amounts to integral action in the controller. This approach is used in software packages such as the MATLAB MPC Control Toolbox, where the default setting assumes only the disturbance **n** in (2.57) which effects only the process output.

In the formulations used in many industrial type MPC controllers, a simplified version of output

feedback is used which is equivalent to the previously described method with only integrated white noise on the output assumed, i.e. with $\mathbf{E} = 0$ and $\mathbf{A}_n = 1$ [36]. This effectively becomes the equivalent of passing the difference between the measured and predicted outputs at the given sampling instant to the MPC controller, which in turn adds this estimated disturbance to the output of the predictions in the optimisation process. This method can be applied to linear and nonlinear models alike. This disturbance is formulated as:

$$\hat{\mathbf{d}}(k) = \mathbf{y}_m(k) - \hat{\mathbf{y}}(k|k) \tag{2.66}$$

where $\hat{\mathbf{y}}(k|k)$ is the predicted value of the output at the present time step. The performance index in (2.51) then becomes:

$$\begin{aligned} V(\mathbf{u},\mathbf{x},\boldsymbol{\delta}) = &\sum_{j=1}^{N_p} (\mathbf{y}_{ref}(k+j|k) - (\hat{\mathbf{y}}(k+j|k) + \hat{\mathbf{d}}))^T \mathbf{Q} (\mathbf{y}_{ref}(k+j|k) - (\hat{\mathbf{y}}(k+j|k) + \hat{\mathbf{d}})) \\ &+ \sum_{i=1}^{N_c} \Delta\mathbf{u}(i+k|k)^T \mathbf{R} \Delta\mathbf{u}(i+k|k) + \boldsymbol{\delta}(k)^T \boldsymbol{\Psi} \boldsymbol{\delta}(k) \end{aligned} \tag{2.67}$$

This method will yield zero offset for any plant model mismatch or unmeasured disturbance which always occur in practice, provided that the constraints on the inputs are not reached. This method is widely employed in industrial MPC control techniques such as Dynamic Matrix Control [36], [41]. It should be noted that the simplicity of this method does not require any state estimation techniques, as the initial state passed to the MPC algorithm is that predicted by the plant model as is the case in other MPC formulations such as Dynamic Matrix Control. Fig. 2.7 shows the block diagram of this type of MPC structure with output feedback.

2.3.2.3 Linear Quadratic Optimal Control

Optimal control is a precursor to MPC which minimises some performance index over either a finite or infinite horizon subject to the dynamics of the system as well as input and state constraints [42]. The theory has been well developed for the case where the performance index is quadratic, the plant is linear and there are no constraints on the inputs or the states. Hence the term Linear Quadratic Optimal control. For the case where the output is to track some reference, the Linear Quadratic Tracking problem is formulated as:

$$\min_{\mathbf{u}} \quad J(\mathbf{u}) = \frac{1}{2} \sum_{k=k_0}^{\infty} [(\mathbf{r}(k) - \mathbf{y}(k))^T \mathbf{Q} (\mathbf{r}(k) - \mathbf{y}(k)) + \mathbf{u}(k)^T \mathbf{R} \mathbf{u}(k)] \tag{2.68}$$

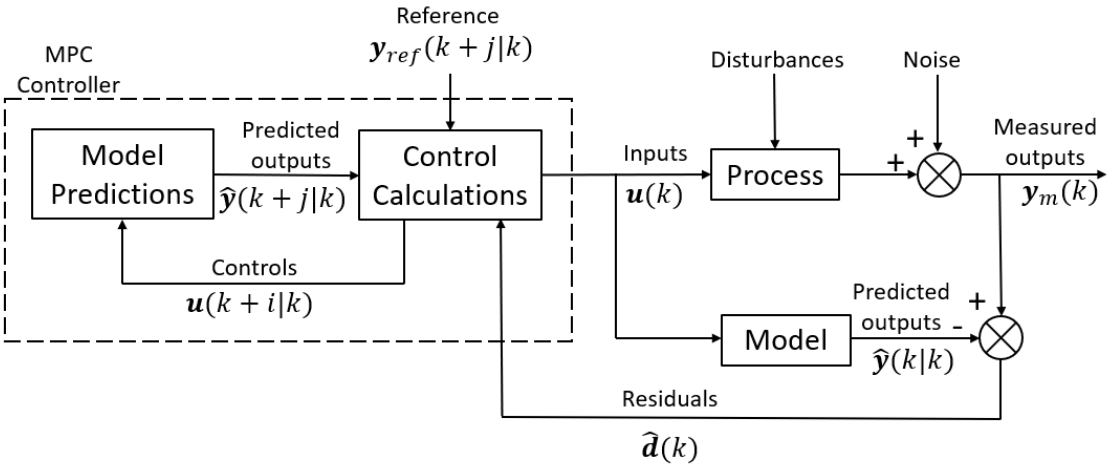

Figure 2.7. MPC with output feedback block-diagram.

subject to:

$$\begin{aligned} \mathbf{x}(k+1) &= \mathbf{A}\mathbf{x}(k) + \mathbf{B}\mathbf{u}(k) \\ \mathbf{y}(k) &= \mathbf{C}\mathbf{x}(k) \end{aligned} \tag{2.69}$$

for the discrete time case where $\mathbf{Q}$ and $\mathbf{R}$ are positive semi-definite and positive definite weighting matrices respectively. A linear feedback control law can be found for the LQT problem using Pontryagin's minimum principle which is of the form:

$$\mathbf{u}(k) = -\mathbf{L}\mathbf{x}(k) + \mathbf{L}_g\mathbf{g}_c\mathbf{r}(k) \tag{2.70}$$

where

$$\mathbf{L} = [\mathbf{R} + \mathbf{B}'\mathbf{P}\mathbf{B}]^{-1}\mathbf{B}'\mathbf{P}\mathbf{A} \tag{2.71}$$

$$\mathbf{L}_g = [\mathbf{R} + \mathbf{B}'\mathbf{P}\mathbf{B}]^{-1}\mathbf{B}' \tag{2.72}$$

$$\mathbf{g}_c = [\mathbf{I} - [\mathbf{A}'[\mathbf{I} - [\mathbf{P}^{-1} + \mathbf{E}]^{-1}\mathbf{E}]]^{-1}\mathbf{Q} \tag{2.73}$$

and $\mathbf{P}$ is the solution of the algebraic Riccati equation:

$$\mathbf{P} = \mathbf{A}'\mathbf{P}[\mathbf{I} + \mathbf{B}\mathbf{R}^{-1}\mathbf{B}'\mathbf{P}]^{-1}\mathbf{A} + \mathbf{Q} \tag{2.74}$$

Thus the optimal control law has two terms, one being a state feedback component and the other a feed-forward term dependant on the value of the reference signal $\mathbf{r}$.

Typically this type of controller is combined with a state-estimator to provide an estimate for the state feedback part of the controller as full state measurement is typically not available. In the case where a Kalman filter is used, the solution is called Linear Quadratic Gaussian control [38].

2.3.2.4 Predictions for nonlinear models

In the case where a linear model is used for predictions (linear MPC), it is possible to calculate the precise solution of the system by converting the continuous time system to a discrete time system according to (2.30) - (2.32). In the case where a nonlinear model is used (nonlinear MPC) a solution needs to be approximated using some sort of numerical integration [38]. For the purposes of this work, wherever the solution of a nonlinear system needs to be approximated, a fourth order Runge-Kutta will be used. This is described as:

$$\mathbf{x}(k+h) \approx \mathbf{x}(k) + \frac{1}{6}(\mathbf{k}_1 + 2\mathbf{k}_2 + 2\mathbf{k}_3 + \mathbf{k}_4) \tag{2.75}$$

where

$$\mathbf{k}_1 = \mathbf{f}(\mathbf{x}(k), \mathbf{u}(k)) \tag{2.76}$$

$$\mathbf{k}_2 = \mathbf{f}(\mathbf{x}(k) + h\frac{\mathbf{k}_1}{2}, \mathbf{u}(k)) \tag{2.77}$$

$$\mathbf{k}_3 = \mathbf{f}(\mathbf{x}(k) + h\frac{\mathbf{k}_2}{2}, \mathbf{u}(k)) \tag{2.78}$$

$$\mathbf{k}_4 = \mathbf{f}(\mathbf{x}(k) + h\mathbf{k}_3, \mathbf{u}(k)) \tag{2.79}$$

where h is the sampling interval.

2.4 CONCLUSION

An overview of trends in migrating the automation hierarchy to the cloud has been presented. Existing research has focused on practical issues such as communication infrastructure and sampling rates as well as the cost and redundancy benefits of having controllers in the cloud. The idea of a platform which can facilitate competition between controllers does not seem to have been addressed.

Due to the fact that the competing controllers are assumed to be at remote locations, delays in the communication between controllers and the plant is expected, in addition to computational time required to evaluate each performance index. These factors thus put a limit on the achievable sampling rate. Thus if the process dynamics are slow enough (ω small enough), the sampling period can be made large enough such that time delays in communication networks can be ignored. This does not pose limitations on the scope of applicable control problems, as large sampling times are common in

the process control industry, with the same argument applicable to MPC due to the time required to solve the optimisation problem at each time step [20], [38].

Relevant control philosophies including conventional feedback control (PI and $\mathcal{H}_\infty$) and MPC have been discussed. It is evident that MPC is more complex from a practical implementation point of view, but does present advantages for multi-variable systems in that the problem formulation inherently takes care of process interactions and constraints without explicit information required in the synthesis of the controller.

CHAPTER 3 PLATFORM FORMULATION AND DEFINITION

3.1 CHAPTER OVERVIEW

This Chapter presents an access economy platform which can potentially facilitate the procurement of advanced control solutions in the industrial automation and control industry. This philosophy would allow for a number of vendors to develop a control strategy for a particular plant with the best performing controller, as determined by the selector, being chosen for control. An analysis is given of what may be required to make such a platform function in practice with a general requirements being discussed in Section 3.2, system identification and modelling in Section 3.3, controller performance measurement in Section 3.4, bump-less transfer in Section 3.5, constraint handling in Section 3.6, the necessity of a fallback strategy in Section 3.7, system stability in Section 3.8, plant security in Section 3.9 and controller remuneration in Section 3.10. Section 3.11 presents a loop diagram of the proposed philosophy with all practical considerations taken into account.

3.2 PLATFORM FORMULATION

It is proposed that a platform could exist where a 'selector' would evaluate any number of different controllers over a period of time, and at the end of each period, select and thus implement the controller which has been determined optimal based on some type of performance measure. Fig. 3.1 illustrates the philosophy. There are a number of issues that will need to be addressed and clarified in order for such a platform to be practically viable. These include:

1. In order to evaluate the performance of the competing controllers, it would be necessary to simulate the control actions provided by each controller on a model of the plant over a period of

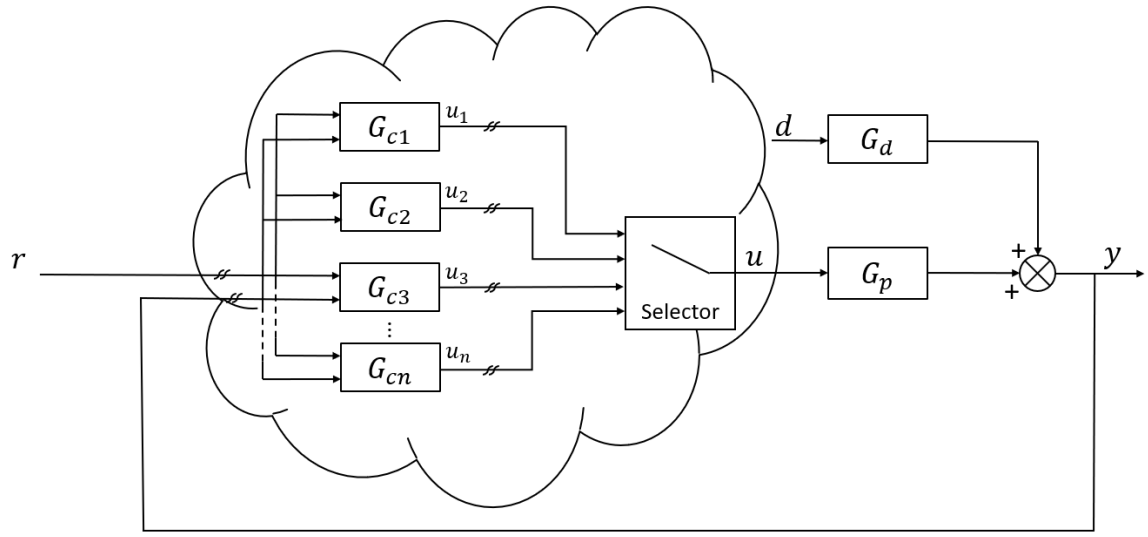

Figure 3.1. Competing controllers.

time.

2. A process model would thus be needed by the selector for the evaluation of each controller, as well as by each competing vendor for controller development.
3. A bump-less transfer mechanism may need to be employed when switching takes place.
4. Constraints on the MVs and CVs will need to be communicated to the competing controllers, as well as the selector.
5. It would be necessary to have a local controller to serve as a fall-back strategy in the event of a technical fault.
6. Overall stability of the system would need to be addressed.
7. Cyber security as well as issues relating to possible sabotage attempts would need to be addressed.

These issues are discussed in more detail in the following sections.

3.3 SYSTEM IDENTIFICATION AND MODELLING

System identification and modelling typically makes up a large portion of the development of a control solution. This would typically include modelling the system dynamics as well as determining all the

relevant plant specific information such as actuator and sensor capabilities, constraints and models [35].

The typical modelling procedure would involve deriving transfer function or ARX models from step test data [26]. It is possible that each competing vendor could develop their own model from input-output data. The selector will use the most accurate model available to evaluate the performance of the competing controllers. This would thus involve supplying each controller with the output **y** of the plant as well as the control actions **u** implemented on the plant. Although this may be the most viable approach in practice, it would however be ideal that a validated first-principles state-space model be made available to the selector and all competing controllers.

All relevant sensor and actuator information would need to be made available to the controllers, which would include all constraints on the the MVs and CVs such as the upper and lower saturation levels as well as any rate of change limits. It would also be necessary for all constraints on the MVs to be made available to the selector in order to ensure that no attempt is made to implement any unachievable control actions on the plant.

It is often the case in practice that much of this information, particularly the measured output data, would be considered as sensitive and confidential information. In this case all values made available by the plant (including measurement data, constraints and plant model) could simply be scaled. It is also possible that potential vendors be vetted on non-critical or non IP sensitive processes (or even on a simulation if that is preferable). Although this would still render the proposed platform feasible, the concept behind an access economy involves a much greater level of openness and access to information than more traditional economic models [2]. The proposed platform would thus have a greater potential for improving system performance if as much information as possible about the plant was shared, allowing for as much expertise as possible to be attracted to the proposition of supplying a solution.

3.4 CONTROLLER PERFORMANCE MEASUREMENT

In order to evaluate the performance of the competing controllers, it would be necessary to simulate each controller in closed-loop on a model of the plant. In terms of reference following, this process

is straight forward so long as the desired reference is supplied to the selector. Determining the disturbance rejection capabilities of the competing controllers will however require knowledge of the actual disturbances $\mathbf{d}$ which affect the process through $\mathbf{G}_d$ as shown in Fig. 3.1 (a plant output disturbance is assumed). If the disturbances can be measured, they could readily be supplied to the selector, whereas if they are not, an estimate thereof would need to be determined by the selector through the use of an observer.

Some type of performance measure will be needed to determine the best controller based on the simulated outputs and generated control moves of each controller. One such performance index could be the sum of the squares of the error (SSE) in the simulated outputs for each evaluation horizon:

$$J_i = \sum_{j=k-N_e+1}^{k} (\mathbf{r}(j) - \mathbf{y}_i(j))^T \mathbf{W}_e (\mathbf{r}(j) - \mathbf{y}_i(j)) \tag{3.1}$$

where $\mathbf{y}_i$ is the simulated output of the i^{th} controller, $\mathbf{W}_e$ is a positive semi-definite weighting matrix which is used to place more or less emphasis on the different outputs and N_e is an evaluation horizon or time period over which the controller is simulated.

The performance measure in (3.1) would typically favour a more aggressive controller due to the exclusive penalisation of the deviation of the simulated outputs $\mathbf{y}_i$ from the reference $\mathbf{r}$. A slightly modified version could be represented as:

$$\begin{aligned} J_i = \sum_{j=k-N_e+1}^{k} & (\mathbf{r}(j) - \mathbf{y}_i(j))^T \mathbf{W}_e (\mathbf{r}(j) - \mathbf{y}_i(j)) \\ & + \Delta\mathbf{u}_i^T(j) \mathbf{W}_u \Delta\mathbf{u}_i(j) \end{aligned} \tag{3.2}$$

where $\mathbf{u}_i$ is the control move generated by the i^{th} controller, $\Delta\mathbf{u}_i(j) = \mathbf{u}_i(j) - \mathbf{u}_i(j-1)$ and $\mathbf{W}_u$ is a positive semi-definite weighting matrix used to place more or less emphasis on the utilisation of the respective control actions. This measure would also penalise excessive control action and therefore not favour a more aggressive controller.

The performance measure and relevant weighting factors such as $\mathbf{W}_e$ and $\mathbf{W}_u$ may or may not be known to the controllers, with this decision possibly lying in the hands of the plant or the selector. Again, from an access economy point of view, the more knowledge the controllers have regarding the

desired performance specifications of the plant, the better they would be able to tailor their proposed solutions to these requirements.

The proposed manner of switching is for the selector to simulate the controllers on the plant model, in parallel with the running plant using the actual reference signal **r** and disturbance **d** (measured or estimated) over a particular evaluation horizon N_e. At the end of each evaluation horizon, a performance measure such as (3.1) or (3.2) would be calculated based on the simulated outputs and generated control moves of each controller. The controller which achieves the best value for the performance index will then automatically be selected and control of the actual plant switched over to this controller once it has been initialised. The performance indices for each controller would then be set to zero and the process repeated.

It is is worth noting that other manners of switching are possible with the proposed platform philosophy. For example, evaluation does not have to be done in discreet blocks with the performance index being reset at the end of each one, but in a receding horizon approach. The decision to switch could also lie with the plant, with the controllers being simulated by the selector in advance on predetermined reference and disturbance signals **r** and **d** which are representative of the expected future conditions of the system. This would allow for the best controller to be selected in advance in a predictive manner.

The main goal of the platform is to facilitate the procurement of an advanced control solution in a manner similar to that of how Uber facilitates the procurement of transportation services. Thus it is the goal of the platform to provide the plant with the best available control option given the operating conditions of the plant and the specified performance requirements.

3.5 BUMP-LESS TRANSFER

In the event that one of the competing controllers is determined to be optimal and is to be selected, it will likely be the case that the control moves generated by this controller in simulation with the plant model are not equal to the current control moves implemented on the actual plant, but may in fact differ substantially. This will require a bump-less transfer mechanism to be employed by each controller in the event that it is awarded control of the actual plant.

In order to achieve this, knowledge of the present control moves implemented on the plant at the time when switching is to take place will be required by the new controller. This responsibility would inherently fall with the individual controllers and would be achieved in different manners depending on the type of controller. For illustrative purposes, two methods are proposed: one for MPC controllers and the other for conventional feedback controllers.

For MPC controllers using the state-space formulation described in Section 2.3.2, bump-less transfer can be achieved by employing two observers for state/disturbance estimation. One would estimate the states and disturbances based on the measurement of the actual plant output and the actual control action implemented on the plant (both pieces of information which are available to the controllers), and a second would provide estimates based on the model it is controlling. When the MPC controller is not selected, the estimate derived from the simulated plant model and control signal are used in the MPC optimisation algorithm. If the MPC controller is selected, the estimate derived from the actual plant output and control signal (which will now become the control signal generated by this controller) is used in the MPC optimisation algorithm and seamless transfer of control takes place.

The conventional feedback controllers would employ a different principle in which the integral term of the controller is back initialised to yield a control action equal to that of the previous control action applied to the plant. Any conventional, linear feedback controller can be discretised and represented in the state state-space form given in (2.32) and (2.33). In order to back initialise the controllers, it follows from (2.32):

$$\mathbf{x}_{ci}(k) = \mathbf{C}_{ci}^{\dagger}(\mathbf{u}(k-1) + \mathbf{D}_{ci}\mathbf{e}(k)) \tag{3.3}$$

where $\mathbf{C}_{ci}^{\dagger}$ is the pseudoinverse of the matrix $\mathbf{C}_{ci}$, $\mathbf{u}(k-1)$ is the previous control action applied to the plant and $\mathbf{e}(k)$ is the actual error based on the measured output of the plant. This method will successfully initialise the controllers to output a control action which is representative of the current state of the plant and prevent the controllers from generating any excessive control action in the event that control is switched over to them.

Since it is the responsibility of the controller to perform this back initialisation, it may be necessary for the selector to ensure that the newly selected controller does not present a control move which deviates significantly from the previous value when switching takes place. If it does happen that the controller fails to back initialise, it would then be necessary for control of the plant to remain with the

previously selected controller or be switched to the local controller (assuming that the initialisation of this controller is guaranteed).

3.6 CONSTRAINT HANDLING

Constraints on the MVs and CVs will need to be communicated to the competing controllers and the selector. This information is required for controller development, and to prevent the implementation of control moves which violate the constraints. Constraint handling is typically incorporated into most MPC formulations as part of the optimisation problem, but there is no explicit constraint handling present in the conventional feedback controller form. This would have to be implemented ad-hoc by each conventional feedback controller by setting an output equal to its given constraint in the event that the output generated by the controller exceeds this constraint. If this is the case, the $\mathbf{\Gamma}_c$ matrix of the controller formulation given in (2.32) is set to zero to disable any integral action and thus prevent any integral windup. Other more sophisticated anti reset windup schemes may also be employed [26].

The selector would also assist in this matter by restricting the plant inputs to their relevant constraints should the active controller attempt to violate them. This would also be true for any rate of change constraints on the MVs. Should this happen, it would be possible to flag a controller and incorporate this information in future switching decisions, and if a controller violated any of the MV constraints during the simulation over an evaluation horizon, it could be automatically excluded from selection at the end of that particular horizon.

3.7 FALLBACK STRATEGY

With the competing controllers possibly all being in a remote location, it would be necessary to have a local controller to serve as a fall-back strategy in the event of a technical fault with a sensor or actuator, a communication fault with the selector or between the selector and active controller, or some undesirable control actions from the active controller. By the very nature of the requirements placed on this controller, it is necessary that it be locally installed at the plant. Controllers $\mathbf{G}_{c1}, \mathbf{G}_{c2} \ldots \mathbf{G}_{cn}$ would typically be Advanced Process Controllers (APCs), and it is assumed that all base layer control would be pre-existing and locally installed.

It is common practice in today's industrial environment for plant personnel to have a generally low skill level, with advanced control solutions being procured from large vendors. This local fall-back controller would thus typically be a rudimentary controller (such as a heuristically tuned PI controller) implemented by plant personnel with inferior performance to an APC. The goal of the platform is to thus facilitate a new method of procuring an APC.

3.8 SWITCHING AND SYSTEM STABILITY

The idea of switching between controllers to achieve better performance has been covered in the field of switched systems [44] - [48]. From the literature, a switched system is defined as:

$$\dot{x} = f_\sigma(x), \quad x \in \Re^n \tag{3.4}$$

where

$$\dot{x} = f_p(x), \quad p \in P \tag{3.5}$$

is a family of individual systems and

$$\sigma : [0,\infty) \to P \tag{3.6}$$

is the switching signal [43]. The predominant philosophies propose switching between controllers in a predetermined way after a certain time has elapsed (time-dependant switching), or based on the discrete values of the states (state-dependant switching) [43]. An aspect of switched systems which has been of predominant interest is the fact that switching signals (σ) may exist which will drive a system unstable, even if the individual systems are independently stable [43] - [48].

A common approach to prove stability of hybrid and switched systems is based on Lyapunov Stability Theory which states that a dynamical system given by:

$$\dot{x} = f(x), \quad x \in \Re^n \tag{3.7}$$

is stable if there exists a positive definite function $V(x)$ such that the time derivative of this function along the solution of the system satisfies:

$$\dot{V} = \frac{\partial V}{\partial x} f(x) \leq 0 \quad \forall x \neq 0 \tag{3.8}$$

[43]. Such a function, if it exists, is called a Lyapunov function of the system. It follows that if there exists a Lyapunov Function which is common to all the individual systems in (3.4), the switched system will be stable for any arbitrary switching signal σ.

In the case where a common Lyapunov function does not exist, and all the individual subsystems are stable, overall stability of the switched system can be guaranteed if switching is limited to take place at intervals which are long enough to allow the transient response of the slowest subsystem to sufficiently dissipate [43], [44]. For the LTI case, the length of time which is sufficient (dwell-time) can be determined from the parameters of the individual subsystems [49].

Work has been done in the field of switched systems which does draw some parallels to the proposed switching philosophy [49] - [51]. This work assumes there is uncertainty in the modelling of the plant, and different controllers are designed for a set of plants which fall into the range of this uncertainty. Predictions are made for each plant model in the set in parallel with the real plant using the same control actions as are implemented on the actual plant. The SSE of the error between the predictions and the actual output is then determined for each model in the set over a certain time horizon. At specified regular intervals, the controller designed for the plant model yielding the smallest SSE is selected. The idea behind this is that the best performance will be achieved when the controller which was designed on the plant model which most accurately represents the actual plant is used.

Fig. 3.2 shows the loop diagram of this philosophy where $O_1 ... O_n$ represent the predictions performed on each model in the set and the performance measure is the SSE of these prediction errors.

Stability proofs have been derived for this switching philosophy based on the dwell-time principle under the assumption that the system is LTI, all individual controllers are stable and the plant parameters remain within their uncertainty regions [50], [51].

The proposed method to facilitate competing controllers is thus different from what has previously been proposed in the switched systems literature in that it makes use of an evaluation horizon to simulate each controller on a plant model and subsequently evaluate the performance of each controller according to some performance index. Thus the value of the switching signal σ in (3.4) is dependent on the discrete integral of a function of the predicted output of the system as well as possibly the

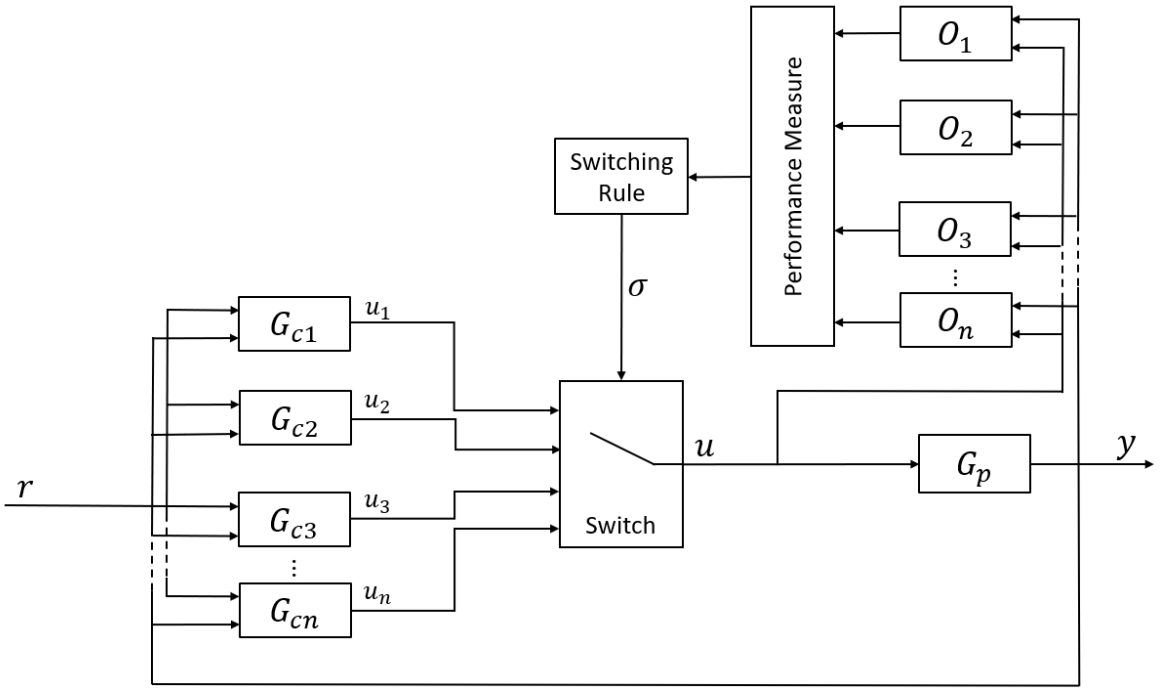

Figure 3.2. Switching controllers (adapted from [51], © 1998 IEEE).

change in the control input presented by each controller at each time step, i.e. the controller yielding the minimum J given in (3.1) or (3.2). This yields a more complex switching signal than those typically considered. Ensuring system stability for the proposed platform would require knowledge of the formulations of each controller, and for this to be done using existing stability analysis results would require all controllers to be conventional linear feedback controllers. It would most likely be the case that the result of such an analysis would require a minimum time between switching, provided that all individual controllers are stable.

For the purposes of the proposed platform it would therefore be required to specify a minimum bandwidth requirement for each competing controller, and switch at intervals which are several orders of magnitude larger than the corresponding period. This would need to be determined and specified by the plant from the process dynamics and input constraints and communicated to the controllers via the selector. It would seem counter intuitive that a very sluggish controller would be determined optimal and thus selected, but the actual transient response dynamics may need to be verified by the selector before selecting the controller.

It is worth noting that switching at intervals longer that the slowest expected closed-loop dynamics

is a sufficient condition for stability (given all individual systems are stable) but not a necessary condition [48]. To guarantee stability otherwise would require knowledge of the individual controller realisations that is not available to the platform, thus switching at longer intervals is necessary to guarantee stability.

3.9 PLANT SECURITY

In the proposed platform philosophy, where potentially any willing party may be awarded control (and hence access to local control loops) of the plant, there would need to be a certain amount of trust in the controllers, or at least some level of accountability. The level of security and trust required by a plant may differ from process to process depending on safety concerns, the impact of mistakes, and IP, among others.

This security and trust could be provided by the platform in a similar manner as to how Uber facilitates trust and accountability between commuters and transport providers. Controllers do need to prove their ability to control the plant by evaluating their performance on a model of the plant, but this may not prevent a malicious agent from being awarded control of the plant and subsequently attempting to sabotage the process if selected. If this is the case, or if a controller exhibits any undesirable behaviour, the controller could be penalised by a rating system similar to how Uber drivers are rated according to the service they offer. Controllers which are frequently selected and never exhibit any undesirable behaviour would subsequently improve their rating. Plants which require a high level of trust could then specify a certain minimum performance rating for controllers allowed to compete to control their process.

Similar to the issue of sabotage is that of cyber security, as it may be possible for malicious agents to hack into the platform in order to gain access to local control loops of the plant. The problem of cycber security is one which is being increasingly dealt with in the realm of IoT, with solutions readily being made available [5], [6]. The issue of cyber security is thus not dealt with further in this work.

3.10 CONTROLLER REMUNERATION

Remuneration would need to be provided to controllers for the service they provide when they are selected to control the plant. This would ideally be dependant on the marginal benefit achieved from using a controller such as when controlling a highly lucrative process or when frequent control moves are required for optimal plant operation. Remuneration could readily be done through the use of blockchain technologies such as a crypto currency or smart contract, both of which are receiving increasing amounts of interest in IoT and access economy applications [3], [5].

3.11 SYSTEM LOOP DIAGRAM

All the aforementioned considerations are incorporated into the schematic in Fig. 3.1 and the result is shown in Fig. 3.3 which shows the measured disturbances **d** and reference **r** supplied to the selector, the feedback channel used to simulate the competing controllers, the implemented control move **u** fed back to the controllers $\mathbf{G}_{c1}$, $\mathbf{G}_{c2}$..., $\mathbf{G}_{cn}$, as well as the local fall-back controller $\mathbf{G}_{c\_local}$.

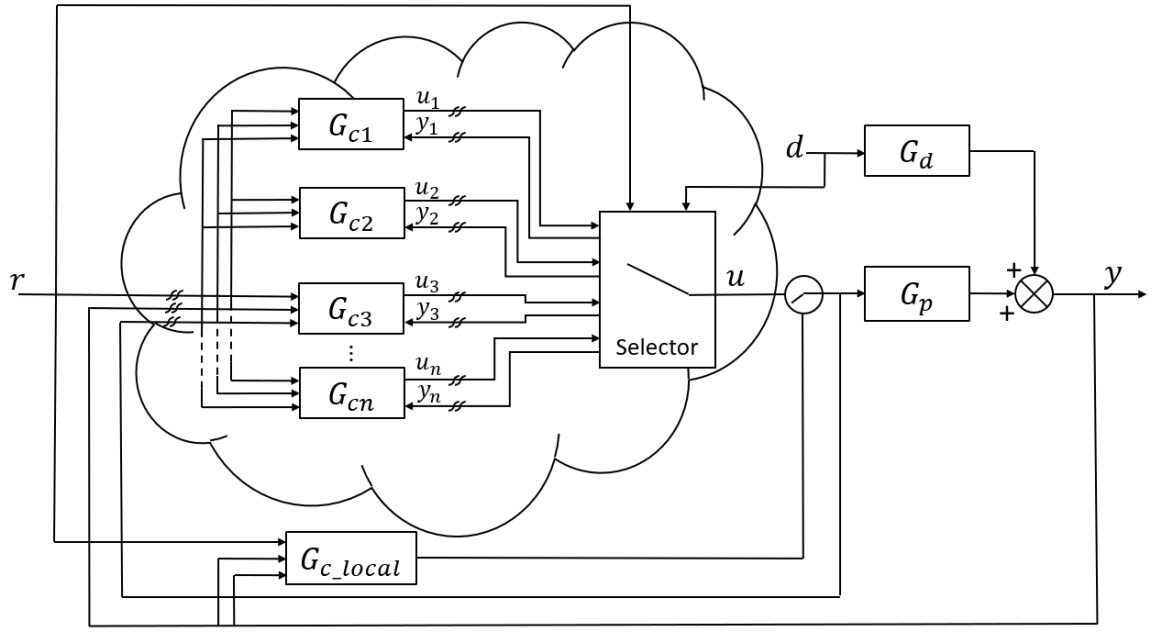

Figure 3.3. Competing controllers with local fall-back controller.

3.12 CONCLUSION

It is concluded that:

- The selector will need to simulate each controller on the plant model to evaluate its performance. This means the reference signal as well as either measured or estimated disturbances will need to be made available to the selector.
- A plant model and relevant operating constraints would need to be supplied to each controller for development purposes, as well as to the selector for controller evaluation and in order to ensure that control signals which violate the plant constraints are not sent to the plant. This may possibly be done by each controller from input-output data, but it would be ideal if a validated first-principles state-space model can be made available to the selector and all competing controllers.
- Controllers need to initialise themselves in the event they are selected, thus the current control move implemented on the plant needs to be supplied to the controllers.
- Constraint handling is the responsibility of the individual controllers, but the selector will also implement these constraints for purposes of redundancy and may penalise a controller which attempts to violate these constraints.
- A local fall back controller is needed in the event of any technical fault between the selected controller and the selector or the selector and the plant.
- Switching intervals need to be longer than the slowest expected closed-loop system dynamics, which thus translates to a minimum system bandwidth which would need to be made known to the controllers.
- The platform could rank controllers according to their performance and could possibly facilitate remuneration through the use of blockchain technology.

CHAPTER 4 SURGE TANK CASE STUDY: MODEL DEVELOPMENT AND ANALYSIS

4.1 CHAPTER OVERVIEW

This Chapter presents a detailed model of the surge tank process at Sibanye-Stillwater's Platinum bulk tailings treatment (BTT) plant in Section 4.2. The nonlinear model is linearised and an input-output controllability analysis is done in Section 4.3 in order to ascertain if it is possible to keep the plant outputs within specified bounds from their references using the available actuator authority in the presence of disturbances. This includes determination and analyses of the modal controllability and observability, multivariable poles and zeros, relative gain array, scaled plant and functional controllability.

4.2 PROCESS MODEL

Fig. 4.1 shows a schematic of the plant which is a surge tank with an input tailings feed of variable density ρ_i and flow rate q_i, a water supply to the tank with a flow rate q_w and a constant flow rate out of the tank q_o. The control objective is to keep the output density ρ constant, given the variable density of the input feed ρ_i by adjusting the input feed rate and water flow rates q_i and q_w while preventing the tank from overflowing or running dry [52].

The mass balance is given as:

$$\frac{d(\rho v)}{dt} = \rho_i q_i + \rho_w q_w - \rho q_0 \tag{4.1}$$

where ρ_i is the density of feed from tailings in $^t/_{m^3}$, q_i is the flow rate of feed from tailings in $^{m^3}/_h$, ρ_w

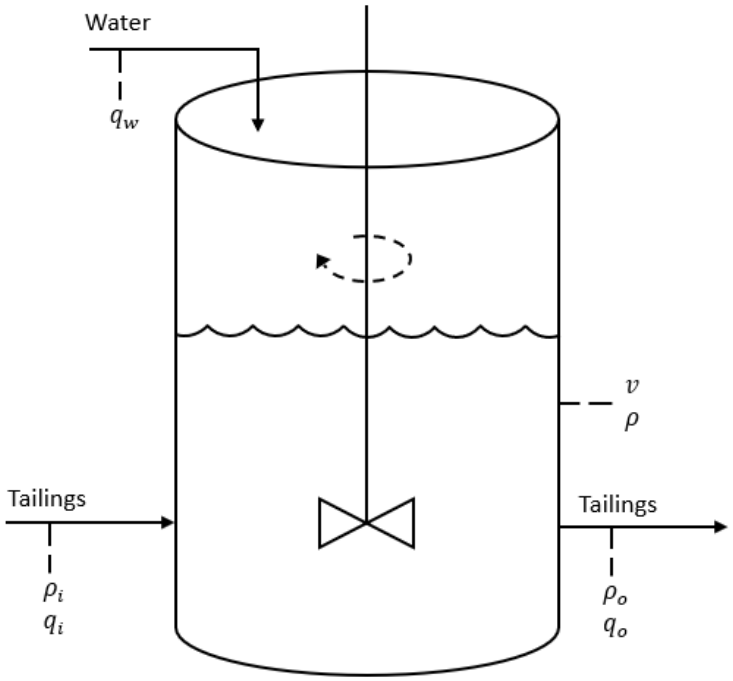

Figure 4.1. Surge tank [52].

is the density of water with fixed value of 1 $^t/_{m^3}$, q_w is the flow rate of water in $^t/_{m^3}$, ρ is the density of product in $^t/_{m^3}$, q_o is the flow rate of slurry out of tank to Chrome plant in $^{m^3}/_h$ and v is the volume of fluid in tank in m^3.

It is assumed that perfect mixing takes place and that the density of the product flowing out of the tank ρ_o is consistent in density with the product in the tank ρ. The volume balance gives:

$$\frac{dv}{dt} = q_i + q_w - q_0 \tag{4.2}$$

Differentiating the left hand side of (4.1):

$$v\frac{d\rho}{dt} + \rho\frac{dv}{dt} = \rho_i q_i + q_w - \rho q_0 \tag{4.3}$$

Substitution of (4.2) into (4.3) and simplifying gives:

$$v\frac{d\rho}{dt} = \rho_i q_i + q_w - \rho(q_i + q_w) \tag{4.4}$$

Equations (4.2) and (4.5) combined give the nonlinear state-space model:

$$\begin{bmatrix} \dot{v} \\ \dot{\rho} \end{bmatrix} = \begin{bmatrix} q_i + q_w - q_0 \\ \frac{1}{v}(\rho_i q_i + q_w - \rho(q_i + q_w)) \end{bmatrix} \tag{4.5}$$

which is of the form:

$$\dot{\mathbf{x}} = \mathbf{f}(\mathbf{x}, \mathbf{u}, \mathbf{d}) \tag{4.6}$$

In this case the states $\mathbf{x}$ are ρ and v, the inputs $\mathbf{u}$ are q_i, q_w and q_o and the disturbance $\mathbf{d}$ is ρ_i. A system of the form in (4.6) is linearised around an equilibrium as follows:

$$\delta\dot{\mathbf{x}} = \left(\frac{\partial \mathbf{f}}{\partial \mathbf{x}}\right)^* \delta\mathbf{x} + \left(\frac{\partial \mathbf{f}}{\partial \mathbf{u}}\right)^* \delta\mathbf{u} + \left(\frac{\partial \mathbf{f}}{\partial \mathbf{d}}\right)^* \delta\mathbf{d} \tag{4.7}$$

where $\delta\mathbf{x}$, $\delta\mathbf{u}$ and $\delta\mathbf{d}$ are deviation variables around the equilibrium values $\mathbf{x}^*$, $\mathbf{u}^*$ and $\mathbf{d}^*$ which satisfy:

$$\mathbf{f}(\mathbf{x}^*, \mathbf{u}^*, \mathbf{d}^*) = 0 \tag{4.8}$$

Applying (4.7) to (4.5) gives:

$$\begin{aligned} \begin{bmatrix} \delta\dot{v} \\ \delta\dot{\rho} \end{bmatrix} = & \begin{bmatrix} 0 & 0 \\ -\frac{1}{v^2}(\rho_i q_i + q_w - \rho(q_i + q_w)) & -\frac{1}{v}(q_i + q_w) \end{bmatrix}^* \begin{bmatrix} \delta v \\ \delta\rho \end{bmatrix} \\ & + \begin{bmatrix} 1 & 1 & -1 \\ \frac{1}{v}(\rho_i - \rho) & \frac{1}{v}(1-\rho) & 0 \end{bmatrix}^* \begin{bmatrix} \delta q_i \\ \delta q_w \\ \delta q_0 \end{bmatrix} + \begin{bmatrix} 0 \\ \frac{q_i}{v} \end{bmatrix}^* \delta p_i \end{aligned} \tag{4.9}$$

The operating conditions are as follows:

$$\rho_i^* = 1.5 \ {}^{t}/_{m^3}$$

$$q_i^* = 600 \ {}^{m^3}/_{h}$$

$$\rho_w^* = 1 \ {}^{t}/_{m^3}$$

$$q_w^* = 150 \ {}^{m^3}/_{h}$$

$$\rho^* = 1.4 \ {}^{t}/_{m^3}$$

$$q_0^* = 750 \ {}^{m^3}/_{h}$$

$$v^* = 10 \ m^3$$

Substitution of these values into (4.5) confirms that these conditions constitute an equilibrium and

(4.8) is satisfied. Substitution of these values into (4.9) yields the following LTI state-space model:

$$\begin{bmatrix}\dot{x}_1\\ \dot{x}_2\end{bmatrix} = \begin{bmatrix}0 & 0\\ 0 & -75\end{bmatrix}\begin{bmatrix}x_1\\ x_2\end{bmatrix} + \begin{bmatrix}1 & 1 & -1\\ 0.01 & -0.04 & 0\end{bmatrix}\begin{bmatrix}u_1\\ u_2\\ u_3\end{bmatrix} + \begin{bmatrix}0\\ 60\end{bmatrix} d_1 \tag{4.10}$$

It is assumed that the flow rate of water out of the tank q_o remains fixed at the nominal value of 750 m^3/h. In this case (4.10) simplifies to:

$$\begin{bmatrix}\dot{x}_1\\ \dot{x}_2\end{bmatrix} = \begin{bmatrix}0 & 0\\ 0 & -75\end{bmatrix}\begin{bmatrix}x_1\\ x_2\end{bmatrix} + \begin{bmatrix}1 & 1\\ 0.01 & -0.04\end{bmatrix}\begin{bmatrix}u_1\\ u_2\end{bmatrix} + \begin{bmatrix}0\\ 60\end{bmatrix} d_1 \tag{4.11}$$

as the deviation variable δq_0 or u_3 is fixed at zero. Converting (4.11) to a transfer function matrix model yields:

$$\begin{bmatrix}X_1\\ X_2\end{bmatrix} = \begin{bmatrix}\frac{1}{s} & \frac{1}{s}\\ \frac{0.01}{s+75} & \frac{-0.04}{s+75}\end{bmatrix}\begin{bmatrix}U_1\\ U_2\end{bmatrix} + \begin{bmatrix}0\\ \frac{60}{s+75}\end{bmatrix} D_1 \tag{4.12}$$

Consider a change in the disturbance variable ρ_i. From (4.5) it can be seen that if all other parameters are held constant, the model of input density ρ_i to output density ρ is linear and is identical to the linearised model in (4.9). This is confirmed by a step change in the input feed disturbance shown in Fig. 4.2. The nonlinearities proceed from the multiplication of ρ with q_i and q_w. This is seen in Figs. 4.3 and 4.4 for a step change of 100 $^{m^3}/_h$ in q_i and q_w respectively.

4.3 INPUT-OUTPUT CONTROLLABILITY

In order to gain insight into the plant behaviour and achievable control, an input-output controllability analysis as described in [27] is conducted. Input-output controllability is defined as the ability to keep the plant outputs within specified bounds from their references in spite of unknown but bounded variations, such as disturbances and plant uncertainty, using the available plant inputs and measurements [27]. This analysis comprises the following points:

1. Perform a modal/state controllability and observability analysis.
2. Determine the poles and multi-variable zeros of the plant.

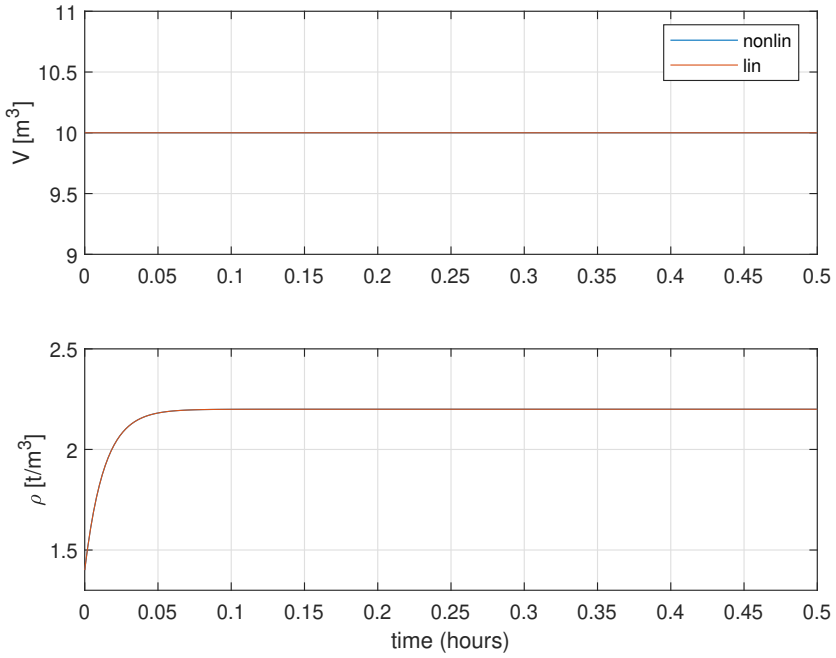

Figure 4.2. Response of linear and nonlinear models to a step of unit magnitude in ρ_i.

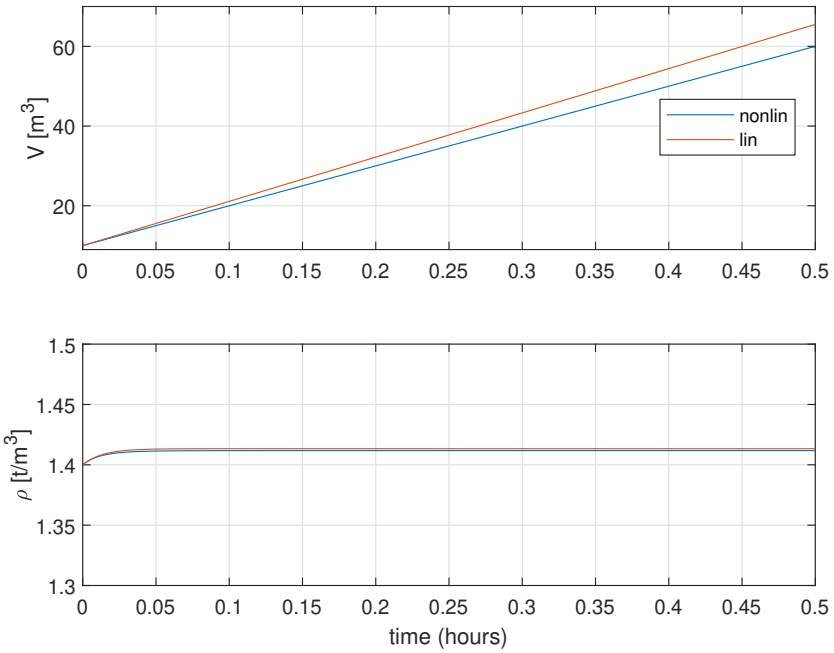

Figure 4.3. Response of linear and nonlinear models to a step of 100 in the magnitude of q_i.

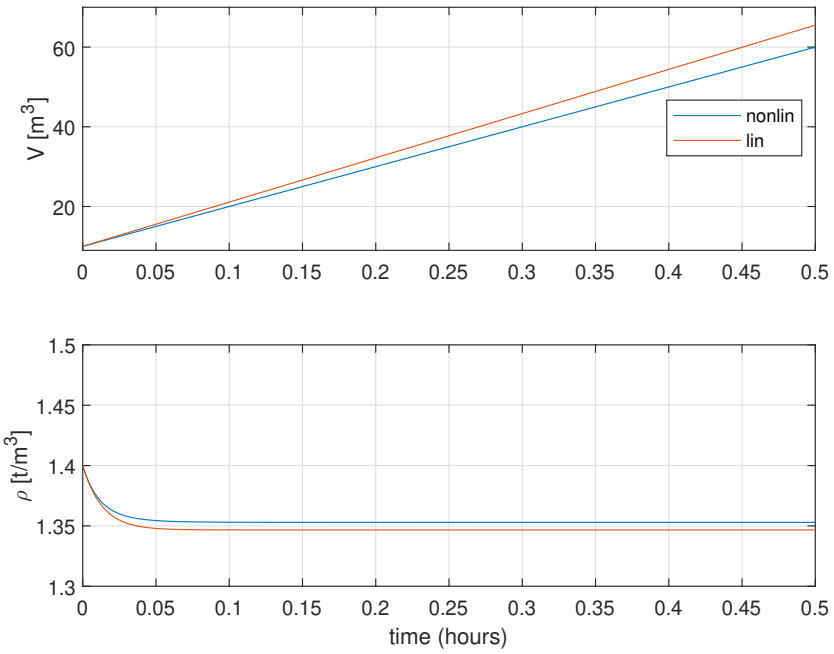

Figure 4.4. Response of linear and nonlinear models to a step of 100 in the magnitude of q_w.

3. Determine the relative gain array of the plant.
4. Scale the plant such that all (scaled) inputs, outputs and disturbances are confined to values between zero and one.
5. Plot the singular values of the scaled plant model $\tilde{\mathbf{G}}_p$ as a function of frequency. If the minimum singular value is less than one at certain frequencies it means that a change in the plant output of one in magnitude cannot be made with a unit change in the magnitude of the plant input at those frequencies. It is thus desired that the minimum singular value of the scaled plant model $\tilde{\mathbf{G}}_p$ is large at frequencies where control is needed.
6. Plot the singular values of the disturbance model $\tilde{\mathbf{G}}_d$ as a function of frequency. Large values indicate the need for control action to reject the disturbances.
7. Determine the elements of the matrix product $\tilde{\mathbf{G}}_p^{-1}\tilde{\mathbf{G}}_d$. If all elements are less than one over all frequencies then perfect disturbance rejection is possible.

4.3.1 Modal/state controllability and observability analysis

A dynamic system given by

$$\dot{\mathbf{x}} = \mathbf{A}\mathbf{x} + \mathbf{B}\mathbf{u} \tag{4.13}$$

$$\mathbf{y} = \mathbf{C}\mathbf{x} + \mathbf{D}\mathbf{u} \tag{4.14}$$

is said to controllable if for any initial state $\mathbf{x}_0$ and final state $\mathbf{x}_f$ there exists a control signal $\mathbf{u}$ which can bring the state from $\mathbf{x}_0$ to $\mathbf{x}_f$ in finite time. Similarly the system is said to be observable if for any time $t_1 > 0$, the initial state $\mathbf{x}_0$ can be determined from the history of the input $\mathbf{u}$ and the output $\mathbf{y}$ in the interval $[0, t_1]$ [20], [27].

It is known that if a dynamic system is controllable, the following matrix (termed the controllability matrix) given by:

$$C = \begin{bmatrix} \mathbf{B} & \mathbf{AB} & \mathbf{A}^2\mathbf{B} & \cdots & \mathbf{A}^{n-1}\mathbf{B} \end{bmatrix} \tag{4.15}$$

has a rank of n, where n is the number of states in the system which is equivalent to the dimensions of $\mathbf{A}$. This means that C has n linearly independent rows and columns. Similarly, if a dynamic system is observable, the following matrix (called the observability matrix) given by:

$$O = \begin{bmatrix} \mathbf{C} \\ \mathbf{CA} \\ \mathbf{CA}^2 \\ \vdots \\ \mathbf{CA}^{n-1} \end{bmatrix} \tag{4.16}$$

has a rank of n. Consider the linearised state-space model of the tank system given by (4.11). The $\mathbf{A}$ and $\mathbf{B}$ matrices are given by:

$$\mathbf{A} = \begin{bmatrix} 0 & 0 \\ 0 & -75 \end{bmatrix} \tag{4.17}$$

$$\mathbf{B} = \begin{bmatrix} 1 & 1 \\ 0.01 & -0.04 \end{bmatrix} \tag{4.18}$$

and $\mathbf{C}$ is simply the identity matrix. Computing the controllability and observability matrices C and O gives:

$$C = \begin{bmatrix} 1 & 1 & 0 & 0 \\ 0.01 & -0.04 & -0.75 & 3 \end{bmatrix} \tag{4.19}$$

$$O = \begin{bmatrix} 1 & 0 \\ 0 & 1 \\ 0 & 0 \\ 0 & -75 \end{bmatrix} \tag{4.20}$$

It is evident that both matrices have 2 linearly independent rows and columns and the system is thus completely controllable and observable.

Another test for controllability and observability is the modal analysis which gives particular insight into the behaviour of the system [27]. In the modal analysis, the plant **A** is broken down into its constituent eigenvalues and eigenvectors which allow the influence of each input on each 'mode', as well as the influence of each mode on each output to be seen.

The solution of any LTI system as given in (4.13) and (4.14) can be determined analytically as [28]:

$$\mathbf{y}(t) = \mathbf{C}e^{\mathbf{A}t}\mathbf{x}_0 + \mathbf{C}\int_0^t e^{\mathbf{A}(t-\tau)}\mathbf{B}\mathbf{u}(\tau)d\tau + \mathbf{D}\mathbf{u}(t) \tag{4.21}$$

It is also known that any matrix **A** of full rank can be broken down into its eigendecomposition which is given as:

$$\mathbf{A} = \mathbf{W}\mathbf{\Lambda}\mathbf{V}^T \tag{4.22}$$

where $\mathbf{\Lambda}$ is a diagonal matrix consisting of the eigenvalues of the matrix **A** on the diagonal and **W** and **V** are matrices of the left and right eigenvectors respectively with:

$$\mathbf{W}^T = \mathbf{V}^{-1}. \tag{4.23}$$

If this decomposition is applied to the **A** matrix of (4.13), the time domain solution in (4.21) can be written as:

$$y_q(t) = \sum_{i=1}^{n}(\mathbf{c}_q\mathbf{v}_i)(\mathbf{w}_i'\mathbf{x}_0)e^{\lambda_i t} + \sum_{i=1}^{n}\sum_{k=1}^{m}(\mathbf{c}_q\mathbf{v}_i)(\mathbf{w}_i'\mathbf{b}_k)\int_0^t e^{\lambda_i(t-\tau)}u_k(\tau)d\tau + \mathbf{d}_q\mathbf{u}(t) \tag{4.24}$$

for the qth output where $\mathbf{x}_0$ is the initial value of the states, $\mathbf{c}_q$ and $\mathbf{d}_q$ are the qth row of the **C** and **D** matrices respectively, $\mathbf{b}_k$ is the kth column of the **B** matrix and λ_i, $\mathbf{v}_i$ and $\mathbf{w}_i$ are the ith eigenvalue, right and left eigenvectors of the **A** matrix respectively. In this formulation the system is represented in

terms of its 'modes', which correspond to the eigenvalues and eigenvectors of the system. The ith mode is said to be controllable from the kth input if and only if:

$$\mathbf{w}_i'\mathbf{b}_k \neq 0 \quad \forall\, i = 1,...,n \tag{4.25}$$

Similarly the ith mode is said to be observable from the qth input if and only if:

$$\mathbf{c}_q'\mathbf{v}_i \neq 0 \quad \forall\, i = 1,...,n \tag{4.26}$$

Therefore a particular mode is controllable if it is controllable from at least one input, and similarly a mode is observable if it is observable from at least one output [28].

The eigenvalues of the **A** matrix given in (4.17) are equal to the diagonal elements of the matrix, as the matrix itself is diagonal. The two eigenvalues are therefore:

$$\lambda_1 = 0, \quad \lambda_2 = -75 \tag{4.27}$$

while the two right eigenvectors $\mathbf{v}_1$ and $\mathbf{v}_2$ are found to be:

$$\mathbf{v}_1 = \begin{bmatrix} 1 \\ 0 \end{bmatrix}, \quad \mathbf{v}_2 = \begin{bmatrix} 0 \\ 1 \end{bmatrix}. \tag{4.28}$$

This yields:

$$\mathbf{V} = \mathbf{W}^T = \begin{bmatrix} 1 & 0 \\ 0 & 1 \end{bmatrix} \tag{4.29}$$

The first mode corresponding to the first eigenvalue λ_1 relates to the tank volume v as it is directly linked to the first state (δv in (4.9)) as is evident from the corresponding eigenvector $\mathbf{v}_1$. Similarly the second mode corresponding to the second eigenvalue λ_2 relates to the output density ρ, as it is directly linked to the second state (δp in (4.9)) as is evident from the corresponding eigenvector $\mathbf{v}_2$.

For controllability it follows:

$$\mathbf{w}_1'\mathbf{b}_1 = \begin{bmatrix} 1 & 0 \end{bmatrix} \begin{bmatrix} 1 \\ 0.01 \end{bmatrix} = 1 \tag{4.30}$$

$$\mathbf{w}_1'\mathbf{b}_2 = \begin{bmatrix} 1 & 0 \end{bmatrix} \begin{bmatrix} 1 \\ -0.04 \end{bmatrix} = 1 \tag{4.31}$$

$$\mathbf{w}_2'\mathbf{b}_1 = \begin{bmatrix} 0 & 1 \end{bmatrix} \begin{bmatrix} 1 \\ 0.01 \end{bmatrix} = 0.01 \tag{4.32}$$

$$\mathbf{w}_2'\mathbf{b}_2 = \begin{bmatrix} 0 & 1 \end{bmatrix} \begin{bmatrix} 1 \\ -0.04 \end{bmatrix} = -0.04 \tag{4.33}$$

It is therefore evident that both modes are controllable from both inputs. Intuitively, this means that, since the first mode corresponds with tank volume v, both inputs have an equal effect on the tank volume. This is due to the fact that the two inputs are flow rates of liquid into the tank. Similarly both inputs have an effect on the second mode corresponding with the output density ρ but to differing extents and with one having a positive effect and the other a negative. Intuitively, the first input corresponding with the input flow rate would serve to increase the density of the liquid in the tank while the second input corresponding with the water flow rate into the tank would serve to decrease the density of the liquid in the tank. It is worth noting that the results in (4.30) - (4.33) correspond with the elements of the **B** matrix of the linearised model given in (4.11).

For observability it follows:

$$\mathbf{c}_1'\mathbf{v}_1 = \begin{bmatrix} 1 & 0 \end{bmatrix} \begin{bmatrix} 1 \\ 0 \end{bmatrix} = 1 \tag{4.34}$$

$$\mathbf{c}_1'\mathbf{v}_2 = \begin{bmatrix} 1 & 0 \end{bmatrix} \begin{bmatrix} 0 \\ 1 \end{bmatrix} = 0 \tag{4.35}$$

$$\mathbf{c}_2'\mathbf{v}_1 = \begin{bmatrix} 0 & 1 \end{bmatrix} \begin{bmatrix} 1 \\ 0 \end{bmatrix} = 0 \tag{4.36}$$

$$\mathbf{c}_2'\mathbf{v}_2 = \begin{bmatrix} 0 & 1 \end{bmatrix} \begin{bmatrix} 0 \\ 1 \end{bmatrix} = 1 \tag{4.37}$$

It is evident that the first mode is only observable in the first output and the second mode in the second output. It is evident from the linearised plant model in (4.9) that the states of the system themselves

(δv and δp) are the outputs of the system. Combining this with the fact that each mode represents the two different states independently, it follows intuitively that each mode is observable only in a single output.

4.3.2 Plant poles and multivariable zeros

The plant poles are defined as the eigenvalues of the **A** matrix of the plant [27], [28]. As noted in the previous subsections the plant thus has two poles, one at the origin corresponding to the eigenvalue of 0 and another at -75 corresponding to the second eigenvalue. This is also evident from the transfer function matrix representation of the plant given in (4.12). It is thus evident that the plant has a pole at the origin which corresponds with the tank volume which by nature is an integrating process when the discharge flow rate is regulated by a pump.

A plant model has a multivariable zero if, at some frequency or for some frequency range, the transfer function matrix loses rank [27]. Thus for the transfer function matrix in (4.12), the normal rank of the matrix is two and there is no frequency ω where substitution of $s = j\omega$ will cause the matrix to lose rank. The plant model therefore does not have any multivariable zeros. If present, multivariable zeros mean that there is a certain direction in which the input will have no effect on the plant output which is undesirable for control purposes [27].

4.3.3 Relative gain array

The relative gain array (RGA) of a non-singular square plant model is defined as:

$$RGA(\mathbf{G}_p) = \mathbf{G}_p \times (\mathbf{G}_p^{-1})^T \tag{4.38}$$

where $\times$ indicates the element by element multiplication of the matrix [27]. The relative gain array provides an indication of the controllability of a plant in a number of ways. Firstly, large RGA elements indicate that the plant is fundamentally difficult to control due to sensitivity to uncertainty. Secondly the RGA indicates the preferred input-output pairing if decentralised control is to be used, with the preferred pairing chosen corresponding to the RGA closest to one, and avoiding pairings which correspond to negative RGA elements [27].

Applying (4.38) to the plant model in (4.12) gives:

$$\begin{aligned} RGA(\mathbf{G}_p) &= \begin{bmatrix} \frac{1}{s} & \frac{1}{s} \\ \frac{0.01}{s+75} & \frac{-0.04}{s+75} \end{bmatrix} \times \begin{bmatrix} 0.8s & 0.2s \\ 20(s+75) & -20(s+75) \end{bmatrix} \\ &= \begin{bmatrix} 0.8 & 0.2 \\ 0.2 & 0.8 \end{bmatrix} \end{aligned} \tag{4.39}$$

It can be seen from (4.39) that the diagonal elements are closer to one than the off diagonal elements, thus for decentralised control, input-output pairing should be done alone the diagonal elements. In real terms, the flow rate of the product into the tank would be best used to control the tank volume, where the flow rate of water into the tank would best be used to control the density of the liquid in the tank. The magnitude of the RGA elements also provide an indication of the interaction between inputs and outputs, where a value of zero would indicate no interaction and a value close to one indicating that only the corresponding input effects the corresponding output. A completely decoupled, diagonal plant will therefore have a RGA matrix equal to the identity matrix [27]. In this case, the RGA is not equal to the identity matrix but does indicate a relatively good level of decoupling between inputs and outputs. It is also evident that uncertainty will not be an issue in controlling the plant due to the small values of the RGA elements.

4.3.4 Plant scaling

For the remaining analysis which needs to be done in terms of input-output controllability, the plant needs to be scaled such that the scaled inputs take on values between zero and one [27]. The scaling factors are chosen according to the maximum and minimum values of the outputs $\mathbf{y}$, inputs $\mathbf{u}$ and disturbances $\mathbf{d}$. The scaling factors D_{yi}, D_{ui} and D_{di} for each output y_i, input u_i and disturbance d_i are chosen as:

$$D_{yi} = min(|y_{i-max}|, |y_{i-min}|) \tag{4.40}$$

$$D_{ui} = min(|u_{i-max}|, |u_{i-min}|) \tag{4.41}$$

$$D_{di} = min(|d_{i-max}|, |d_{i-min}|) \tag{4.42}$$

The plant model can then be written in terms of scaled outputs $\hat{\mathbf{y}}$, inputs $\hat{\mathbf{u}}$ and disturbances $\hat{\mathbf{d}}$ as:

$$\begin{aligned} \mathbf{D}_y\hat{\mathbf{y}} &= \mathbf{G}_p\mathbf{D}_u\hat{\mathbf{u}} + \mathbf{G}_d\mathbf{D}_d\hat{\mathbf{d}} \\ \therefore \quad \hat{\mathbf{y}} &= \mathbf{D}_y^{-1}\mathbf{G}\mathbf{D}_u\hat{\mathbf{u}} + \mathbf{D}_y^{-1}\mathbf{G}_d\mathbf{D}_d\hat{\mathbf{d}} \end{aligned} \tag{4.43}$$

where $\mathbf{G}_p$ and $\mathbf{G}_d$ are the plant and disturbance transfer function matrix models given in (4.12).

The nominal values along with maximum and minimum values for the output variables v and ρ, input variables q_i and q_w and the disturbance variable ρ_i in (4.5) are summarised in Table 4.1 below. For the

Table 4.1. Operating constraints

Variable	Nominal	Minimum	Maximum	Unit
v	10	3	20	m^3
ρ	1.4	1	1.5	t/m^3
q_i	600	300	1200	m^3/h
q_w	150	0	750	m^3/h
ρ_i	1.5	1	2	t/m^3

linearised model in (4.11) and (4.12) these constraints need to be written in terms of the deviation variables y_1, y_2, u_1, u_2 and d. This is given in Table 4.2 below. This yields the following scaling

Table 4.2. Deviation operating constraints

Variable	Minimum	Maximum	Unit
y_1 (δv)	-7	10	m^3
y_2 $(\delta \rho)$	-0.4	0.1	t/m^3
u_1 (δq_i)	-300	600	m^3/h
u_2 (δq_w)	-150	600	m^3/h
d $(\delta \rho_i)$	-0.5	0.5	t/m^3

matrices according to (4.40) - (4.42):

$$\mathbf{D}_y = \begin{bmatrix} 7 & 0 \\ 0 & 0.1 \end{bmatrix} \tag{4.44}$$

$$\mathbf{D}_u = \begin{bmatrix} 600 & 0 \\ 0 & 150 \end{bmatrix} \tag{4.45}$$

$$\mathbf{D}_d = \begin{bmatrix} 0.5 \end{bmatrix} \tag{4.46}$$

The scaled plant and disturbance models $\tilde{\mathbf{G}}_p$ and $\tilde{\mathbf{G}}_d$ are found to be:

$$\tilde{\mathbf{G}}_p = \begin{bmatrix} \frac{85.71}{s} & \frac{21.43}{s} \\ \frac{60}{s+75} & \frac{-60}{s+75} \end{bmatrix} \tag{4.47}$$

$$\tilde{\mathbf{G}}_d = \begin{bmatrix} 0 \\ \frac{300}{s+75} \end{bmatrix} \tag{4.48}$$

4.3.5 Functional controllability

This subsection incorporates the last three points of the input-output controllability analysis which are concerned with the possibility of achieving the desired plant set-point given the magnitude of the plant and disturbance gains of the scaled model given in (4.47). Figs. 4.5 and 4.6 show plots of the singular values of these two models versus frequency.

It can be seen from Fig. 4.5 that at low frequencies the smaller of the two singular values takes on a value very close to one, while the larger of the two appears to increase indefinitely with decreasing frequency. This can be explained intuitively as the larger singular value corresponds with the volume

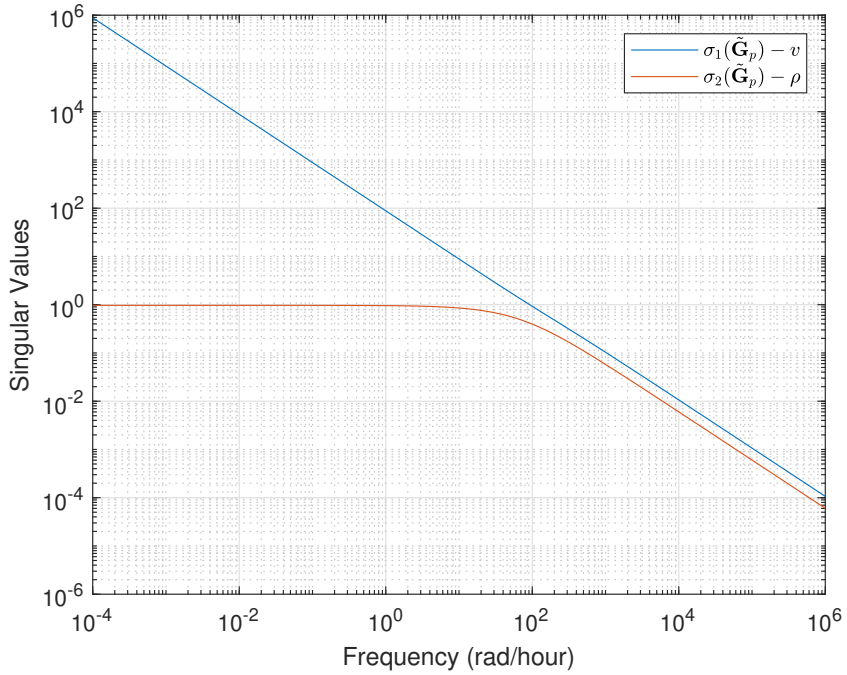

Figure 4.5. Singular values of scaled plant model $\tilde{\mathbf{G}}_p$.

of the tank v (i.e. integrators in the plant model) while the smaller singular value corresponds with the density ρ. As stated previously, if the minimum singular value is less than one at low frequencies, it means that, in that particular direction, it is not possible to achieve a change in the output of unit magnitude with a change in the inputs of unit magnitude [27]. In this case, any tank level can be achieved due to the integrating nature of the process, hence the larger singular value increases as frequency decreases. The reason as to why the smaller singular value takes on a value of one at low frequencies can be seen by examining the input and output constraints. The maximum and minimum values of the density of 1 and 1.5 t/m^3 correspond with the densities of the input water and feed respectively. Thus in order to achieve an output density ρ of 1 or 1.5 t/m^3, either the feed flow rate or water flow rate will need to be set to zero which is the lower constraint of both inputs (assuming the input density remains fixed at the nominal value). The minimum singular value is thus equal to 1 at frequencies where control is necessary and the density ρ is functionally controllable.

As mentioned previously, large singular values in the disturbance model indicate a need for control in order to reject disturbances, and if all elements of $\tilde{\mathbf{G}}_p^{-1}\tilde{\mathbf{G}}_d$ are less than one, perfect disturbance rejection is possible, with the outputs staying within bounds without any control. It can be seen in

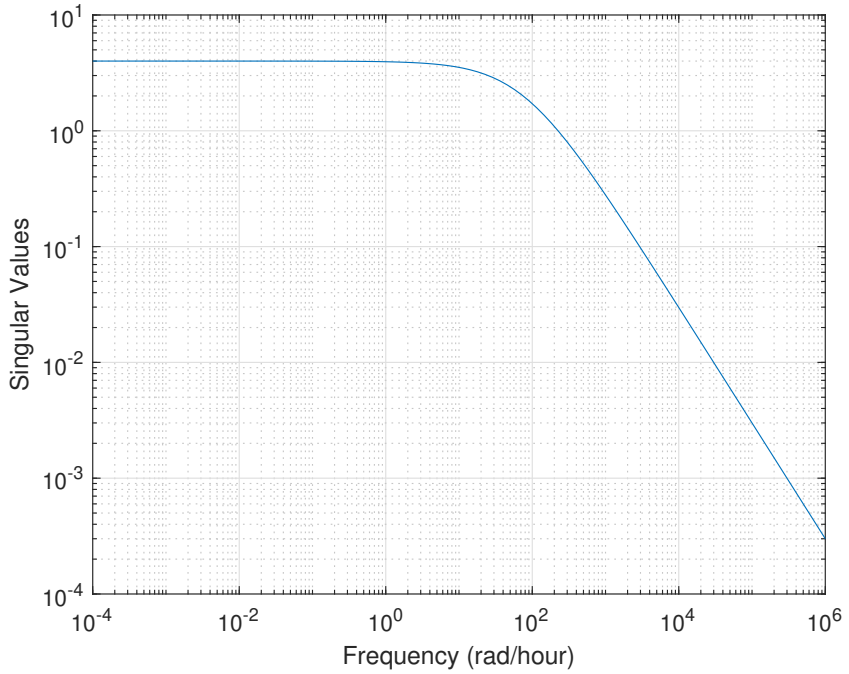

Figure 4.6. Singular value of scaled disturbance model $\tilde{\mathbf{G}}_d$.

Fig. 4.6 that the singular value of the disturbance model does exceed one at low frequencies and thus

control is needed. The analytical calculation of $\tilde{\mathbf{G}}_p^{-1}\tilde{\mathbf{G}}_d$ gives:

$$\tilde{\mathbf{G}}_p^{-1}\tilde{\mathbf{G}}_d = \begin{bmatrix} 0.00933s & 0.00333(s+75) \\ 0.00933s & -0.01333(s+75) \end{bmatrix} \begin{bmatrix} 0 \\ \dfrac{300}{s+75} \end{bmatrix} = \begin{bmatrix} 1 \\ 4 \end{bmatrix} \tag{4.49}$$

It is thus evident that perfect disturbance rejection is not possible. This can be intuitively deduced from the system constraints given in Table 4.1. The disturbance variable ρ_i can vary between 1 and 2 t/m^3, thus if the set-point for the density ρ is fixed at the nominal value of 1.4 t/m^3 it will not be possible to maintain this density if the density of the feed falls below 1.4 t/m^3, in which case the water feed will be shut off $q_w = 0$ and the input feed q_i flow rate will be set to the output feed flow rate of 750 m^3/h to keep the level constant. Perfect disturbance rejection is therefore not possible for the range of input densities given in Table 4.1.

It is worth noting that there is a certain amount of inaccuracy between the linear and nonlinear models in terms of the change in the feed flow rate q_i and the water flow rate q_w required to reject a given change in the feed density ρ_i. For example if there is an increase of 0.5 t/m^3 in ρ_i to its maximum value of 2 t/m^3, the new values of the feed and water flow rates q_i and q_w required to keep the output density ρ at the nominal 1.4 t/m^3 can be calculated from the mass balance equation:

$$\rho q_0 = \rho_i q_i + q_w \tag{4.50}$$

In order for the tank level to remain fixed at steady state, it is required that the increase in the water flow rate q_w be equal to the decrease in the feed flow rate q_i. Denoting this change as x and substitution into (4.50) yields:

$$\begin{aligned} 1.4 \cdot 750 &= (600 - x) \cdot 2 + (150 + x) \\ x &= 300 \ m^3/h \end{aligned} \tag{4.51}$$

This means the feed flow rate q_i would need to decrease by 300 m^3/h and the water flow rate would need to increase by a corresponding 300 m^3/h in order to reject this disturbance and keep the tank volume steady. It is also worth noting that since this value of 2 t/m^3 is the maximum value of the disturbance variable ρ_i, it is confirmed that there is sufficient input range available in q_i and q_w to reject the worst case disturbance.

If a similar calculation is performed using deviation variables and the linearised model in (4.12), the following result is obtained for steady state conditions:

$$\begin{aligned} 0 &= -0.01 \cdot x - 0.04 \cdot x + 60 \cdot 0.5 \\ x &= 600 \ m^3/h \end{aligned} \tag{4.52}$$

This is double the result which was obtained from the nonlinear mass balance equation. A similar calculation for an increase in 0.1 t/m^3 in ρ_i yields a required increase and decrease in the input flow rates q_w and q_i of 100 m^3/h for the nonlinear model and 120 m^3/h for the linear model. This is a significantly smaller difference than for the larger change in ρ_i of 0.5 t/m^3. It is thus evident that nonlinearities in the model have an effect on the input magnitude required to reject a given disturbance with the magnitude of the effect increasing with the magnitude of the disturbance. As shown in Figs. 4.2 - 4.4, the nonlinear and linear models are identical in response to changes in the disturbance variable ρ_i, with mild nonlinearities resulting from the flow rates q_i and q_w with the linear model accurate over a wide operating range.

4.4 CONCLUSION

A detailed nonlinear model of Sibanye-Stillwater's Platinum tailings treatment plant has been derived. The model was subsequently linearised and a detailed input-output controllability analysis was performed. It has been shown that the system is input-output controllable, so long as the input density does not drop below the output set-point, making it unachievable.

CHAPTER 5 SURGE TANK CASE STUDY: CONTROLLER DESIGN AND ANALYSIS

5.1 CHAPTER OVERVIEW

This chapter presents six controllers for the surge tank process presented in Chapter 4. Four conventional feedback controllers are presented in Section 5.2 which include an inverse, modified inverse, decentralised PI and mixed sensitivity $\mathcal{H}_\infty$ controller. Section 5.3 presents two MPC controllers (one linear and the other nonlinear).

5.2 CONVENTIONAL FEEDBACK CONTROL

In this subsection, four different feedback control strategies are presented and their performance is compared. First the case of ideal control is analysed, followed by a slightly modified version of the ideal controller. A decentralised PI controller with SIMC tuning is then presented followed by a mixed sensitivity $\mathcal{H}_\infty$ controller.

5.2.1 Inverse based (ideal) controller - $\mathbf{G}_{c1}$

As stated in section 2.3.1, ideal feedback control is achieved when the controller takes the form:

$$\mathbf{G}_c = \frac{k}{s}\mathbf{G}_p^{-1} \tag{5.1}$$

where $\mathbf{G}_p$ is the plant transfer function matrix and k is a tuning factor that determines the bandwidth and aggressiveness of the controller. In this instance perfect control is theoretically possible as the plant model in (4.11) is invertible. This gives a controller of the form:

$$\mathbf{G}_{c1} = k \begin{bmatrix} 0.8 & \dfrac{20(s+75)}{s} \\ 0.2 & \dfrac{-20(s+75)}{s} \end{bmatrix} \tag{5.2}$$

Fig. 5.1 shows the singular values of the sensitivity transfer function **S** for increasing values of k. This shows the increasing bandwidth with increasing k, as well as the fact that there is no amplification of the error signal at any frequency. Figs. 5.2 and 5.3 show the inputs and outputs resulting from the

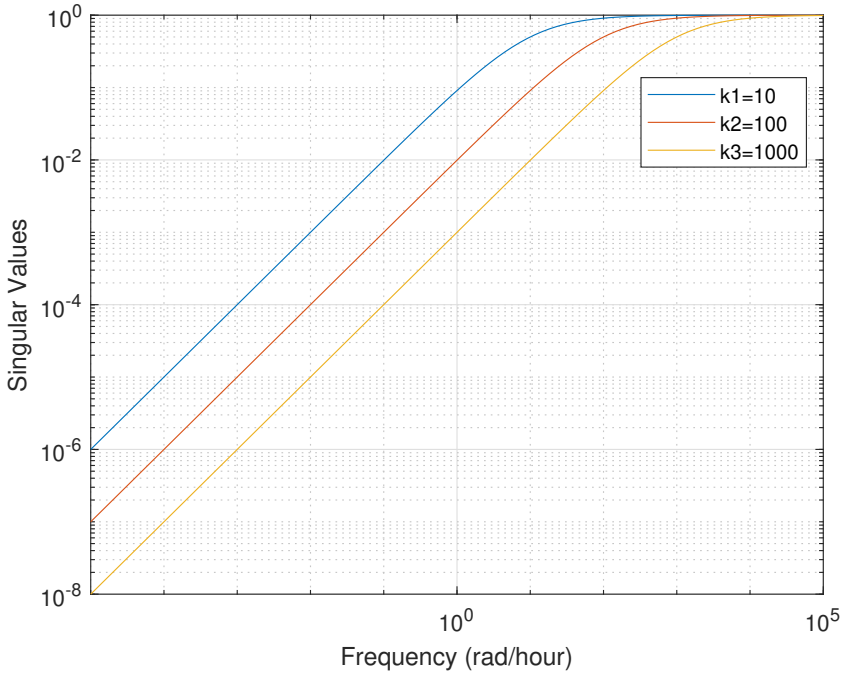

Figure 5.1. Sensitivity function singular values for $k = 10$, $k = 100$ and $k = 1000$.

controller given in (5.2) with $k = 100$ acting on both the linear and nonlinear plants given in (4.5) and (4.9) respectively. The output density ρ of the nonlinear and linear plants reach a maximum value of 1.424 and 1.426 respectively while the tank volume remains constant.

To provide an indication of controller performance for each respective output, the sum of the squares of the error given as:

$$SSE_i = \sum_{k=1}^{N} (r_i(k) - y_i(k)) \cdot (r_i(k) - y_i(k)), \tag{5.3}$$

is used where N is the total number of samples in the simulation and the subscript i denotes the output (i.e. 1 for v and 2 for ρ).

The sum of the squares of the error according to (5.3) in the tank volume v and output density ρ achieved for the nonlinear plant are 0 and 0.0057 respectively. It can be seen from Fig. 5.3 that slightly larger changes in the inputs q_i and q_w are needed to reject the disturbance for the linearised model as opposed to the nonlinear model. This clearly shows the discrepancies between the linear and nonlinear models discussed in the input output controllability analysis in section 4.3. Figs. 5.4 and 5.5 show the response of the same controller ($k = 100$) on the linear and nonlinear plants for a sinusoidal disturbance in ρ_i with a magnitude of 0.1 $^t/_{m^3}$ and frequency 5 $cycles/h$. For the nonlinear plant with no control the resulting sum of the squares of the error in ρ from this disturbance is 0.5983, with the given controller ($k = 100$) it is reduced to 0.1003. Increasing the controller gain k to 1000 further reduces this to 0.0015.

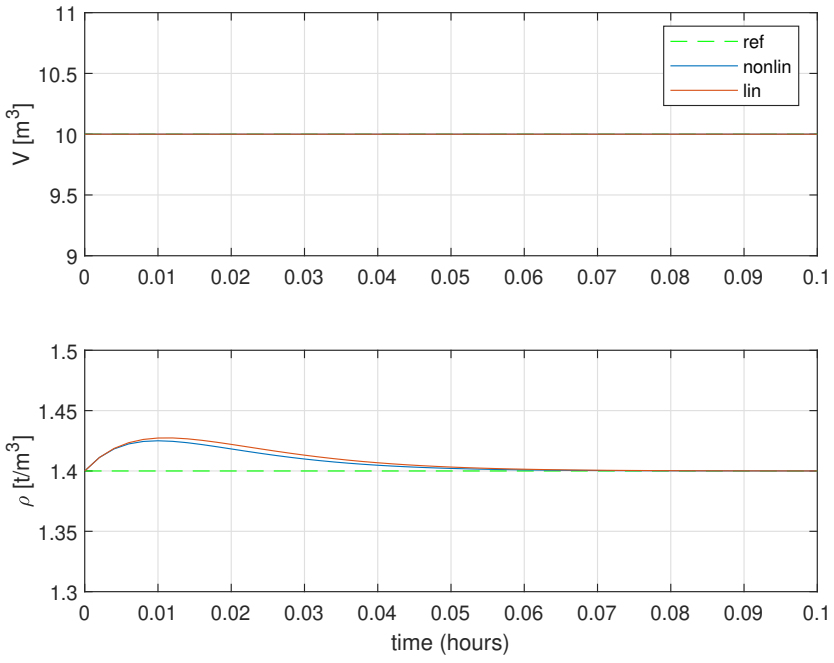

Figure 5.2. Linear and nonlinear outputs for step disturbance of 0.1 $^t/_{m^3}$ in ρ_i.

5.2.2 Modified inverse based control - $\mathbf{G}_{c2}$

It is evident that the two terms in the controller given by (5.2) which correspond with the volume measurement ($\mathbf{G}_{c1}(1,1)$ and $\mathbf{G}_{c1}(2,1)$) are purely proportional terms while the other two terms corresponding with the density measurement take on the standard PI controller form. It is known from the classical control literature that in order to achieve zero steady-state offset in terms of reference following, it is required that there be an integrator in the feedback loop [20], [26], [27]. Since elements in the plant transfer function model which relate to the tank volume v are integrators, purely proportional

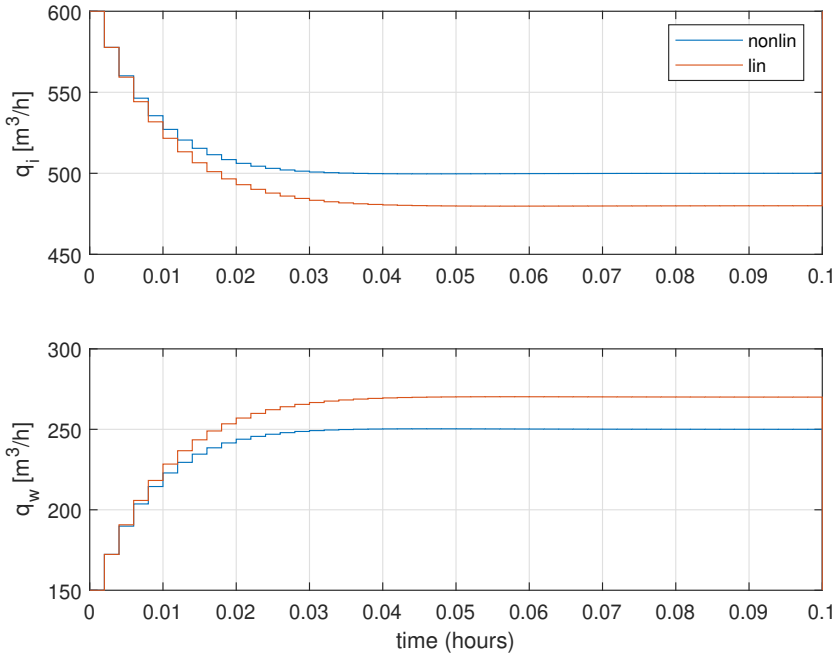

Figure 5.3. Linear and nonlinear inputs for step disturbance of 0.1 t/m^3 in ρ_i.

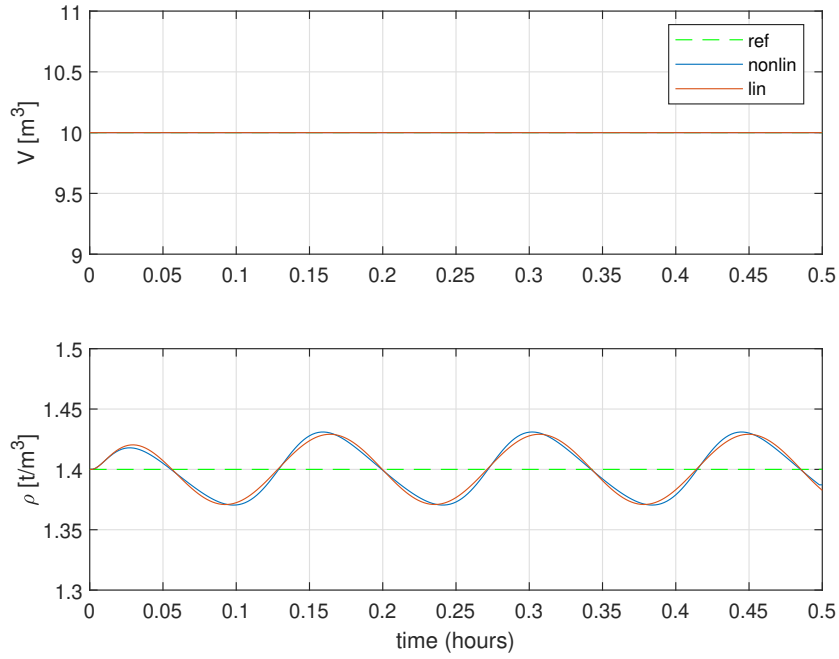

Figure 5.4. Linear and nonlinear outputs for sinusoidal disturbance of 0.1 t/m^3 magnitude and frequency 5 $cycles/h$ in ρ_i.

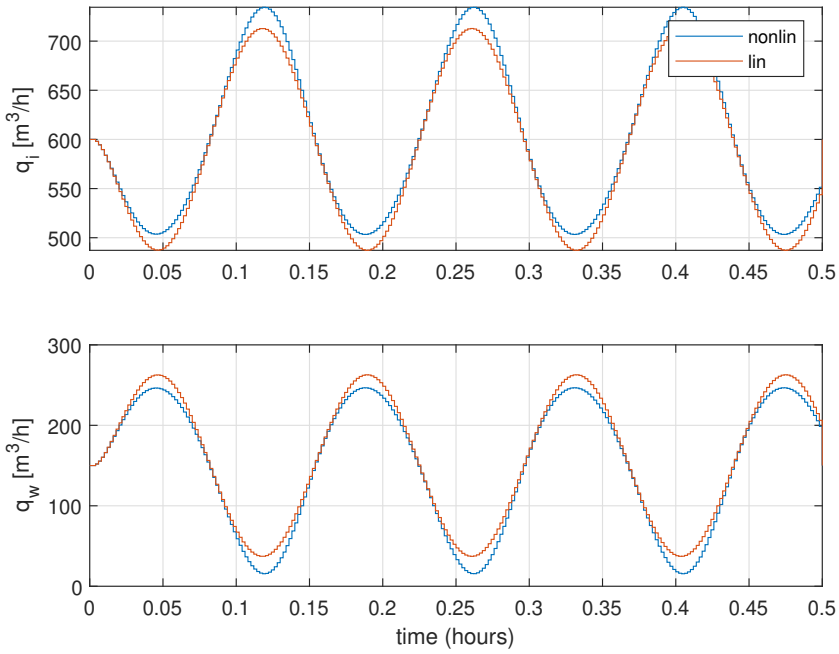

Figure 5.5. Linear and nonlinear inputs for sinusoidal disturbance of 0.1 $^{t}/_{m^3}$ magnitude and frequency 5 $cycles/h$ in ρ_i.

control will suffice. This is however not the case for load disturbances which requires integration in the controller itself to yield zero steady-state error.

If there is any uncertainty in the model gains which relate the input flow rates q_i and q_w to the tank volume v, a steady state offset will result in the tank volume due to set-point changes and disturbances. This is verified by the results shown in Fig. 5.6 which shows the output achieved by the inverse based controller in (5.2) with $k = 100$ for a disturbance of 0.1 $^{t}/_{m^3}$ in ρ_i with 10% gain uncertainty in q_w. It can be seen that the density ρ is effectively brought back to set-point while the tank volume settles with a steady state error. This is due to the absence of integral control on the two corresponding terms of the inverse based controller.

This problem can be overcome by the addition of integral action to the two proportional only elements in the controller ($\mathbf{G}_{c1}(1,1)$ and $\mathbf{G}_{c1}(2,1)$). This yields a controller of the form:

$$\mathbf{G}_{c2} = k \begin{bmatrix} \frac{0.8(s+41.3)}{s} & \frac{20(s+75)}{s} \\ \frac{0.2(s+165)}{s} & \frac{-20(s+75)}{s} \end{bmatrix} \tag{5.4}$$

where a value of 33 was chosen for the gain of the additional integral terms. Figs. 5.7 and 5.8 show the resulting plant outputs and control moves from the controller with $k = 100$ for a step disturbance of 0.1 $^{t}/_{m^3}$ in ρ_i.

In comparison with Fig. 5.6 it is evident that the response in the liquid density ρ is almost identical for the two controllers where the modified controller forces the tank level back to set-point resulting in no steady-state error. The sum of the squares of the error according to (5.3) achieved in the tank volume v and output density ρ are 2.13 and 0.004 respectively for the pure inverse based controller and 0.1992 and 0.0043 respectively for the modified inverse based controller.

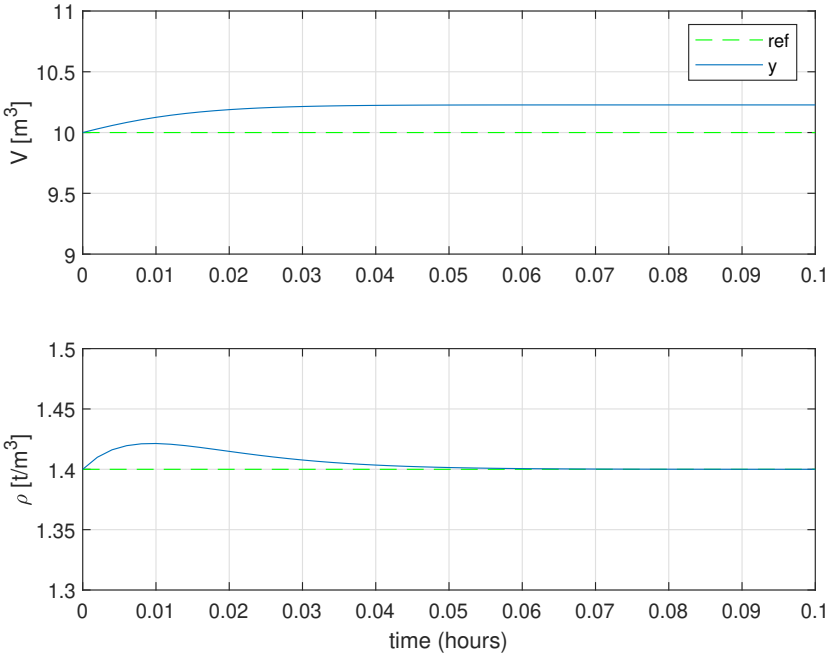

Figure 5.6. Outputs of inverse controller for step disturbance of 0.1 $^{t}/_{m^3}$ in ρ_i with 10% gain uncertainty in q_w.

5.2.3 Decentralised PI control with SIMC tuning - $\mathbf{G}_{c\_local}$

A typical control solution which may be applied in practice is to use decentralised PI controllers which are tuned according to some rules such as the SIMC rules given in Table 2.1. According to the RGA given in (4.39), it is best to pair the inputs in a diagonal fashion with the input flow rate q_i used to

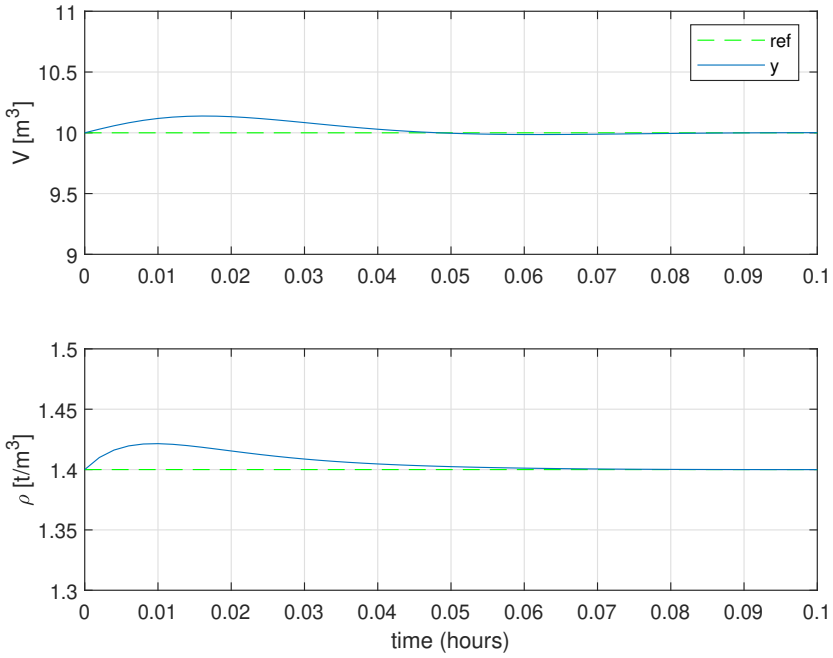

Figure 5.7. Outputs of modified inverse controller for step disturbance of 0.1 $^{t}/_{m^3}$ in ρ_i with 10% gain uncertainty in q_w.

control the tank volume v and the water flow rate q_w used to control the liquid density ρ. Using a tuning value of 0.01 for the tuning factor τ_c in the SIMC rules and applying the rules in Table 2.1 to the relevant models ($\mathbf{G}_p(1,1)$ and $\mathbf{G}_p(2,2)$) for each input output pairing, the following controller is derived:

$$\mathbf{G}_{c3} = \begin{bmatrix} \dfrac{4(s+25)}{s} & 0 \\ 0 & \dfrac{-2500(s+75)}{s} \end{bmatrix} \tag{5.5}$$

Figs. 5.9 and 5.10 show the resulting plant outputs and control moves from the controller for a step disturbance of 0.1 $^{t}/_{m^3}$ in ρ_i. In this case there is also a 10% gain uncertainty in q_w. It is evident from these figures that the response of this controller with respect to the tank volume v is very poor, with large oscillations occurring which take almost an hour to settle within 10% of the set-point, though it does settle to this set-point without any steady state error. These oscillations are due to the interactions that occur in the plant which are ignored when designing the controllers for the two individual loops. The sum of the squares of the error according to (5.3) achieved in the tank volume v and output density ρ are 1609 and 0.0049 respectively for the first 0.1 hours of the simulation. The performance in the

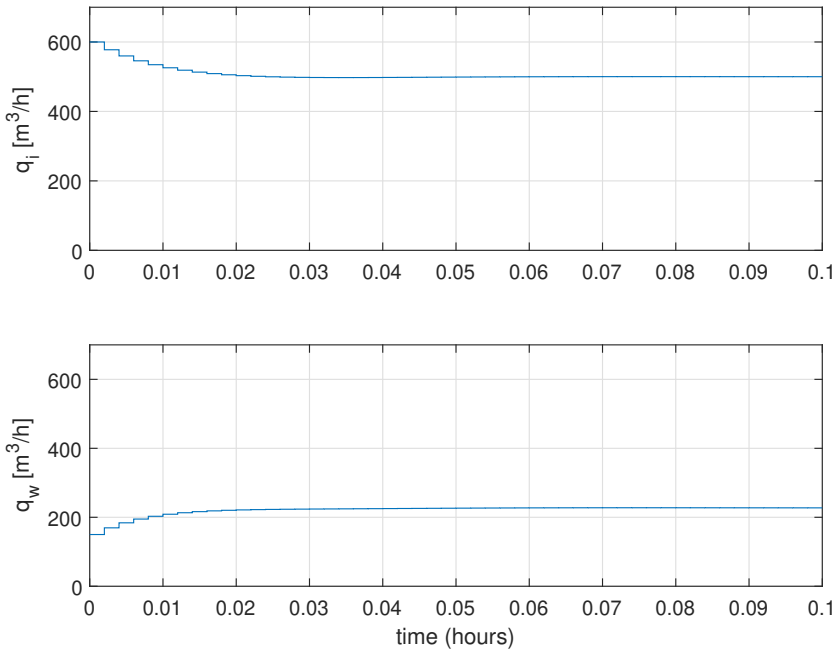

Figure 5.8. Plant inputs of modified inverse controller for step disturbance of 0.1 $^{t}/_{m^3}$ in ρ_i with 10% gain uncertainty in q_w.

density ρ is thus only slightly poorer in comparison with the previous two controllers.

5.2.4 Mixed sensitivity $\mathcal{H}_\infty$ loop shaping control - $\mathbf{G}_{c3}$

A mixed sensitivity $\mathcal{H}_\infty$ controller, with only **S** and **T** weighted, as described in Section 2.3.1 was designed for the plant with a desired bandwidth ω_B of 100 rad/s. This gives the weighting transfer function matrices of:

$$\mathbf{W}_p = \frac{s+100}{s+1e^{-3}}\mathbf{I} \tag{5.6}$$

$$\mathbf{W}_T = \frac{s+100}{1e^{-5}s+100}\mathbf{I} \tag{5.7}$$

where the value of A was taken to be 10^{-5}. The weighting matrix $\mathbf{W}_u$ was ignored in the design. Fig. 5.11 shows the singular values of the sensitivity and complementary sensitivity functions along with the inverse of the weights $\mathbf{W}_p$ and $\mathbf{W}_T$ versus frequency. It can be seen that the singular values of **S** and **T** always remain less than or equal to the inverse of their respective weights $\mathbf{W}_p$ and $\mathbf{W}_T$, and thus yield loop shapes close to the ideal.

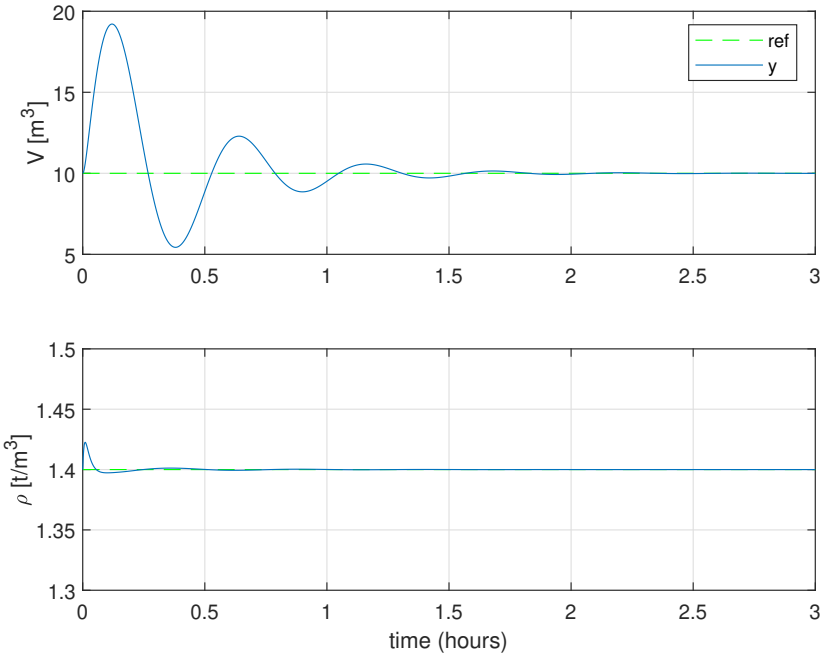

Figure 5.9. Outputs of decentralised PI controller for step disturbance of 0.1 $^{t}/_{m^3}$ in ρ_i with 10% gain uncertainty in q_w.

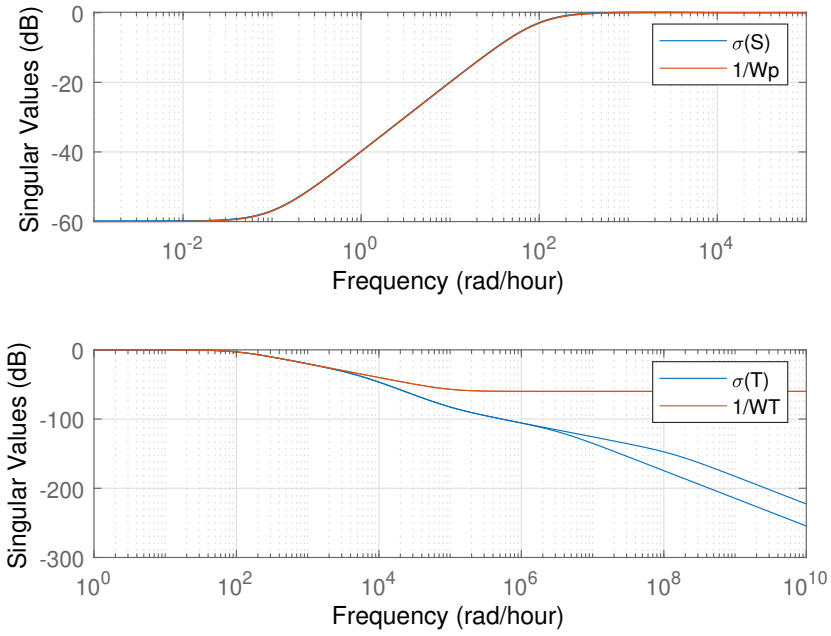

Figure 5.11. Singular values of sensitivity and complementary sensitivity transfer matrices for $\mathcal{H}_\infty$ controller and corresponding weights $\mathbf{W}_p$ and $\mathbf{W}_T$.

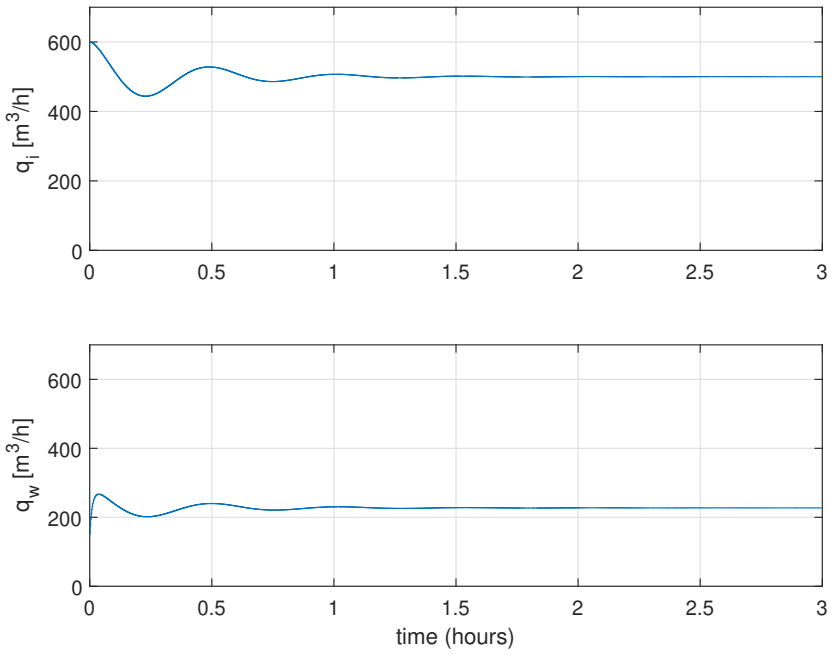

Figure 5.10. Plant inputs of decentralised PI controller for step disturbance of 0.1 $^{t}/_{m^3}$ in ρ_i with 10% gain uncertainty in q_w.

The controller was generated using the MATLAB robust control toolbox and the elements of $\mathbf{G}_c$ given as:

$$\mathbf{G}_{c3}(1,1) = \frac{2.6777e09(s+1.046e10)(s+1e07)(s+9244)(s+0.0009803)}{(s+1.384e11)(s+2.766e09)(s+9246)(s+9242)(s+0.001)} \tag{5.8}$$

$$\mathbf{G}_{c3}(2,1) = \frac{9.9667e09(s+7.019e08)(s+1e07)(s+9254)(s+0.001079)}{(s+1.384e11)(s+2.766e09)(s+9246)(s+9242)(s+0.001)} \tag{5.9}$$

$$\mathbf{G}_{c3}(1,2) = \frac{4.9854e09(s+1.405e11)(s+1e07)(s+9242)(s+75)}{(s+1.384e11)(s+2.766e09)(s+9246)(s+9242)(s+0.001)} \tag{5.10}$$

$$\mathbf{G}_{c3}(2,2) = \frac{-5.3573e09(s+1.307e11)(s+1e07)(s+9242)(s+75)}{(s+1.384e11)(s+2.766e09)(s+9246)(s+9242)(s+0.001)} \tag{5.11}$$

It is evident from (5.8) - (5.11) that the controller generated by the $\mathcal{H}_\infty$ loop shaping algorithm is of high order. Upon evaluation of the multi-variable zeros of the controller, it is found to have a zero at -75 corresponding to the stable pole of the plant as well as two others far into the left half plane. The two elements ($\mathbf{G}_{c3}(1,2)$ and $\mathbf{G}_{c3}(2,2)$) which correspond to the density ρ contain zeros at -75 whereas the two elements ($\mathbf{G}_{c3}(1,1)$ and $\mathbf{G}_{c3}(2,1)$) which correspond to the volume v contain zeros in the left half plane which are very close to the origin. It is also evident that the individual elements do not contain pure integral action but have poles relatively close to the origin at -0.001 which corresponds with the pole in the weight $\mathbf{W}_p$. There is thus no pure integral action present.

Figs. 5.12 and 5.13 show the resulting plant outputs and control moves from the controller for a step disturbance of 0.1 $^{t}/_{m^3}$ in ρ_i. In this case there is also a 10% input gain uncertainty in q_w. Similarly to the inverse based controller, the density ρ is effectively controlled back to set-point after the disturbance, whereas the volume v settles with a steady state error. The sum of the squares of the error according to (5.3) achieved in the tank volume v and output density ρ are 2.2554 and 0.0043 respectively. The performance is thus comparable, although marginally poorer than the inverse based controller.

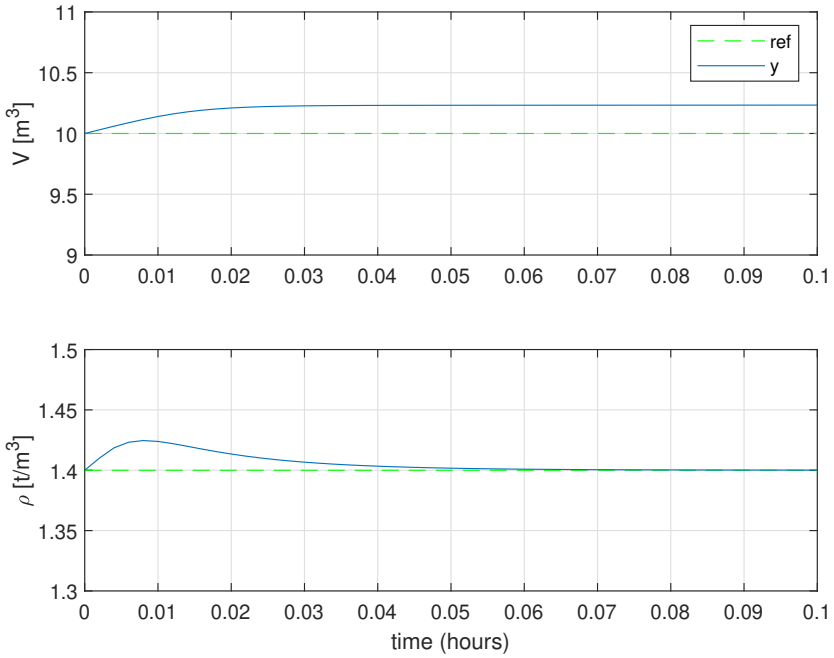

Figure 5.12. Outputs of $\mathcal{H}_\infty$ controller for step disturbance of 0.1 $^{t}/_{m^3}$ in ρ_i with 10% gain uncertainty in q_w.

5.3 MODEL PREDICTIVE CONTROL - $\mathbf{G}_{c4}$, $\mathbf{G}_{c5}$

In this subsection, two model predictive controllers (MPC) are presented, one ($\mathbf{G}_{c4}$) using the linearised model in (4.9) to perform predictions with the other ($\mathbf{G}_{c5}$) using the full nonlinear model in (4.5). As discussed in Section 2.3.2.2, some form of feedback or disturbance estimation is needed for off-set free MPC to be achieved. For both MPC controllers a Kalman filter as described in Section (2.3.2) is used to estimate the states with integrated white noise in the input channel used to provide integral action. This requires the augmentation of the linearised model in (4.9) to the from given in (2.64) with $\mathbf{G} = \mathbf{B}$, $\mathbf{A}_w = \mathbf{I}$ and $\mathbf{A}_n = \mathbf{0}$. This method assumes that any discrepancy between the estimated value of the output $\mathbf{C}\hat{\mathbf{x}}$ and the measured value $\mathbf{y}_m$ in

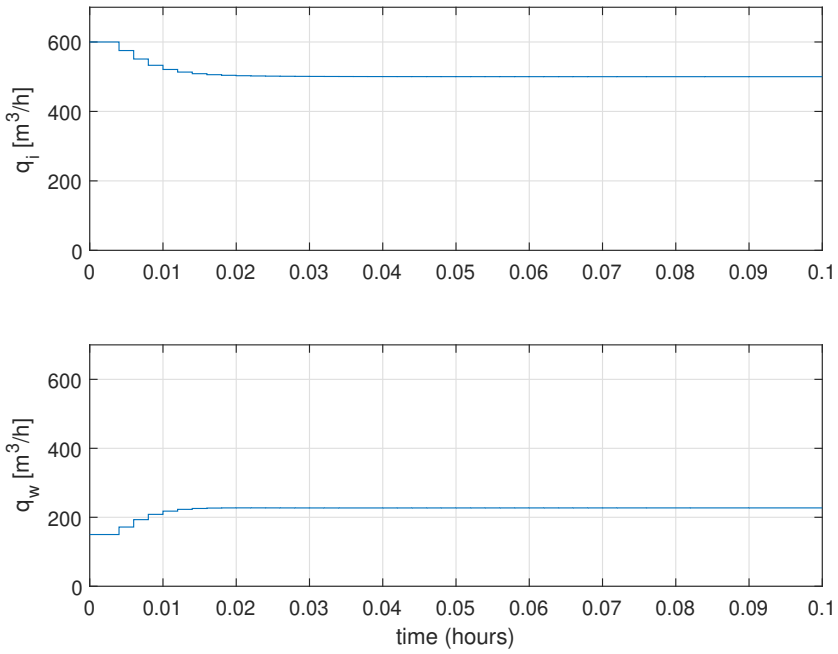

Figure 5.13. Plant inputs of $\mathcal{H}_\infty$ controller for step disturbance of 0.1 $^t/_{m^3}$ in ρ_i with 10% gain uncertainty in q_w.

(2.54) is due to the disturbance estimate **w**. The covariance matrices $\mathbf{Q}_w$ and $\mathbf{R}_n$ for the process and measurement noise **w** and **n**, which are used in the synthesis of the Kalman filter, were chosen to be:

$$\mathbf{Q}_w = \mathbf{I}, \quad \mathbf{R}_n = 1e^{-5} \times \mathbf{I} \tag{5.12}$$

The smaller the value of $\mathbf{R}_n$ in relation to $\mathbf{Q}_w$, the quicker the filter and thus the faster the controller reacts to disturbances, as expected, a smaller $\mathbf{R}_n$ also decreases the robustness of the controller [38]. The objective function used in the MPC controller is that given in (2.51) with the weighting matrices **Q** and **R** chosen as:

$$\mathbf{Q} = \begin{bmatrix} 1e^{-3} & 0 \\ 0 & 1 \end{bmatrix} \quad \mathbf{R} = 0.25e^{-7} \times \mathbf{I} \tag{5.13}$$

Figs. 5.14 - 5.19 show the plant outputs **y**, control moves **u** and disturbance estimates **w** for both the LMPC and NMPC controllers respectively. It can be seen from these figures that the response of the two controllers are practically identical which leads to the conclusion that the added complexity of

using the nonlinear model for predictions in the controller is not justified in this case. The sum of the squares of the error according to (5.3) achieved in the tank volume v and output density ρ are 0.0379 and 0.0039 respectively for the LMPC controller and 0.0405 and 0.0039 respectively for the NMPC controller. These values are thus comparable with the feedback controllers previously presented.

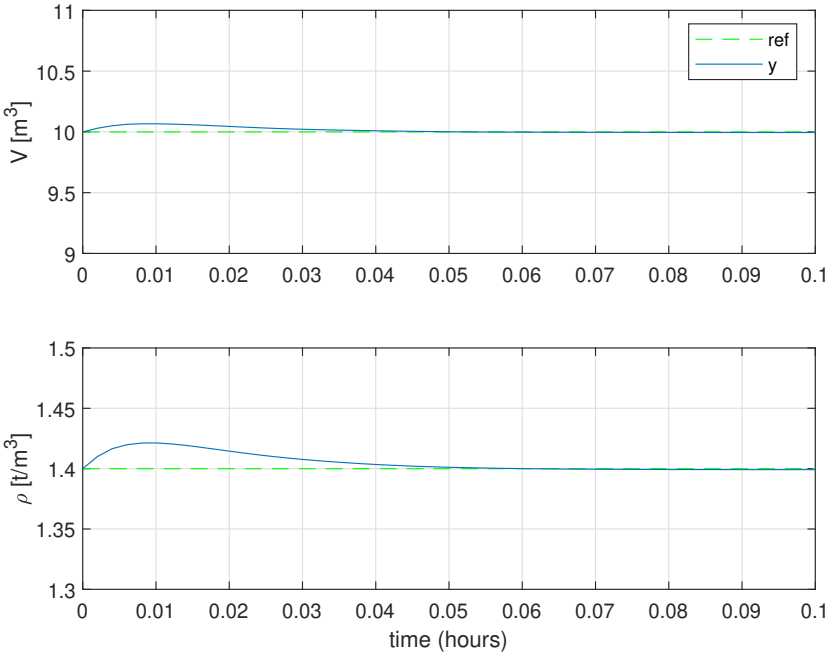

Figure 5.14. Outputs of LMPC controller for step disturbance of 0.1 $^{t}/_{m^3}$ in ρ_i with 10% gain uncertainty in q_w.

5.4 CONCLUSION

Six controllers have been presented for control of the plant. It has been shown that adequate control of the plant cannot be achieved by rudimentary decentralised PI control due to plant interactions. It has been shown that pure inverse and $\mathcal{H}_\infty$ control cannot successfully control the tank volume v to set-point in the presence of plant-model mismatch. The remaining three controllers (modified inverse and the two MPC) provide satisfactory control of the plant.

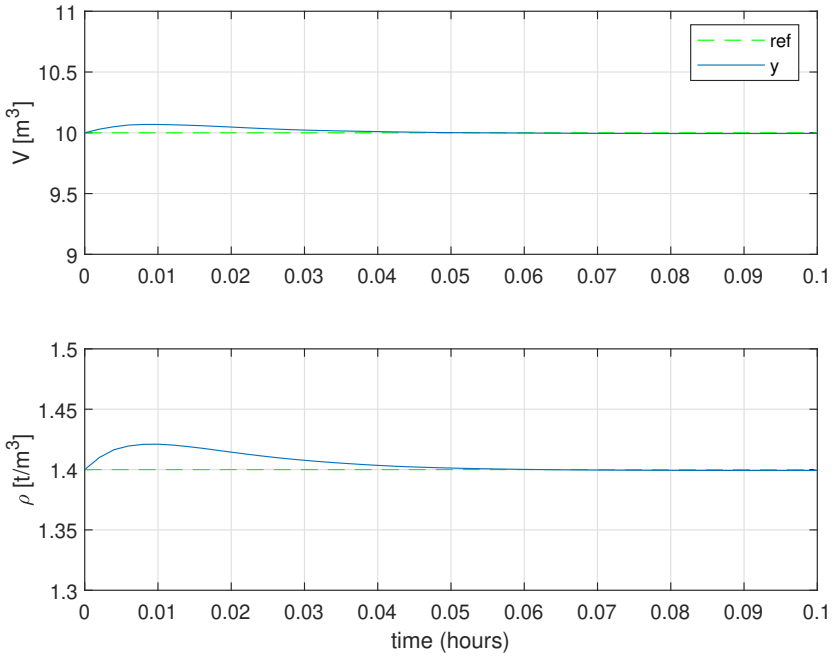

Figure 5.15. Outputs of NMPC controller for step disturbance of 0.1 $^{t}/_{m^3}$ in ρ_i with 10% gain uncertainty in q_w.

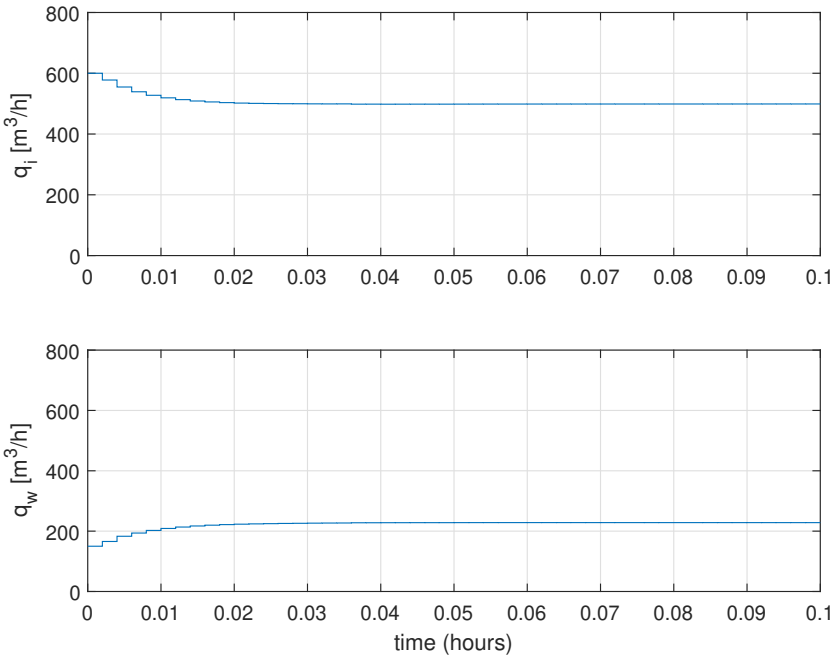

Figure 5.16. Inputs of LMPC controller for step disturbance of 0.1 $^{t}/_{m^3}$ in ρ_i with 10% gain uncertainty in q_w.

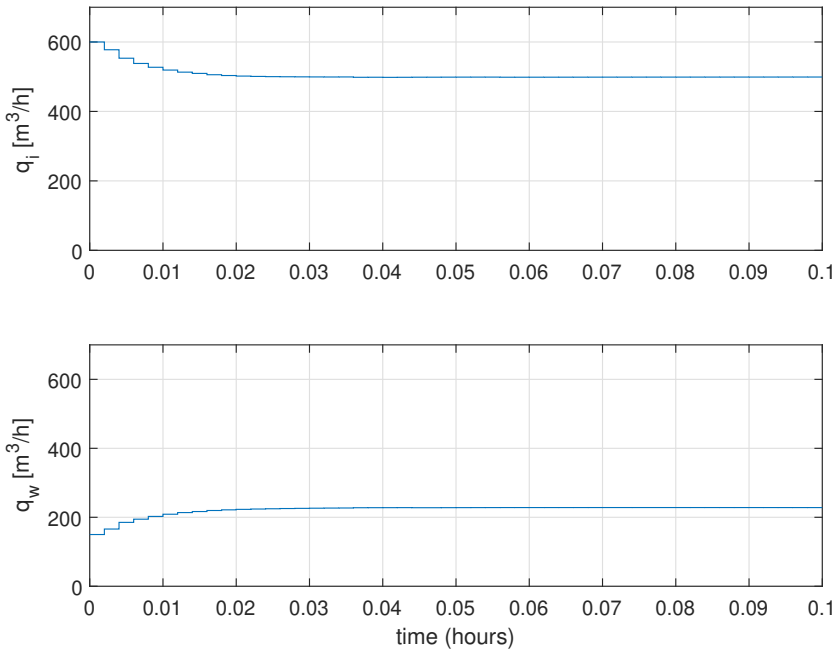

Figure 5.17. Inputs of NMPC controller for step disturbance of 0.1 $^{t}/_{m^3}$ in ρ_i with 10% gain uncertainty in q_w.

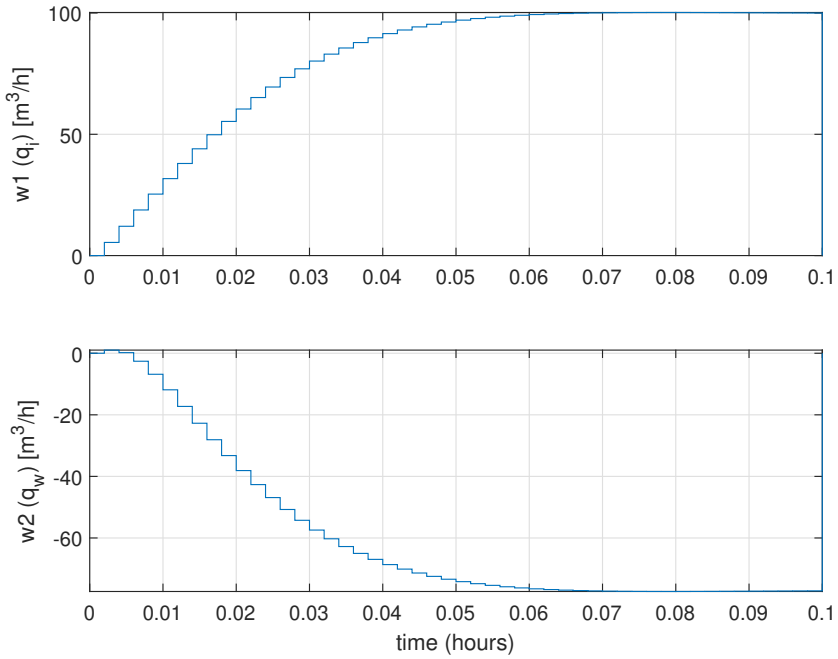

Figure 5.18. Disturbance estimates of LMPC controller for step disturbance of 0.1 $^{t}/_{m^3}$ in ρ_i with 10% gain uncertainty in q_w.

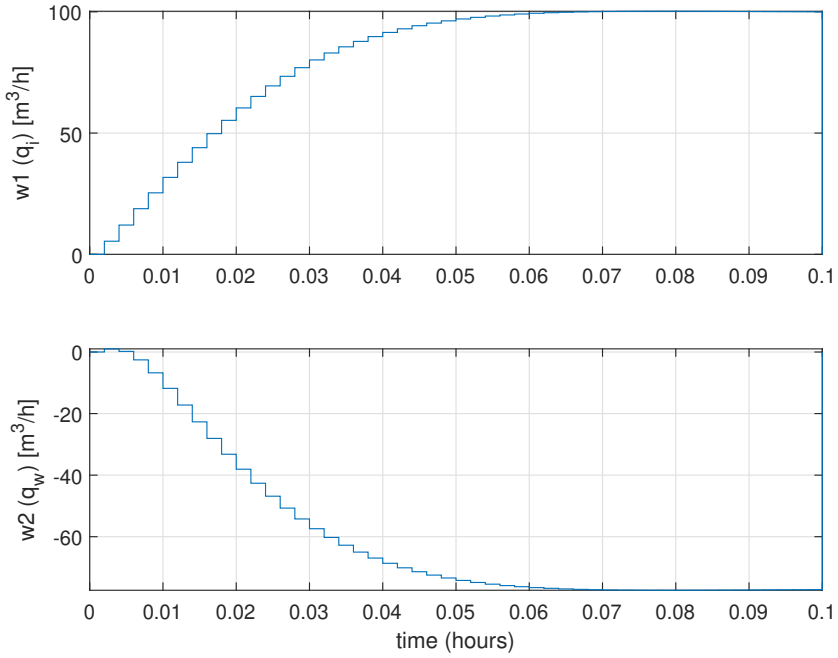

Figure 5.19. Disturbance estimates of NMPC controller for step disturbance of 0.1 $^{t}/_{m^3}$ in ρ_i with 10% gain uncertainty in q_w.

CHAPTER 6 SURGE TANK CASE STUDY: PLATFORM SIMULATION AND RESULTS

6.1 CHAPTER OVERVIEW

A scenario is presented where a platform as described in Chapter 3 facilitates the competition between the six controllers presented in the previous chapter to control the surge tank process presented in Chapter 4. Section 6.2 presents the scenario and assumptions made in conjunction with Chapter 3 while Section 6.3 presents the simulation results.

6.2 PLATFORM SIMULATION

A scenario where the six controllers presented in the previous Chapter compete to control the process in the manner depicted in Fig. 3.3 is presented in this section. It is assumed that the disturbance d (which is the density of the feed ρ_i into the tank) is measured by the selector. The local fall-back controller is taken to be the decoupled PI controller with SIMC tuning as this is the simplest and most generic control structure which would be employed in practice. Fig. 6.1 shows the value of the disturbance variable ρ_i over the simulation period of 6 hours which takes on a maximum value of 1.74 $^t/_{m^3}$ and a minimum of 1.38 $^t/_{m^3}$. The nomenclature of the six controllers is chosen as:

0. De-coupled PI controller with SIMC tuning ($\mathbf{G}_{c\_local}$)
1. Inverse controller ($\mathbf{G}_{c1}$)
2. Modified inverse controller ($\mathbf{G}_{c2}$)
3. $\mathcal{H}_\infty$ controller ($\mathbf{G}_{c3}$)

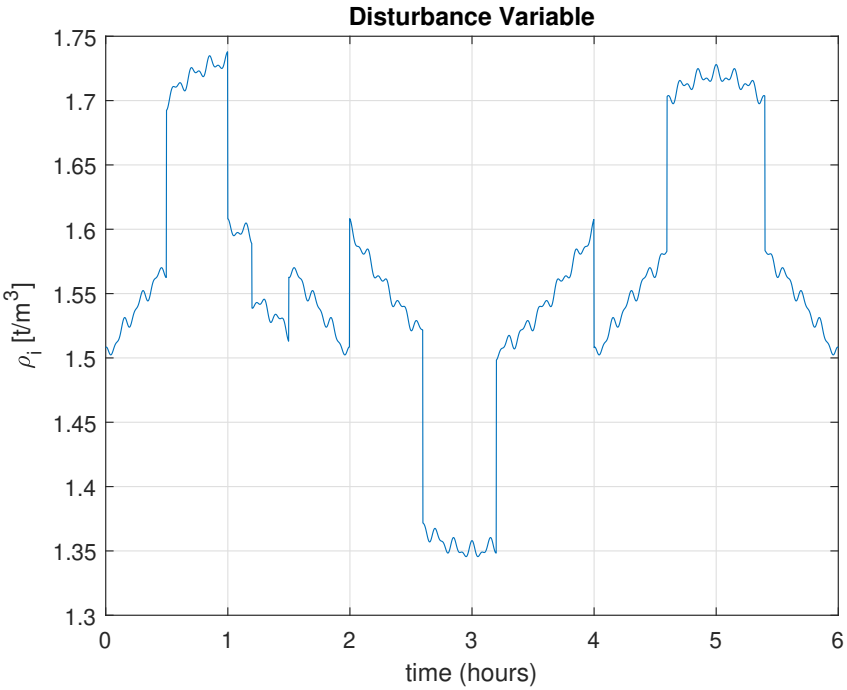

Figure 6.1. Disturbance variable ρ_i.

4. Linear MPC controller ($\mathbf{G}_{c4}$)
5. Nonlinear MPC controller ($\mathbf{G}_{c5}$)

The selector in Fig. 3.3 determines the best controller in the manner described in Section 3.4, using the nonlinear plant model to simulate the controllers and the performance index in (3.1) for evaluation. The weighting matrix $\mathbf{W}_e$ in (3.1) was set to:

$$\mathbf{W}_e = \mathbf{Q} = \begin{bmatrix} 1e^{-3} & 0 \\ 0 & 1 \end{bmatrix} \tag{6.1}$$

which is the same weighting matrix $\mathbf{Q}$ used in the performance index of the two MPC controllers, placing significantly more emphasis on the density ρ than the volume v. It is thus assumed that the performance measure in (3.1) and the weighting matrix $\mathbf{W}_e$ is shared with the controllers, but this does not necessarily have to be the case. The evaluation horizon N_e was set to 0.5 hours in order to be several orders of magnitude greater than that corresponding to the specified bandwidth of the controllers. This ensures the evaluation horizon is much longer than the expected dynamics of the slowest closed-loop system.

A sampling period Δt of 0.002 hours was chosen to satisfy the guideline given in (2.22) where the frequency ω is taken as the specified controller bandwidth ω_B of 100 rad/h. The conventional feedback controllers $\mathbf{G}_{c\_local}$ and $\mathbf{G}_{c1}$ - $\mathbf{G}_{c3}$ were transformed into state-space form and discretised as given in (2.32) and (2.33). The simulation of the nonlinear model was done using a 4^{th}-order Runge-Kutta approximation as described in Section 2.3.2.

Bump-less transfer is performed by the MPC and conventional feedback controllers in the manner described in Section 3.5. This is also the case in terms of constraint handling as described in Section 3.6. For the MPC controllers this is handled as part of the optimisation algorithm as described in Section 2.3.2. For the conventional feedback controllers, if the controller tries to increase the flow rate of the product feed q_i above 750 m^3/h, this flow rate will be capped at this upper constraint and the water flow rate q_w will be set to 0 m^3/h in order to keep the inflow equal to the outflow. In terms of limits on the rate of change constraints on the MVs, it is assumed that both the product and water flow rates q_i and q_w can be increased by a maximum of 100 m^3/h at each sampling instant which corresponds to 100 m^3/h every 0.002 hours or 7.2 seconds (actuator and sensor dynamics are neglected).

It is assumed for the purposes of this simulation that the controllers are completely trusted by the plant with no controller rating or remunerations necessary. The purpose of this simulation is to illustrate the platform concept of providing the plant access to the best performing controller based on the performance it yields when controlling a plant model.

6.3 PLATFORM SIMULATION RESULTS

Figs. 6.2 and 6.3 show the plant outputs and the inputs sent to the plant respectively. Fig. 6.4 shows the controller selected over the 6-hour period. Plant model mismatch was created by adding a 10% gain uncertainty to the input water flow rate q_w. As can be seen in Fig. 6.4, control is initially performed by $\mathbf{G}_{c\_local}$ (de-coupled PI), after which control is switched over to controller $\mathbf{G}_{c1}$ (inverse). For the remainder of the simulation period, control is performed by controller $\mathbf{G}_{c4}$ (linear MPC) apart from a single evaluation period where control is switched back over to ($\mathbf{G}_{c1}$) between the 3.5 and 4 hour mark.

In the period from 2.6 hours to 3.2 hours the set-point density of 1.4 t/m^3 is not achievable as the input density ρ decreases below 1.4 t/m^3 as can be seen in Fig. 6.1, hence the deviation from set-point in the output ρ. During this period, the constraints are taken into account by the selected controller $\mathbf{G}_{c4}$ (linear MPC). The rate of change constraints on the inputs are also never violated by an active controller, with maximum changes between sampling periods of 38.7 and 46.3 m^3/h for q_i and q_w respectively. The spikes seen in the density ρ correspond with the step changes in the input feed density ρ_i as seen in Fig. 6.1.

Figs. 6.5 and 6.6 show the outputs simulated by the platform on the plant model (no plant model mismatch) for each of the six controllers. It can be seen in Fig. 6.5 that the response in density ρ is fairly similar for all controllers with the magnitude of the spikes in the MPC controllers slightly larger than those of the other feedback controllers. It can be seen in Fig. 6.5 that all controllers keep the level constant when controlling the perfect plant model except the local controller $\mathbf{G}_{c\_local}$ which performs very poorly in terms of level control. It can also be seen that the $\mathcal{H}_\infty$ controller performs poorly when recovering from a situation where the constraints are violated. Fig. 6.6 shows that all controllers keep the level constant when controlling the perfect plant model except the local controller $\mathbf{G}_{c\_local}$ which performs very poorly in terms of level control.

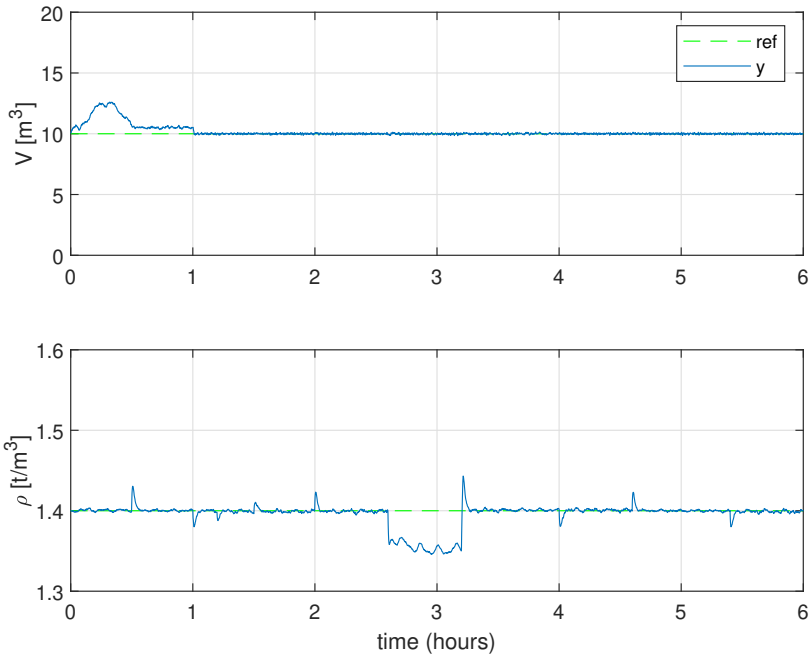

Figure 6.2. Plant outputs.

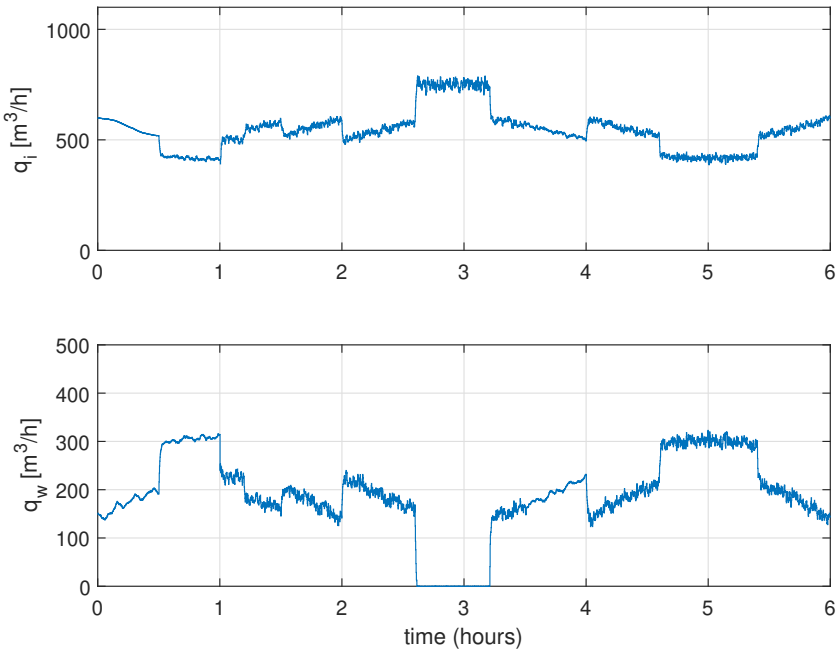

Figure 6.3. Plant inputs.

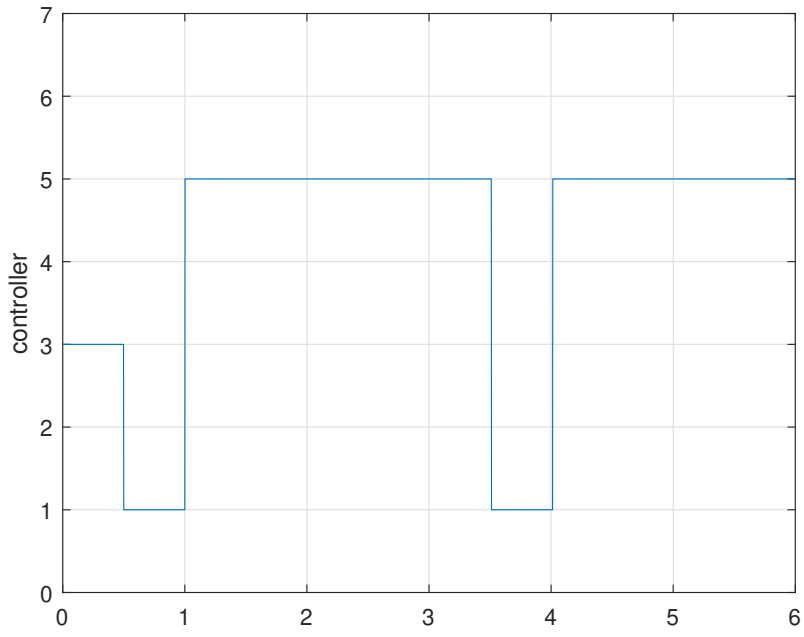

Figure 6.4. Selected controller.

Table 4.2 shows the SSE_i according to (5.3) achieved in the tank volume v and output density ρ as well as the total weighted SSE_{tot} according to (3.1) over the entire six hour simulation period for each controller acting alone for the same disturbance scenario and on the same plant with the 10% gain uncertainty in the input water flow rate q_w. It can be seen that the difference in performance in terms of the density ρ between the different controllers is not very large with a 5% difference between the best and worst controllers.

There is a much bigger discrepancy in terms of the volume v, with the local controller $\mathbf{G}_{c\_local}$ performing extremely poorly and the MPC controllers performing the best by a large margin. In terms of the weighted overall performance, the nonlinear MPC controller $\mathbf{G}_{c_5}$ is the best, outperforming the linear MPC controller $\mathbf{G}_{c_4}$ by only a narrow margin. It can also be seen that a drastic improvement in performance has been achieved through the use of the platform providing the plant access to the better performing controllers.

Table 6.1. Controller performance indices with the platform and for each individual controller acting alone

	SSE_ρ	SSE_v	SSE_{tot}
No Platform ($\mathbf{G}_{c\_local}$)	0.7012	5.258e4	53.28
With Platform	0.6747	826.3	1.501
Inverse Controller ($\mathbf{G}_{c1}$)	0.6664	155.5	0.8219
Mod. Inverse Controller ($\mathbf{G}_{c2}$)	0.6714	25.00	0.6964
$\mathcal{H}_\infty$ Controller ($\mathbf{G}_{c3}$)	2.298	205.0	2.503
Linear MPC Controller ($\mathbf{G}_{c4}$)	0.6717	7.337	0.6790
Nonlinear MPC Controller ($\mathbf{G}_{c5}$)	0.6711	7.605	0.6787

It is evident from Fig. 6.4 that the selector has chosen the linear MPC controller for the majority of the time, where Table 6.1 indicates that the nonlinear MPC controller would have performed better (although very marginally). This can be explained with the help of Table 6.2 which shows the SSE_{tot} determined by the platform from the simulation of each controller on the plant model.

It can be seen in this table that the linear MPC controller marginally outperforms the nonlinear MPC controller, with the performance measure almost equal over some evaluation periods. This can be attributed to the fact that the disturbance estimates in the observer play a major role in the disturbance

rejection properties of the controller, and since both controllers use the same linear observer, their performance is similar.

There is therefore a minor discrepancy in these results between the theoretical performance determined by the selector and the results of the actual simulation in the presence of plant model mismatch. This presents a potential difficulty for this platform philosophy in that plant model mismatch is always present in practice and would be difficult to factor into the decision made by the selector, but in this case, the effect is negligible as the performance of the linear and nonlinear MPC controllers differ by a negligible amount.

Table 6.2. Controller performance indices for each individual controller over each evaluation horizon N_e. The best performance in each row is highlighted.

N_e (hours)	$\mathbf{G}_{c\_local}$ (PI)	$\mathbf{G}_{c1}$ (Inv.)	$\mathbf{G}_{c2}$ (Mod Inv)	$\mathbf{G}_{c3}$ ($\mathcal{H}_\infty$)	$\mathbf{G}_{c4}$ (LMPC)	$\mathbf{G}_{c5}$ (NMPC)
0 - 0.5	7.444e-1	6.693e-4	6.693e-4	6.984e-4	7.822e-4	9.060e-4
0.5 - 1	6.916	6.190e-3	6.190e-3	6.769e-3	5.370e-3	5.443e-3
1 - 1.5	3.716	6.154e-3	6.154e-3	6.483e-3	5.572e-3	5.612e-3
1.5 - 2	2.612	3.247e-3	3.247e-3	3.792e-3	3.207e-3	3.759e-3
2 - 2.5	7.876	4.016e-3	4.016e-3	3.922e-3	3.567e-3	3.573e-3
2.5 - 3	7.029e-1	4.064e-1	4.064e-1	4.206e-1	4.038e-1	4.057e-1
3 - 3.5	9.352e-1	2.275e-1	2.275e-1	1.462	2.369e-1	2.369e-1
3.5 - 4	4.588e-1	2.670e-3	2.670e-3	3.181e-3	2.595e-3	2.960e-3
4 - 4.5	5.401	2.872e-3	2.872e-3	2.670e-3	2.645e-3	2.645e-3
4.5 - 5	3.668	5.079e-3	5.079e-3	5.563e-3	4.479e-3	4.479e-3
5 - 5.5	2.787	4.658e-3	4.658e-3	4.910e-3	4.206e-3	4.206e-3
5.5 - 6	3.859	4.941e-4	4.941e-4	4.936e-4	6.255e-4	6.278e-4

Figs. 6.7 - 6.18 show the plant response as well as the control inputs generated for each of the six controllers acting alone on the plant for the same disturbance scenario as depicted in Fig. 6.1 with the 10 % gain uncertainty in the input water flow rate q_w. These responses are practically indistinguishable from the responses simulated by the platform, the outputs of which are shown in Figs. 6.5 and 6.6.

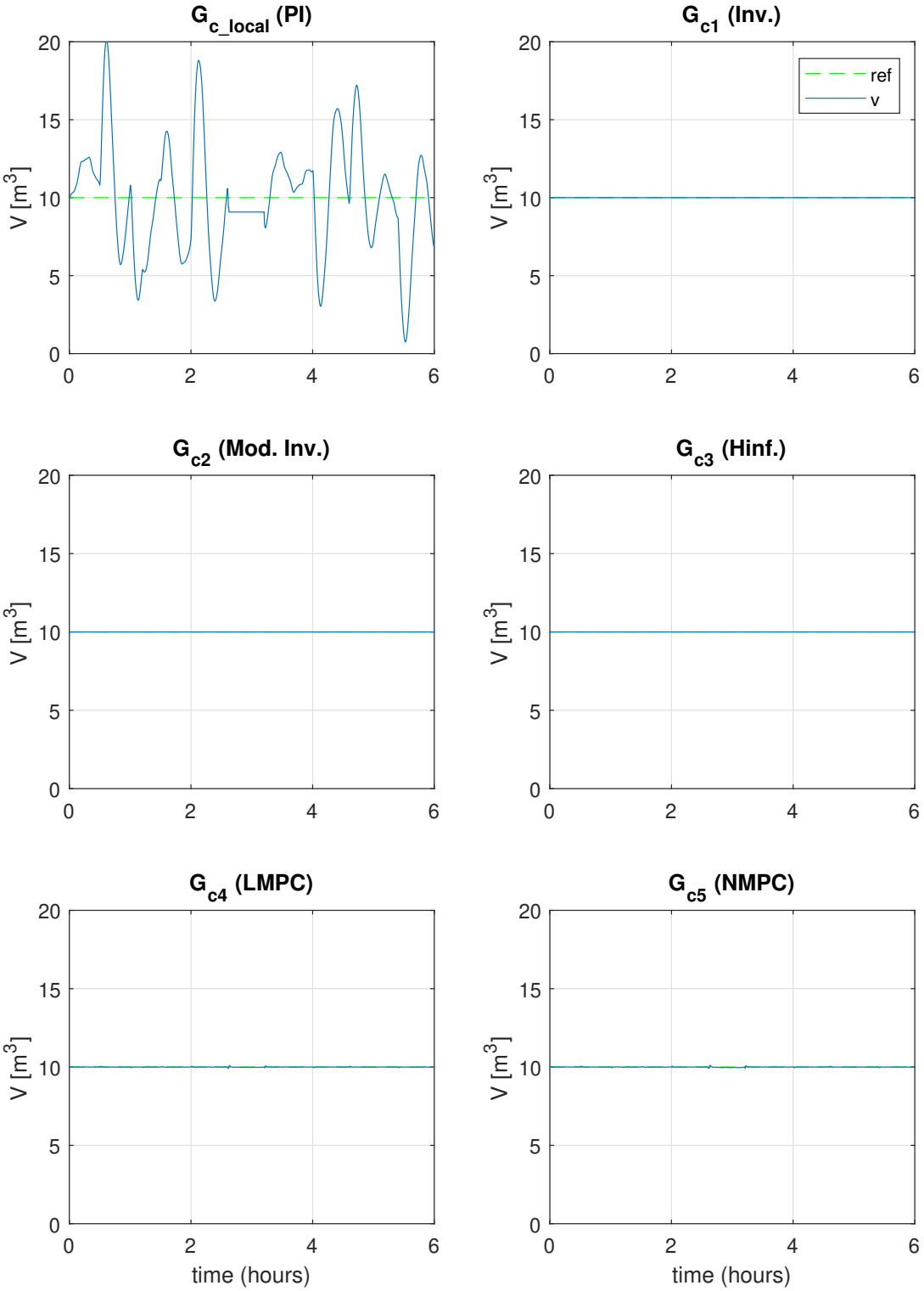

Figure 6.5. Selector simulations - output density ρ.

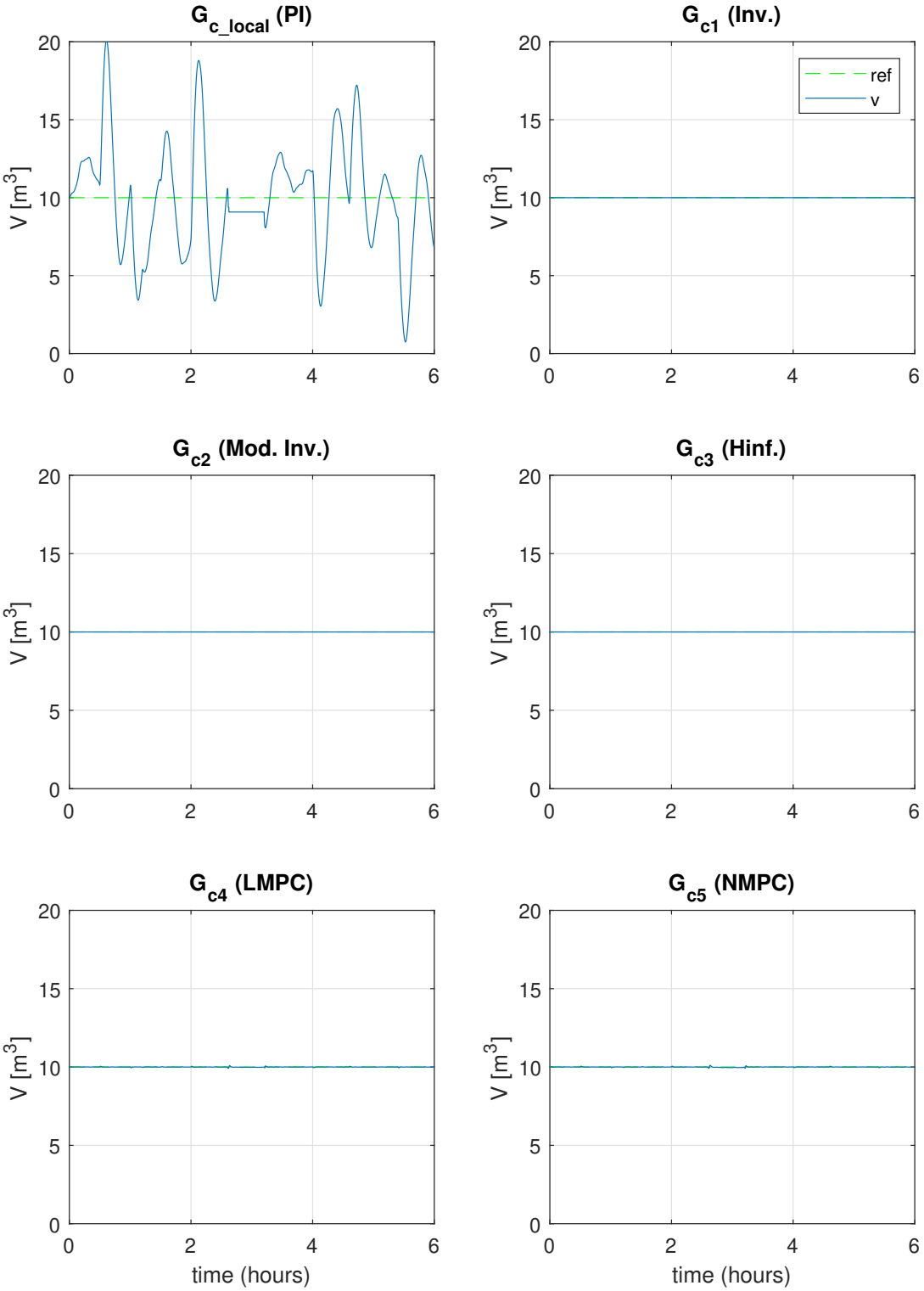

Figure 6.6. Selector simulations - tank volume *v*.

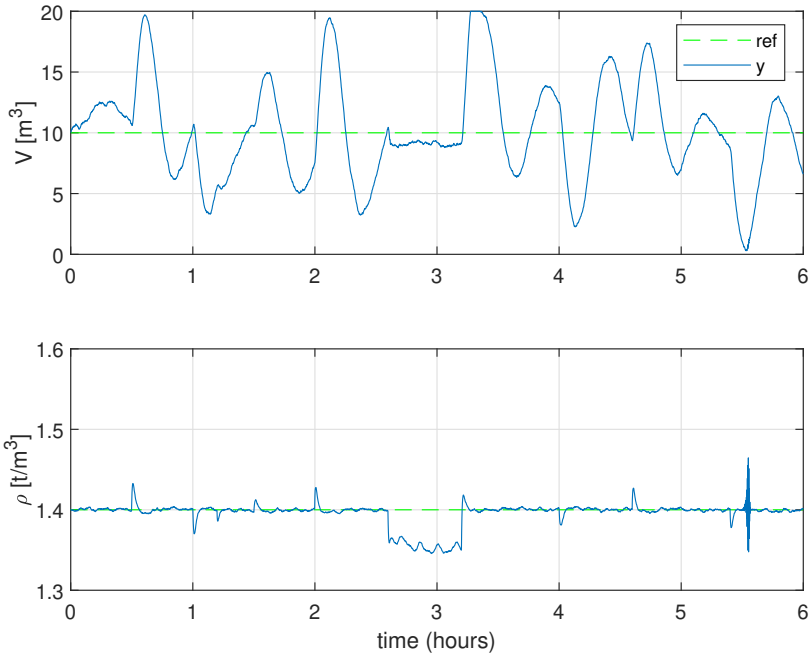

Figure 6.7. Decentralised PI controller ($\mathbf{G}_{c\_local}$) - plant outputs.

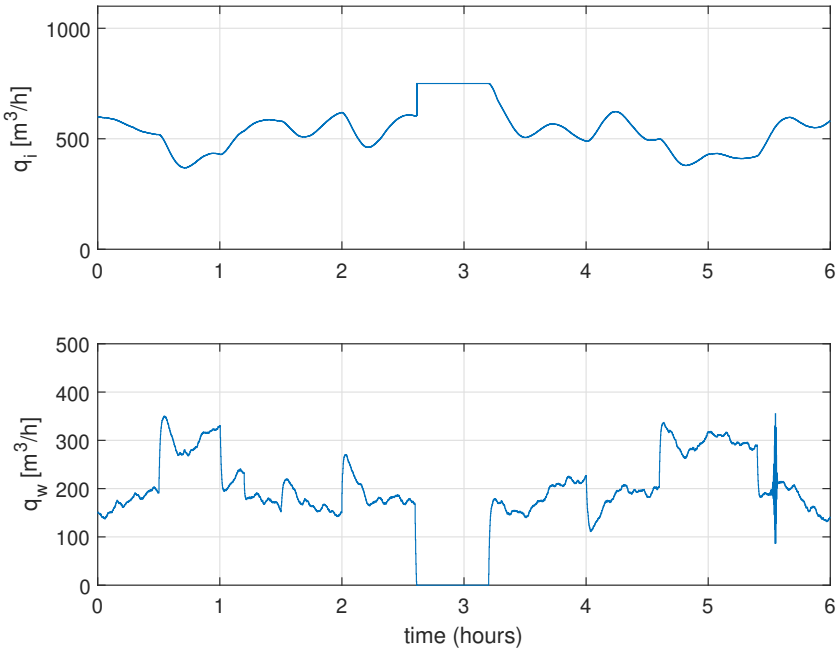

Figure 6.8. Decentralised PI controller ($\mathbf{G}_{c\_local}$) - plant inputs.

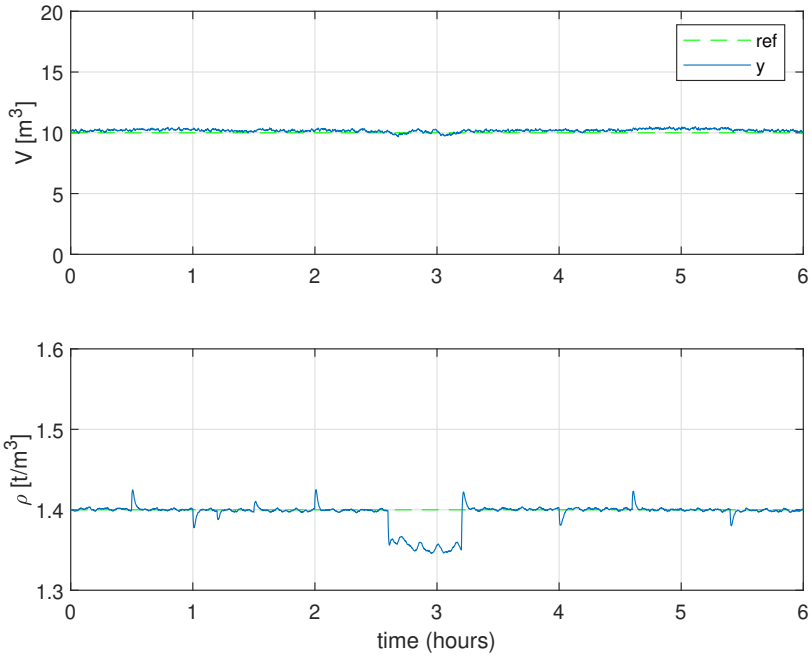

Figure 6.9. Inverse controller ($\mathbf{G}_{c1}$) - plant outputs.

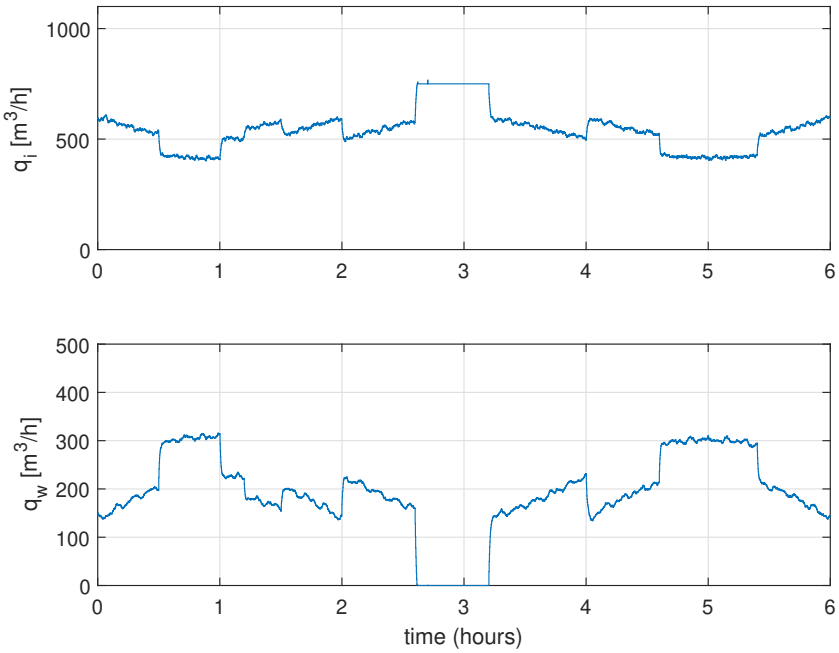

Figure 6.10. Inverse controller ($\mathbf{G}_{c1}$) - plant inputs.

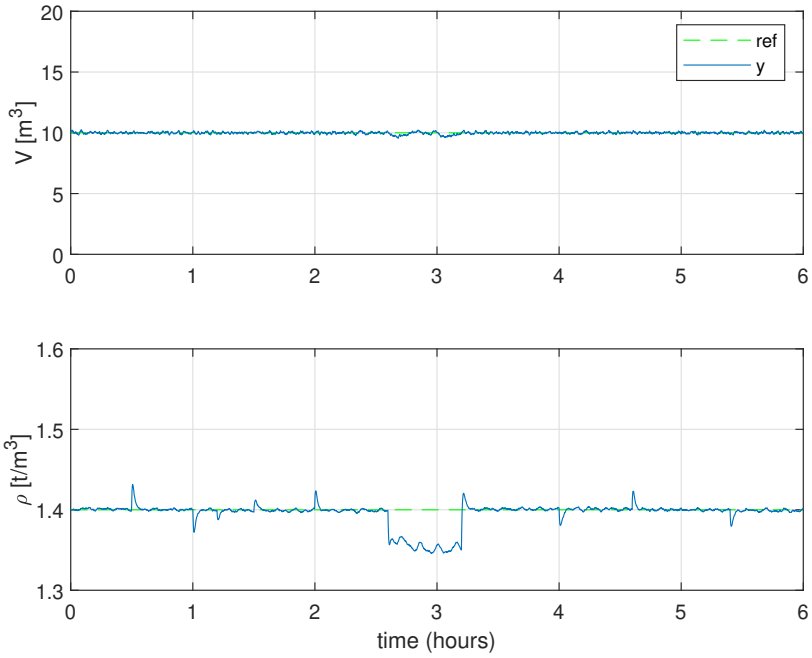

Figure 6.11. Modified inverse controller ($\mathbf{G}_{c2}$) - plant outputs.

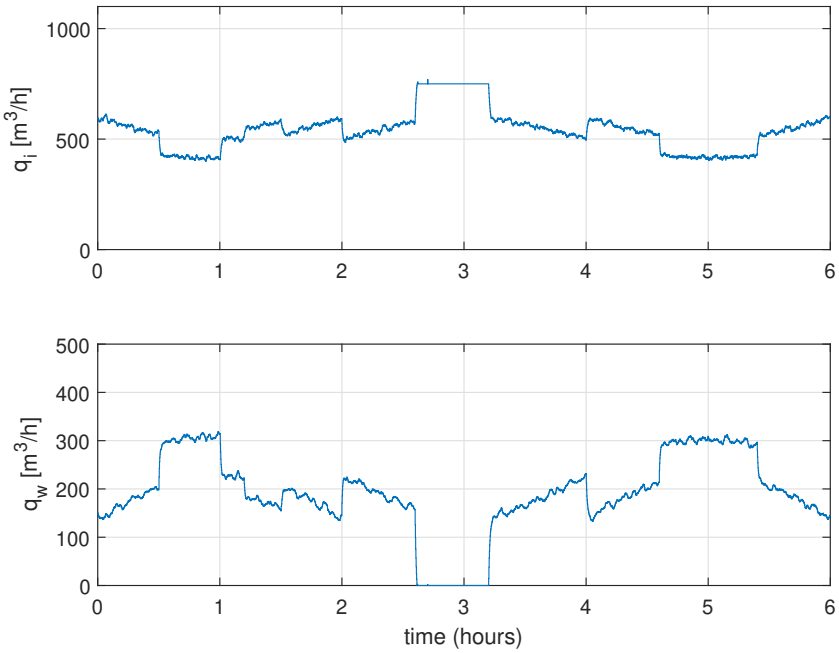

Figure 6.12. Modified inverse controller ($\mathbf{G}_{c2}$) - plant inputs.

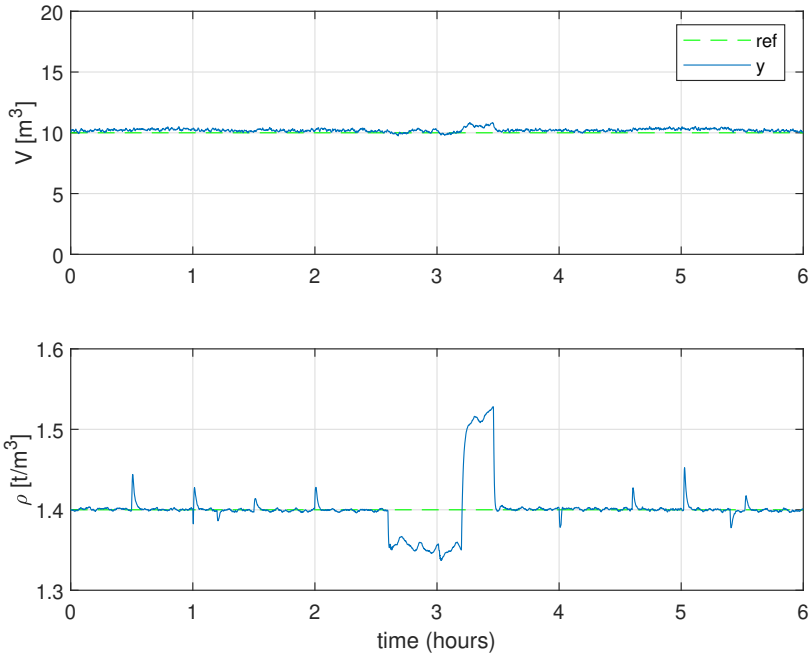

Figure 6.13. $\mathcal{H}_\infty$ controller ($\mathbf{G}_{c3}$) - plant outputs.

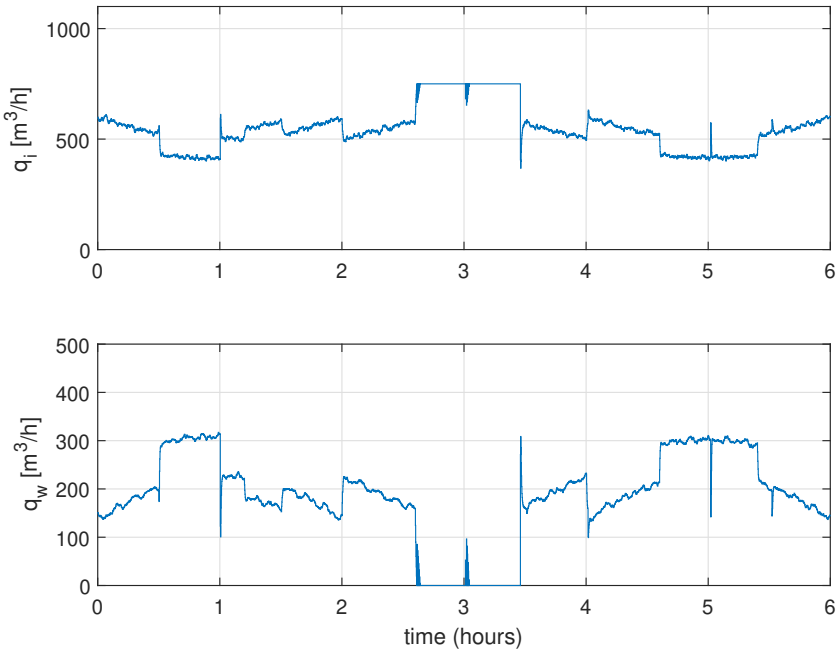

Figure 6.14. $\mathcal{H}_\infty$ controller ($\mathbf{G}_{c3}$) - plant inputs.

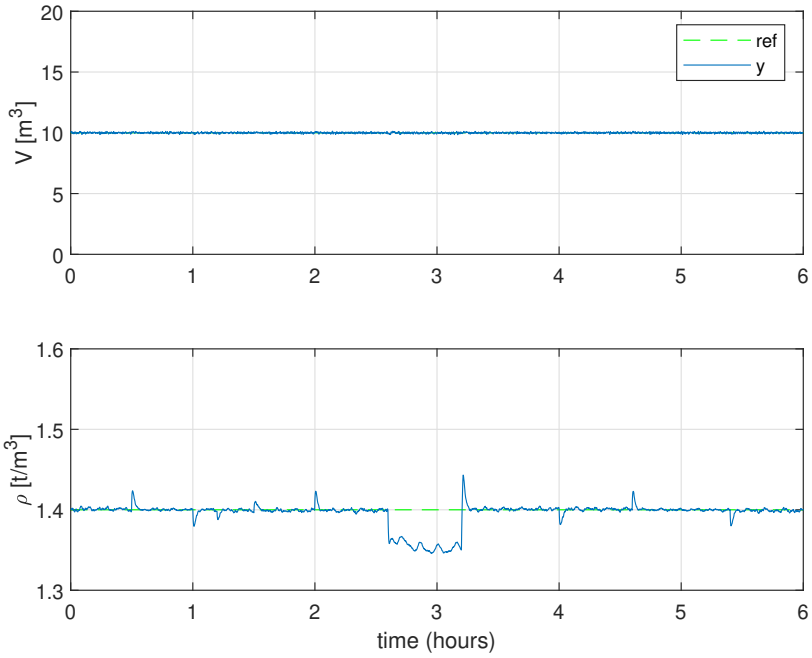

Figure 6.15. Linear MPC controller ($\mathbf{G}_{c4}$) - plant outputs.

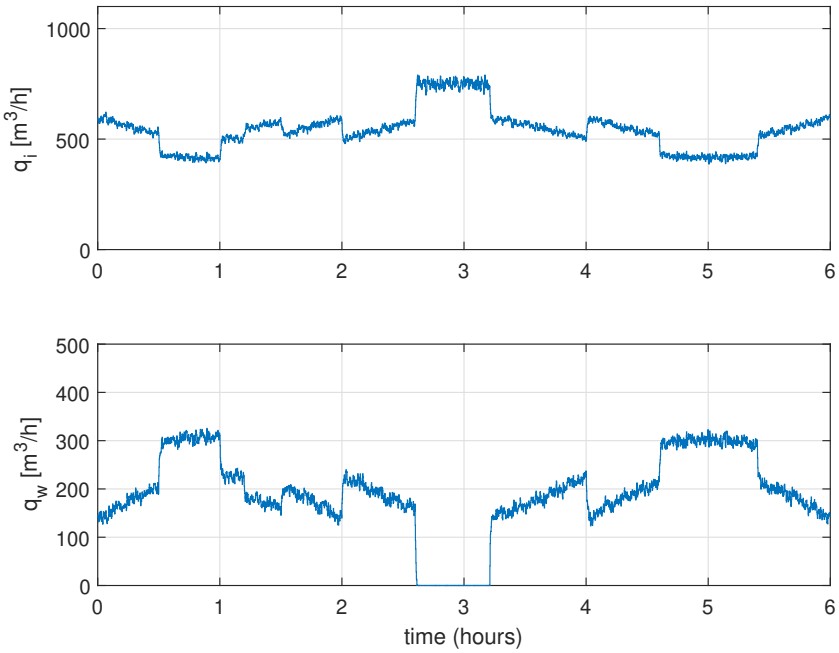

Figure 6.16. Linear MPC controller ($\mathbf{G}_{c4}$) - plant inputs.

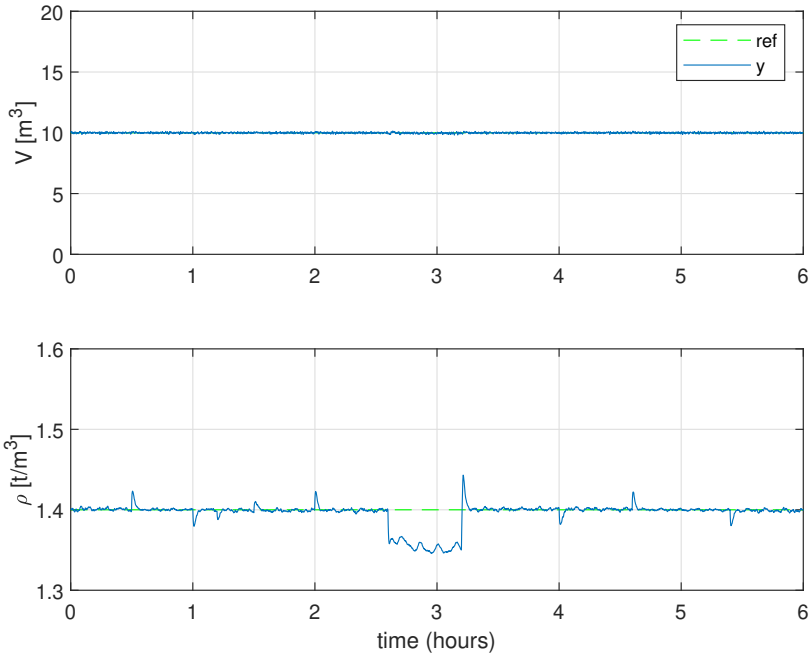

Figure 6.17. Nonlinear MPC controller ($\mathbf{G}_{c5}$) - plant outputs.

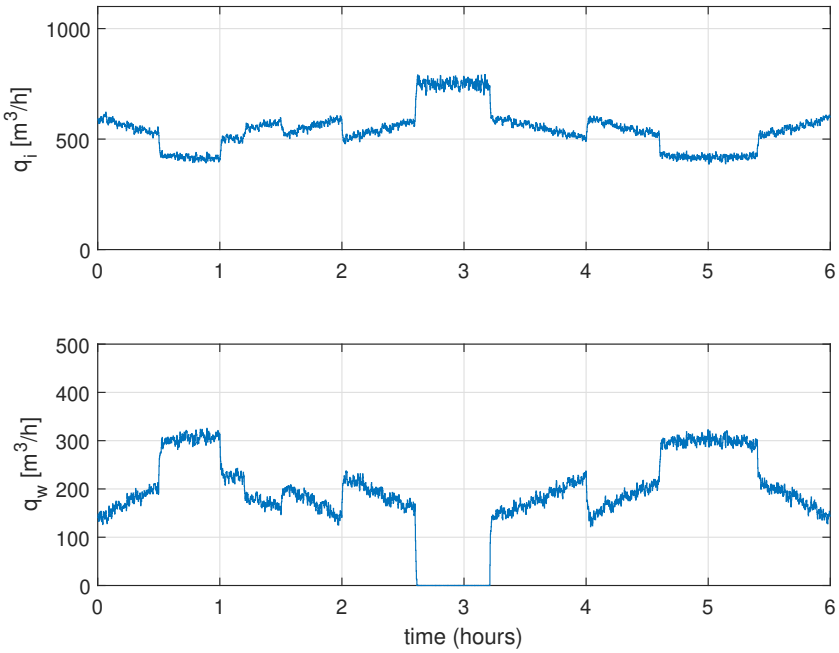

Figure 6.18. Nonlinear MPC controller ($\mathbf{G}_{c5}$) - plant inputs.

6.4 CONCLUSION

A simulation of the platform described in Chapter 3 to facilitate the competition between various controllers has been presented with the six controllers competing to control the surge tank process. It was shown that a drastic improvement in performance can be achieved by more sophisticated techniques with the linear MPC controller being awarded control of the plant for the majority of the simulation. It was also shown that the nonlinear MPC controller would have provided superior performance, but due to the plant model mismatch that was introduced, the linear MPC controller was selected due to the superior performance it provided when controlling the accurate plant model.

In this case, where the de-coupled PI controller is the locally employed controller ($\mathbf{G}_{c\_local}$ in Fig. 3.3), the platform presented will facilitate the access to more advanced controllers, allowing for significantly improved performance to be achieved without the need for directly procuring the services of a large vendor.

CHAPTER 7 CONCLUSION

The following conclusions can be made with respect to the initial hypotheses:

- The hypothesis that the performance measure proposed in [15] cannot give an accurate measure of system performance was confirmed. It was shown that this method can select an unstable controller in the presence of a stable well-tuned controller. This is due, not to the performance index used to determine the optimal controller, but the fact that one step ahead predictions are used to obtain a measure of controller performance. This is not possible with the use of one step ahead predictions and it was concluded that the controller would need to be simulated over a period of time on the plant model to obtain a measure of controller performance.
- For the controllers to develop a control solution it is obvious that the controllers will need the same information about the plant that any control vendor would need. This is a critical issue as a large part of the development of a control solution consists of system identification and modelling and other practical issues such as determining actuator and sensor limitations, input and output constraints and the expected degree of plant model mismatch. The development of the controller is thus only a small part of the process and can be done in isolation from the physical plant if all the process related information is available. It would thus be feasible for the controllers to be in remote locations and develop independent control solutions to be evaluated by the selector using a plant model. Another issue in this regard is the fact that in order for the selector to simulate the controllers, it is necessary for a measurement of all possible disturbances, or at least estimates thereof to be made available.
- It was shown that there are cases where the system performance can be improved in the case were there is a constraint in the rate of change in the input, where a more aggressive controller can be selected so long as the disturbance or reference changes do not cause the controller to

violate this input constraint. This means that switching back to a less aggressive controller is necessary in the event that the controller attempts to violate the constraint.

- A detailed nonlinear model of Sibanye-Stillwater's Platinum tailings treatment plant was derived, linearised and an input-output controllability analysis performed. Six controllers were developed for the process, including four conventional feedback and two MPC controllers. It was shown that both the inverse based and $\mathcal{H}_\infty$ controllers fail to control the tank level to set-point in the event of an unmeasured disturbance. The competing controller platform concept was successfully illustrated on this process with the linear MPC controller being the most often selected controller. It was shown that for this process, the presented platform will facilitate the access to more advanced controllers.

Overall it can be concluded that it is possible to implement a platform where controllers compete to control a process, provided the necessary information as discussed is made available to the controllers and selector. The proposed platform has been shown to work in simulation on the tailings treatments surge tank process. It was shown that the platform facilitates a significant improvement in process performance without the need for directly procuring the services of a large vendor, opening up the industrial control sector to an access economy and service based model of operation.

REFERENCES

[1] G.M. Eckhardt, F. Bardhi, "The Sharing Economy isn't About Sharing at All". [Online] Available: https://hbr.org/2015/01/the-sharing-economu-isnt-about-sharing-at-all, 2015, [October 18 2019].

[2] K. Frenken, "Political economies and environmental futures for the sharing economy", *Philosophical Transactions. Series A, Mathematical, Physical, and Engineering Sciences*, vol. 375, no. 2095, 2017, https://doi.org/10.1098/rsta. 2016.0367.

[3] A. Rahman, R. Mamunur, S. Hossain, E. Hassanain, M.F. Alhamid, M. Guizani, "Blockchain and IoT-Based Cognitive Edge Framework for Sharing Economy Services in a Smart City", *IEEE Open Access*, vol. 7, 2019, pp. 18611-18621.

[4] M.O. Pahl, "Multi-tenant IoT service management towards an IoT app economy", *in HotNSM workshop at the International Symposium on Integrated Network Management (IM)*, Washington DC, USA, 2019.

[5] S. Huckle, M. Bhattacharua, M. White, N. Beloff, "Internet of things, blockchain and shared economy applications", *Procedia Computer Science*, vol. 98, 2016, pp. 461-466.

[6] S. Gershon, "Control in the cloud: Trends in cloud computing and their impact on the world of industrial control". [Online] Available: http://emea.rockwellautomation.com/downloads/Cloud%20Control.pdf, 2013 [March 25, 2018].

[7] R. Drath, A. Horch, "Industrie 4.0: Hit or Hype?", *IEEE Industrial Electronics Magazine*, vol. 8, no.2, 2014, pp. 56-58.

[8] Reali Technologies LTD., “RealiteQ a New (Fourth) Generation of SCADA system”. [Online] Available: http://www.realiteq.com/technologu, 2018 [March 25, 2018].

[9] O. Givehchi, J. Imtiaz, H. Trsek, J. Jasperneite, “Control-as-a-service from the cloud: A case study for using virtualised PLCs”, in *Proc. of IEEE Workshop on Factory Communication Systems (WFCS’14)*, Toulouse, France, May 2014, pp. 1–4.

[10] T. Goldschmidt, M. Murugaiah, C. Sonntag, B. Schlich, S. Biallas, P. Weber, “Cloud-based control: A multi-tenant, horizontally scalable soft-PLC”, in *Proc. of IEEE International Conference on Cloud Computing (CLOUD’15)*, New York, USA, June 2015, pp. 909–916.

[11] T. Hegazy, M. Hefeeda, “Industrial Automation as a cloud service”, *IEEE Transactions on Parallel and Distributed Systems*, vol. 26, no. 10, pp. 2750–2763, Oct. 2015.

[12] A.E. Abdelaal, T. Hegazy, M. Hefeeda, “Event-based control as a cloud service”, in *Proc. 2017 American Control Conference*, Seattle, USA, May 2017.

[13] Y. Xia. “From networked control systems to cloud control systems”. in *Proc. 31st Chinese Control Conference*. Kunming, China, 2012. pp. 5878-5883.

[14] Y. Xia, “Cloud control systems”, *Automatica Sinica*, vol. 2, no. 2, pp. 134–142, April 2015.

[15] L.E. Olivier, “Process automation with competitive controllers”. Report, University of Pretoria, South Africa, Aug. 2017.

[16] Y. Xia , W. Xie, B. Liu, X.Y. Wang. "Data-driven predictive control for networked control systems". *Information Science*, vol. 235, no. 20, pp. 45-54, 2013.

[17] H. Wade. *Basic and Advanced Regulatory Control: System Design and Application*, Research Triangle Park, NC, USA: ISA, 2004, pp. 130-132.

[18] S. Yang, X. Chen, L. Tan, L. Yang, “Time delay and data loss compensation for internet-based process control systems”, *Transactions of the Institute of Measurement and Control*, vol. 27, no. 2,

pp. 103–118, Jun. 2012.

[19] O. Smith, “Closer control of loops with dead time”, *Chemical Engineering Progress*, vol. 53, no. 5, pp. 217–219, May 1957.

[20] K. J. Åström, B. Wittenmark, *Computer Controlled Systems: Theory and Design*, Upper Saddle River, NJ: Prentice Hall, 1997.

[21] R. A. Gupta, M.Y. Chow, “Networked control systems: overview and research trends”, *IEEE Transactions on Industrial Electronics*, vol. 57, no. 7, pp. 2527–2535, Jul. 2010.

[22] J. Baillieul, P.J. Antsaklis, “Control and communication challenges in networked real-time systems”, *Proceedings of the IEEE*, vol. 95, no. 1, pp. 9–28, Jan. 2007.

[23] J. Nilsson, B. Bernhardsson, and B. Wittenmark, “Stochastic analysis and control of real-time systems with random time delays”, *Automatica*, vol. 34, no. 1, pp. 57–64, Jan. 1998.

[24] F. Goktas, J. M. Smith, and R. Bajcsy, “μ-synthesis for distributed control systems with network-induced delays,” in *Proc. 35th IEEE Conf. Decision Control*, 1996, pp. 813–814.

[25] K.J. Åström, R.M. Murray, *Control System Design*, Princeton, NJ: Princeton University Press, 2010.

[26] D.E. Seborg , T.F. Edgar, D.A. Mellichamp, F.J. Doyle, *Process Dynamics and Control*, Hoboken, NJ: John Wiley and Sons, 2011.

[27] S. Skogestad, I. Postlethwaite, *Multi-variable Feedback Control: Analysis and Design*, Hoboken, NJ: John Wiley and Sons, 2005.

[28] I.K. Craig, "Multivariable Control System Design", Class handout for course EMB 732, July 2018.

[29] K.J. Åström, T. Hägglund, “The future of PID control”, *Control Engineering Practice*, vol. 9, pp. 1163-1175, Apr. 2001.

[30] K.J. Åström, T. Hägglund, “Automatic tuning of simple regulators with specifications on phase and amplitude margins,” *Automatica*, vol. 20, no. 5, pp. 645-651, Sept. 1984.

[31] J. Berner, K. Soltesz, T. Hägglund, K.J. Åström, “An experimental comparison of PID autotuners”, *Control Engineering Practice*, vol. 73, pp. 124-133, 2018.

[32] S. Skogestad, "Simple analytic rules for model reduction and PID controller tuning," *Journal of Process Control*, vol. 13, no. 4, pp. 291–309, 2003.

[33] K. Zhou, J.C. Doule, K. Glover, *Robust and Optimal Control*, New York: Prentice-Hall, 1995.

[34] M. Green, D. J. N. Limebeer, *Linear Robust Control*. Englewood Cliffs, NJ: Prentice-Hall, 1995.

[35] M.G. Forbes, R.S. Patwardhan, H. Hamadah, R.B. Gopaluni, “Model Predictive Control in Industry: Challenges and Opportunities”, in *Proc. 9th International Symposium on Advanced Control of Chemical Processes*, British Colombia, Canada, June 2015.

[36] E. F. Camacho, C. Bordons, *Model Predictive Control*. New York: Springer-Verlag, 1999.

[37] D.Q. Mayne, J.B. Rawlings, C.V. Rao, P.O.M. Scokaert, "Constrained model predictive control: Stability and optimality", *Automatica*, vol. 36, pp. 789-814, 2000.

[38] D.Q. Mayne, *Model Predictive Control: Theory and Design*. Madison WI: Nob Hill, 2009.

[39] D.Q. Mayne, "Model predictive control: Recent developments and future promise," *Automatica*, vol. 50, pp. 2967-2986, 2014.

[40] L.E. Olivier, B. Huang, I.K. Craig, "Dual particle filters for state and parameter estimation with application to a run-of-mine ore mill", *Journal of Process Control*, vol. 22, no. 4, pp. 710–717,

2012.

[41] E.S Meadows, J.B. Rawlings (2005). *CACHE Virtual Process Control Book Ch5*, [Online], Available: https://cse.sc.edu/ gatzke/cache/npc-Chapter5-scan.pdf.

[42] D.E. Kirk. *Optimal Control Theory, An Introduction*. Mineola, New York: Dover Publications Inc, 1970.

[43] D. Liberzon, *Switching in Systems and Control*, Boston, MA: Birkhauser, 2003.

[44] D. Liberzon, A.S. Morse, “Basic problems in stability and design of switched system”, *IEEE Control Systems Magazine*, vol. 19, no. 5, pp. 59–70, Oct. 1999.

[45] D.J. Leith, R.N. Shorten, W.E. Leithead, O. Mason, P. Curran, “Issues in the design of switched linear control system: A benchmark study”, *Int. Journal of Adaptive Control and Signal Processing*, vol. 17, pp. 103-108, 2003.

[46] J. Malmborg, B. Bernhardsson and K. J. Åström, "A stabilizing switching scheme for multi controller systems", in *Proc. 13th IFAC World Congress*, vol. F, pp. 229-234, 1996.

[47] M. S. Branicky, “Multiple Lyapunov functions and other analysis tools for switched and hybrid systems”, *IEEE Transactions on Automatic Control*, vol. 43, no. 4, pp. 475–482, Apr. 1998.

[48] H. Lin, P.J. Antsaklis, "Stability and stabilizability of switched linear systems: a survey of recent results", *IEEE Transactions on Automatic control*, vol. 54, no. 2, pp. 308-322, 2009.

[49] J. P. Hespanha and A. S. Morse, “Stability of switched systems with average dwell-time”, in *Proc. 38th IEEE Conf.Decision Control*, 1999, pp. 2655–2660.

[50] A. S. Morse, "Supervisory control of families of linear set-point controllers, part 1: Exact matching", *IEEE Transactions on Automatic control*, vol. 41, no. 10, pp. 1413-1431, 1996

[51] J. Hocherman-Frommer, S. R. Kulkarni, P. J. Ramadge, "Controller switching based on output prediction errors", *IEEE Transactions on Automatic control*, vol. 43, no. 5, pp. 596-607, 1998.

[52] J.J. Burchell, I.K. Craig, "Dynamic Modelling, Simulation and Control of a Tailings Treatment Surge Tank," presented at *18th IFAC Symposium on Control, Optimization and Automation in Mining, Mineral and Metal Processing*, Stellenbosch, South Africa, 28-30 Aug. 2019.

[53] P. Lundström, *Studies on Robust Multivariable Distillation Control*, PhD thesis, Norwegian University of Science and Technology, Trondheim, 1994.

[54] J.C. Doyle, "Analysis of Feedback Systems with Structured Uncertainties", *Proceedings of the IEEE*, vol. 129, no. 6, pp. 242 - 250, 1982.

ADDENDUM A INITIAL SWITCHING PHILOSOPHY

A.1 OVERVIEW

This addendum analyses the performance index used as the switching criteria in [15], and a slightly modified version is presented is Section A.2. Simulations are presented in Section A.3 which show that the criterion presented in [15] cannot accurately determine the performance of a given controller and may even select an unstable controller.

A.2 SWITCHING CRITERION AND PERFORMANCE INDEX

The performance measure which was initially proposed in [15] is described as follows: the sum of the squared errors (SSE) between the desired output and the predicted output, had the input of that particular controller been selected at the previous time step, is calculated over a predetermined evaluation horizon; the controller yielding the smallest sum is selected. This can be expressed as:

$$\min_{i} \quad SSE_i = \sum_{j=k-N_e+1}^{k} (\mathbf{r}(j) - \hat{\mathbf{y}}_i(j))^T \mathbf{W}_e (\mathbf{r}(j) - \hat{\mathbf{y}}_i(j)), \tag{A.1}$$

where k is the present time step, N_e is the evaluation horizon, $\mathbf{r}(j)$ is the desired plant output, $\hat{\mathbf{y}}_i(j)$ is the predicted value of the plant output at time step j had the control input of controller i been applied at the previous time step $j-1$, and $\mathbf{W}_e$ is a positive semi-definite weighting matrix. The predicted outputs are calculated using the discrete time state-space model of the plant:

$$\hat{\mathbf{x}}_i(j) = \mathbf{A}\mathbf{x}_i(j-1) + \mathbf{B}\mathbf{u}_i(j-1) \tag{A.2}$$

$$\hat{\mathbf{y}}_i(j) = \mathbf{C}\hat{\mathbf{x}}_i(j), \tag{A.3}$$

where **A**, **B** and **C** are the system matrices [15]. Switching between controllers is specified to take place if an unselected controller yields a smaller *SSE* than the selected controller, minus a small constant or switching margin:

$$SSE_i < SSE_j - e \tag{A.4}$$

The switching margin e is necessary to prevent frequent switching between controllers.

This performance index was modified slightly to incorporate one step ahead predictions at the present sampling instant, as well as a term which penalises the change in the inputs between time steps (i.e. $\Delta\mathbf{u}$). This can be expressed as:

$$\min_i J_i = \sum_{j=k-N_e+1}^{k} [(\mathbf{r}(j) - \hat{\mathbf{y}}_i(j+1))^T \mathbf{W}_e (\mathbf{r}(j) - \hat{\mathbf{y}}_i(j+1)) + \Delta\mathbf{u}_i(j)^T \mathbf{W}_u \Delta\mathbf{u}_i(j)] \tag{A.5}$$

where

$$\hat{\mathbf{x}}_i(j+1) = \mathbf{A}\mathbf{x}_i(j) + \mathbf{B}\mathbf{u}_i(j) \tag{A.6}$$

$$\hat{\mathbf{y}}_i(j+1) = \mathbf{C}\hat{\mathbf{x}}_i(j+1) \tag{A.7}$$

$$\Delta\mathbf{u}_i(j) = \mathbf{u}_i(j) - \mathbf{u}(j-1)) \tag{A.8}$$

and the weighting matrices $\mathbf{W}_e$ and $\mathbf{W}_u$ in (A.5) are positive semi-definite and positive definite weighting matrices respectively. The performance index is modified in order not to be as susceptible to the selection of an overly aggressive controller as the performance index in (A.1) would be.

A.3 SWITCHING SCENARIO

In this section an example is presented which shows that switching according to the performance index in (A.5) may select a controller which is unstable, even in the presence of a stable well performing controller. The plant being controlled is taken as a general second order system of the form:

$$G_p(s) = \frac{Y(s)}{U(s)} = \frac{\omega_n^2}{s^2 + 2\zeta\omega_n s + \omega_n^2} \tag{A.9}$$

where ω_n and ζ are chosen to be 1/33 and 0.33 respectively. This yields a substantially under damped plant with slow oscillations. There are assumed to be no constraints on the input or output.

Two controllers are used to compete for control of the plant, an LQT controller as presented in Section 2.3 and a PID controller. The weighting matrices $\mathbf{Q}$ and $\mathbf{R}$ in the LQT performance index in (2.68) are chosen to be 1 and $1e^{-3}$ respectively which yields a well tuned response with minimal overshoot. The PID controller is chosen to be of the form:

$$G_c(s) = \frac{U(s)}{E(s)} = \frac{k(s^2 + 2\zeta\omega_n s + \omega_n^2)}{\omega_n^2 s(s+b)} \tag{A.10}$$

This yields ideal control as discussed in Section 2.3.1 which gives the loop and closed-loop transfer functions:

$$L(s) = \frac{Y(s)}{E(s)} = \frac{k}{s^2 + bs} \tag{A.11}$$

and

$$T(s) = \frac{Y(s)}{R(s)} = \frac{k}{s^2 + bs + k}, \tag{A.12}$$

The parameters k and b can therefore be used to shape the closed-loop response. The values of k and b in (A.12) were chosen as follows:

$$k = (7\omega_n)^2$$

$$b = -2 \cdot 0.1 \cdot 7\omega_n$$

which will yield a closed-loop system with two complex poles in the right half-plane (RHP) with a small damping ratio of 0.1 and a natural frequency of 7 times that of the plant. Figs. A.1 and A.2 show the individual closed-loop responses and generated control signals for a unit step in the reference respectively. The LQT controller yields a good closed-loop response with minimal overshoot while the PID controller is tuned to yield an unstable response with large oscillations.

Figs. A.3 - A.7 show the system response, selected input, inputs generated by each controller, predictions made by each controller and the performance index J for each controller respectively. It can be seen in Fig. A.3 that when switching is performed, the unstable controller is selected for the majority of the time yielding an unstable overall response. It can be seen in Fig. A.7 that the

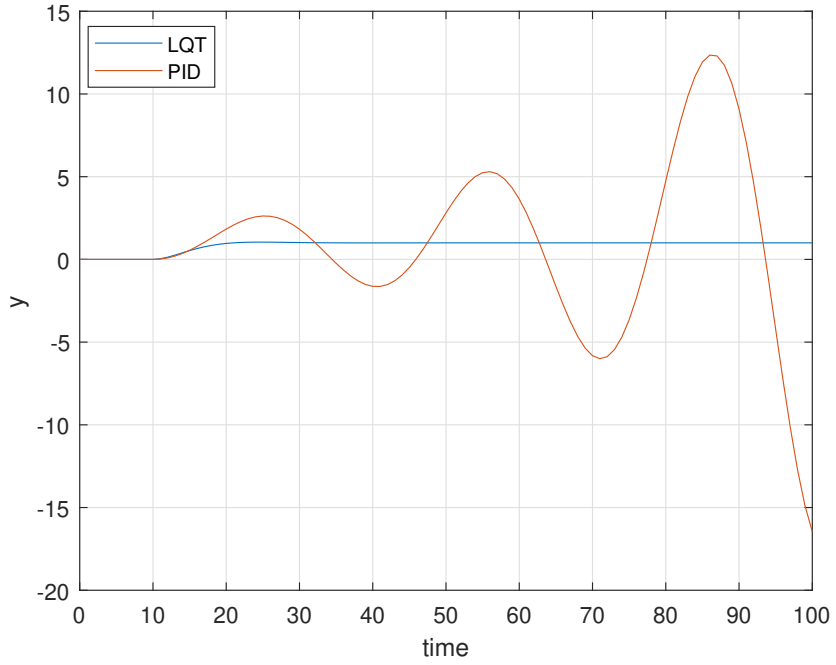

Figure A.1. Scenario 4: Process outputs for controllers acting alone

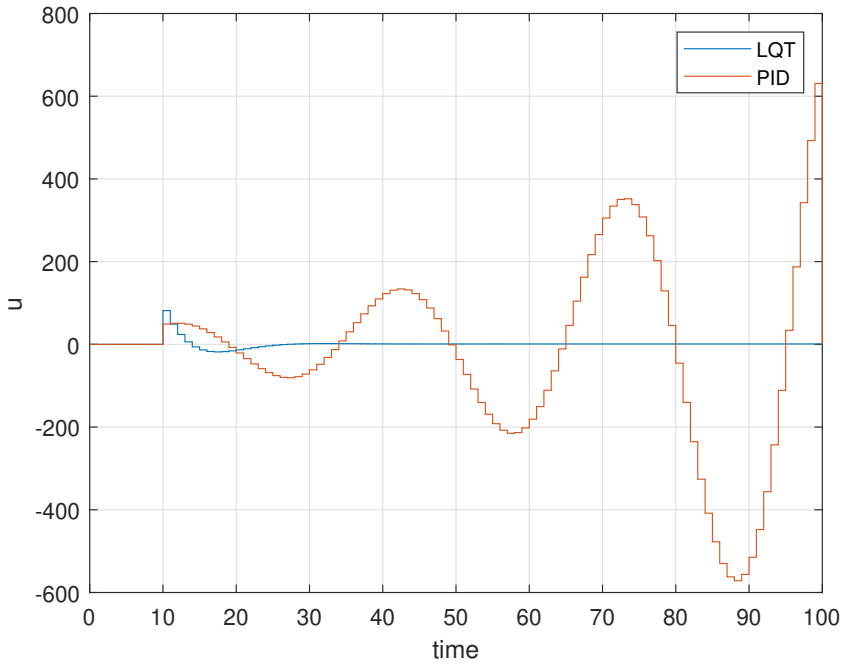

Figure A.2. Scenario 4: Process inputs for controllers acting alone

performance index J generated by the unstable controller is smaller than that generated by the LQT controller for the majority of the time. The switching margin e and evaluation horizon N_e were chosen to be 0.1 and 30 respectively, while the weighting matrices $\mathbf{W}_e$ and $\mathbf{W}_u$ were chosen to be 1 and $1e^{-4}$ respectively. Reducing this was found to have no effect on the outcome, where increasing it to a large value of 0.8 prevented the selection of the unstable controller, provided that the stable controller is selected as the initial controller.

The reason for this behaviour is attributed to the fact that doing one step ahead predictions using a plant model, based on the current state of the process and the input generated by the controller does not provide an adequate representation of the overall controller performance. This is evident from Fig. A.6 where the predictions are very much indistinguishable from the plant response in Fig. A.3.

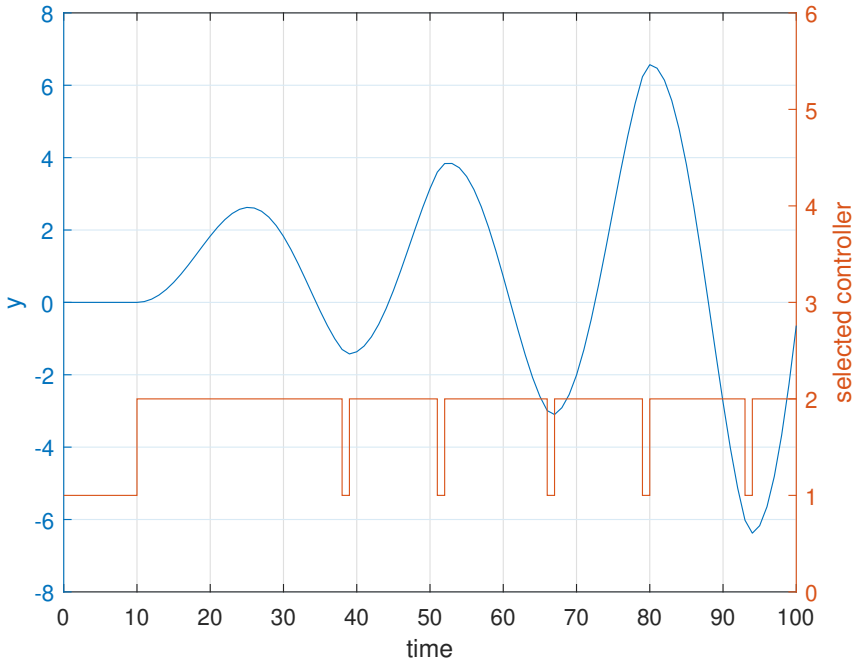

Figure A.3. Scenario 4: Process output with switching

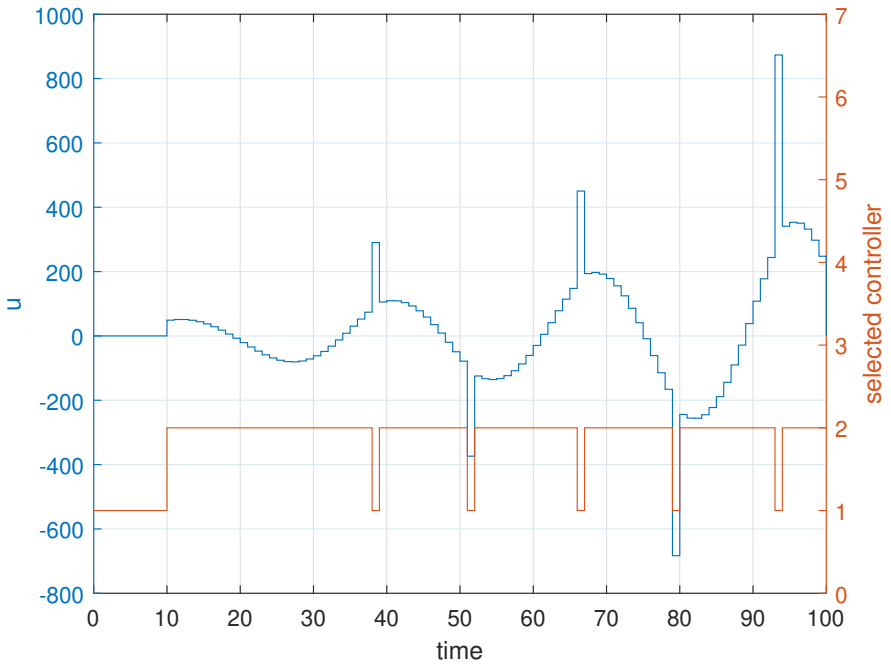

Figure A.4. Scenario 4: Process input with switching

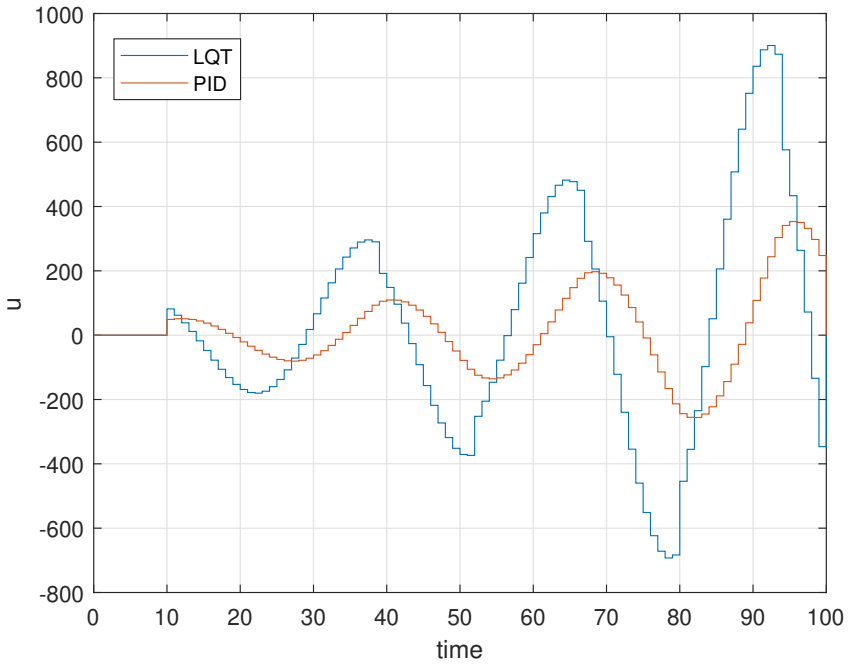

Figure A.5. Scenario 4: Control moves presented by each controller

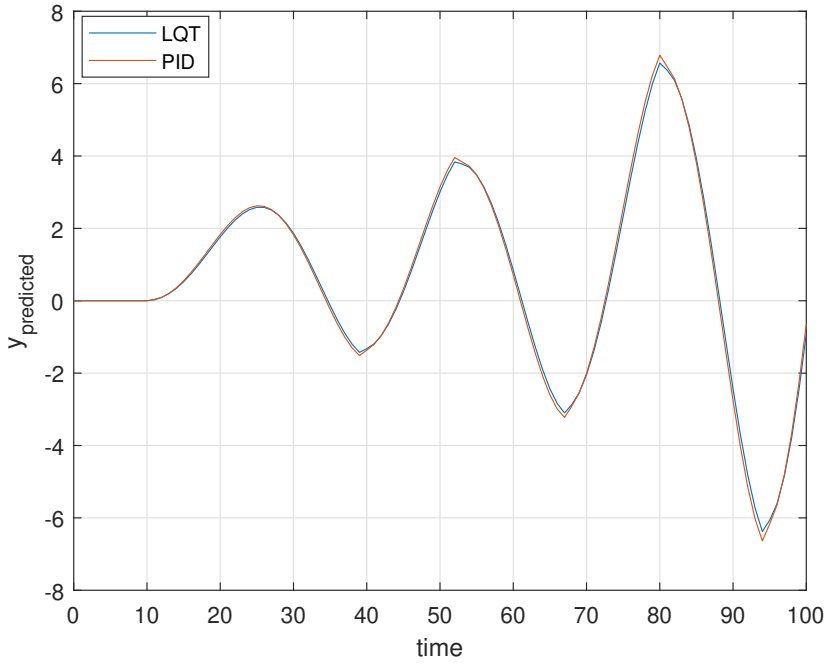

Figure A.6. Scenario 4: Predictions for each controller

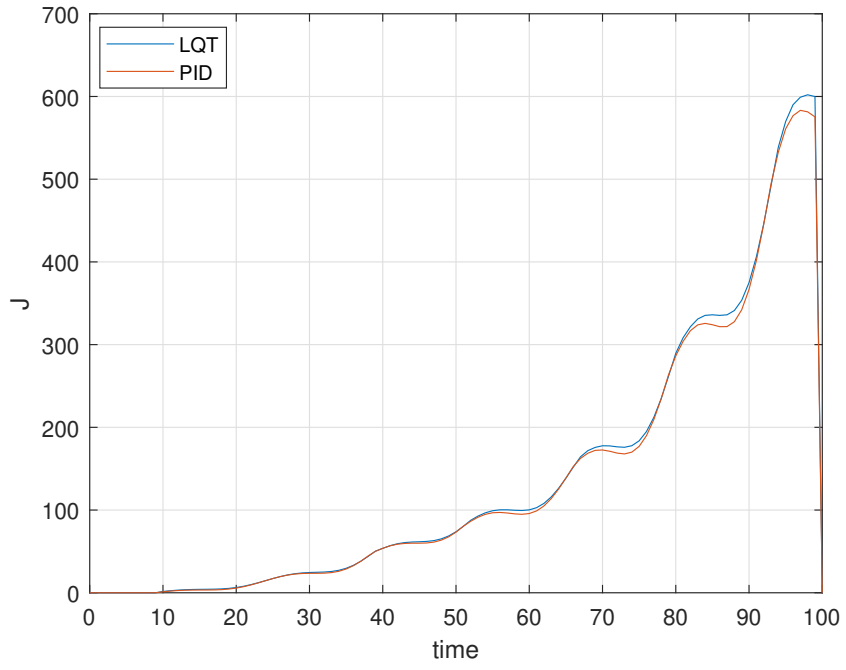

Figure A.7. Scenario 4: Sum of the square of error (SSE) for each controller

A.4 CONCLUSION

It has been shown that it is possible for an unstable controller to be selected according to (A.5) when competing with a stable, well tuned controller. It has also been shown that the performance measure of (A.5) cannot provide an adequate measure of controller performance as one step ahead predictions do not provide meaningful information about controller behaviour. It is thus concluded that the controllers would have to be simulated by the selector over a period of time in order to provide adequate information about controller response.

ADDENDUM B POTENTIAL PERFORMANCE IMPROVEMENT

B.1 OVERVIEW

This addendum illustrates how the platform presented in Chapter 3 could yield an overall improvement in system performance in the presence of rate of change constraints on the plant input. This is illustrated firstly with a simple first order plant in Section B.2 and then with the surge tank process presented in Chapter 4 in Section B.3.

B.2 SIMPLE FIRST ORDER SYSTEM

An overall improvement in system response in the presence of a rate of change constraint on the control input can be achieved by switching between controllers. To illustrate the concept, consider a simple first order process:

$$G_p(s) = \frac{y(s)}{u(s)} = \frac{1}{5s+1} \tag{B.1}$$

and

$$G_d(s) = \frac{y(s)}{u(s)} = G_p(s) \tag{B.2}$$

Consider a local fall-back PI controller G_{c_local} given by:

$$G_{c\_local}(s) = \frac{u_l(s)}{e(s)} = \frac{5s+1}{s} \tag{B.3}$$

where e is the error signal given by $r-y$. This yields a simple loop transfer function:

$$L_l(s) = G_p(s)G_{c\_local}(s) = \frac{1}{s} \tag{B.4}$$

and sensitivity transfer function:

$$S_l(s) = (1 + L_l)^{-1} = \frac{s}{s+1} \tag{B.5}$$

In any physical application, there will be a limit on the rate at which the input can change, that is on $^{du}/_{dt}$. This means that there is maximum amount by which the control move u can be changed between samples (Δu). If it is assumed that the maximum rate of change $(^{du}/_{dt})_{max}$ occurs in the input over a single sampling interval, the change Δu_{max} which occurs is given as:

$$\Delta u_{max} = \left(\frac{du}{dt}\right)_{max} \Delta t \tag{B.6}$$

where Δt is the sampling interval. For this example, consider a maximum allowed $^{du}/_{dt}$ of 3. Which would give:

$$\Delta u_{max} = 3\Delta t \tag{B.7}$$

The expression relating the disturbance d to the control move u generated by a given feedback controller is expressed as:

$$u_l(s) = [-(1 + G_p G_{c\_local})^{-1} G_c G_d] d(s) \tag{B.8}$$

For this example the disturbance transfer function G_d is taken as equal to the plant transfer function G_p, thus (B.8) reduces to:

$$u_l(s) = [-S_l(s) L_l(s)] d(s) = \frac{1}{s+1} d(s) \tag{B.9}$$

where $L(s)$ and $S(s)$ are given by (B.4) and (B.5) respectively. The time derivative of the input u can easily be found from (B.9) as:

$$\frac{du_l}{dt} \rightarrow s u_l(s) = \frac{s}{s+1} d(s) \tag{B.10}$$

It follows from (B.10) that the maximum rate of change in the input u_l resulting from a unit step in the disturbance d, or a sinusoidal disturbance of unit amplitude, is one. Therefore, if the maximum value of the disturbance d never exceeds one in magnitude, the rate of change in the control signal u_l generated by the controller G_{c_local} given in (B.3) will never exceed a value of one, which is within the defined limit of three.

Consider now a controller G_{c1} which is competing to control the plant given by:

$$G_{c1}(s) = \frac{u_{c1}(s)}{e(s)} = \frac{5s+1}{0.1s} \tag{B.11}$$

This gives loop and sensitivity transfer functions L and S:

$$L_{c1}(s) = G_p(s)G_{c1}(s) = \frac{10}{s} \tag{B.12}$$

$$S_{c1}(s) = (1+L_l)^{-1} = \frac{s}{s+10} \tag{B.13}$$

G_{c1} therefore has a bandwidth which is 10 times larger than that of G_{c_local}. Applying the same principles as in (B.8), (B.9) and (B.10) to G_{c1} gives:

$$u_{c1}(s) = [-S_{c1}(s)L_{c1}(s)]d(s) = \frac{10}{s+10}d(s) \tag{B.14}$$

$$\frac{du_{c1}}{dt} \rightarrow su_{c1}(s) = \frac{10s}{s+10}d(s) \tag{B.15}$$

It follows from (B.10) that the maximum rate of change in the input u_{c1} resulting from a unit step in the disturbance d, or a sinusoidal disturbance of unit amplitude, is ten. Therefore, if the maximum value of the disturbance d never exceeds one in magnitude, the rate of change in the control signal u_{c1} generated by the controller G_{c1} given in (B.11) will never exceed a value of ten, which exceeds the defined limit of three.

If the disturbance d is less than or equal to one in magnitude, controller G_{c_local} will never violate the constraint on $^{du}/_{dt}$ where it is possible that G_{c1} may violate this constraint, depending on the magnitude and frequency of the disturbance d. It should also be noted however that for certain disturbances, controller G_{c1} may not violate the constraint on $^{du}/_{dt}$ and due to the much larger bandwidth, provide superior disturbance rejection properties compared with controller G_{c_local}.

Consider a hypothetical scenario where G_{c_local} is the fall-back controller and G_{c1} is the only controller competing to control the plant. In the competing procedure, the selector simulates the control moves provided by G_{c1} on a model of the plant and feeds the simulated outputs back to G_{c1}. Any competing controller which is not selected would thus be controlling a model of the plant in closed-loop. See Fig. 3.3. Switching is specified to take place as described in Section 3.4 with the performance index in (3.1) used to determine the best controller. The output $\mathbf{y}$ is a scalar in this instance, thus the weighting

term $\mathbf{W}_e$ is also a scalar. The evaluation horizon N_e was chosen to be 20 in order to be several orders of magnitude larger than corresponding bandwidth of the slowest controller.

Figs. B.1 and B.2 show the outputs and control moves generated by controllers G_{c_local} and G_{c1} respectively for the load disturbance d shown in Fig. B.3. This disturbance is a constant sinusoidal disturbance with an amplitude of 0.5 over a period of 10 hours, with a step of 0.5 occurring at 150 hours. The peak value of the disturbance therefore does not exceed a value of 1. The reference value r is 0. It can be seen from Fig. B.1 that controller G_{c1} outperforms controller G_{c_local} by a large margin. If the overall performance is measured according to:

$$J_i = \sum_{k=1}^{N} (r(k) - y_i(k)) \cdot (r(k) - y_i(k)), \tag{B.16}$$

where N is the total number of time steps, index J_{local} is found to be 66.73 for controller G_{c_local}, whereas J_1 is found to be 0.93 for controller G_{c1}. This is drastic improvement in the output response, especially when considering the difference in the control signals u generated by the two controllers. A sampling time of 0.01 hours was chosen in accordance with (2.22).

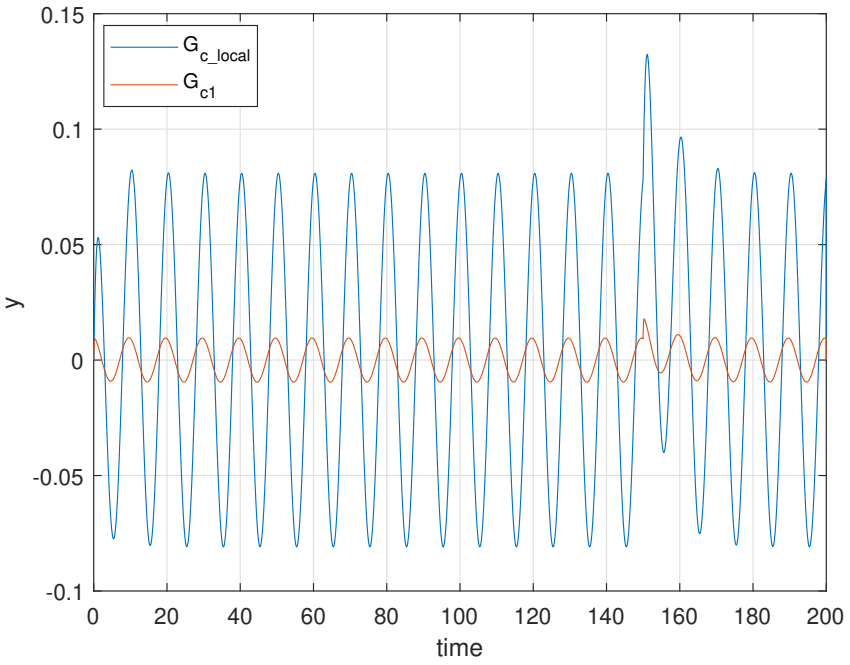

Figure B.1. Outputs generated by controllers G_{c_local} and G_{c1}.

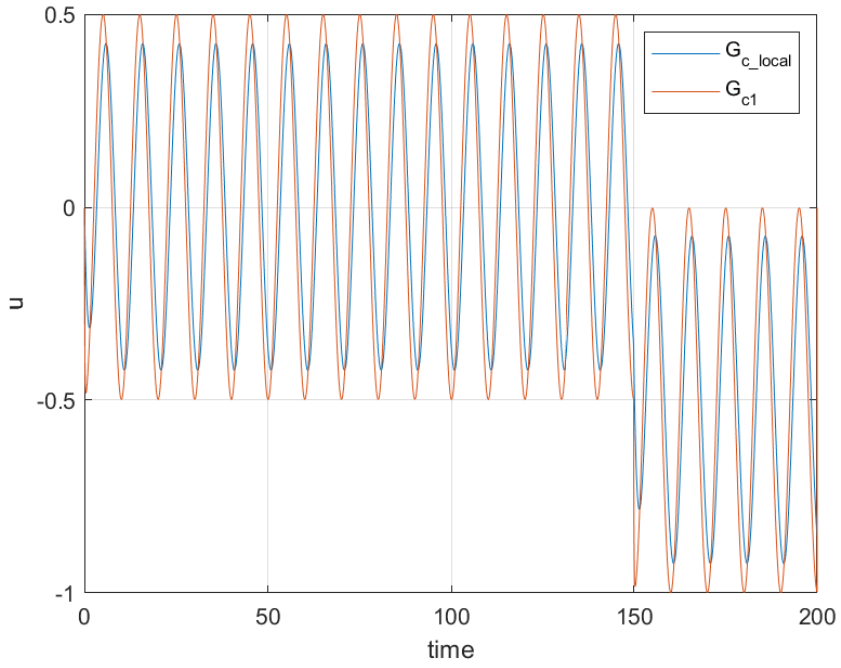

Figure B.2. Inputs generated by controllers G_{c_local} and G_{c1}.

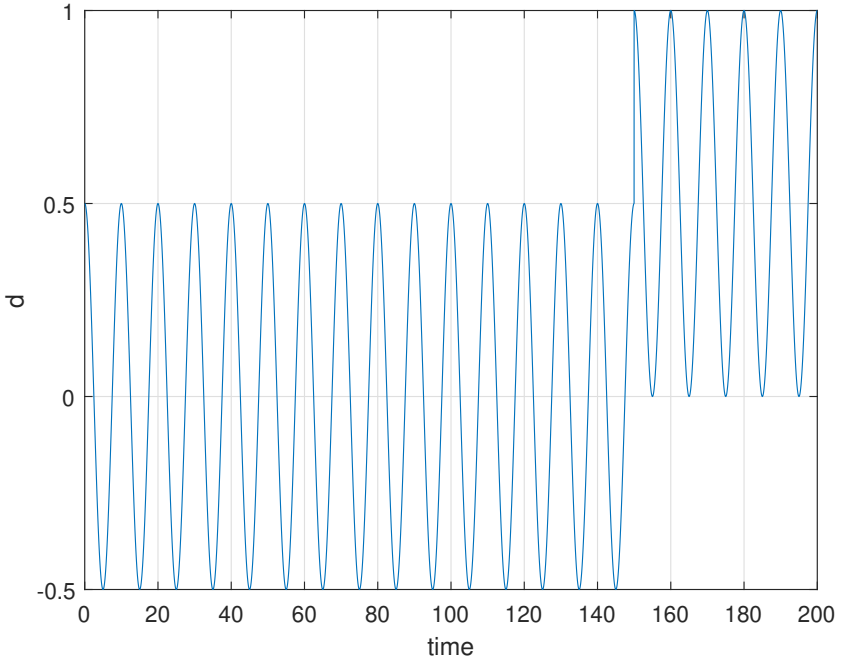

Figure B.3. Disturbance d.

If a similar performance measure to that of (B.16) given by:

$$J_{u_i} = \sum_{k=1}^{N} u_i(k) \cdot u_i(k), \tag{B.17}$$

is used to evaluate the input usage over the entire simulation, controller G_{c_local} yields a value of 2955 and controller G_{c1} yields a value of 3730. This is a 26% deterioration, which is however much less compared to the 99% improvement in the output performance. The rate of change of the control signal $^{du_i}/_{dt}$ generated by controller G_{c_local} never exceeds the limit of 3, whereas that of controller G_{c1} does with a maximum value of 5.02 which results due to the step change of 0.5 in the disturbance at 150 hours.

Figs. B.4 and B.5 show the system output and implemented control signal when switching between controllers according to (3.1) is performed with an evaluation horizon N_e of 20 hours. It can be seen from these figures that control is switched from G_{c_local} to G_{c1} at the 40 hour mark, then from G_{c1} back to G_{c_local} at the 150 hour mark when the step change of 0.5 occurs in the disturbance, and finally back to controller G_{c1} at the 180 hour mark. This results in an output performance measure J according to (B.16) of 22.13 which is substantially better than controller G_{c_local} acting alone.

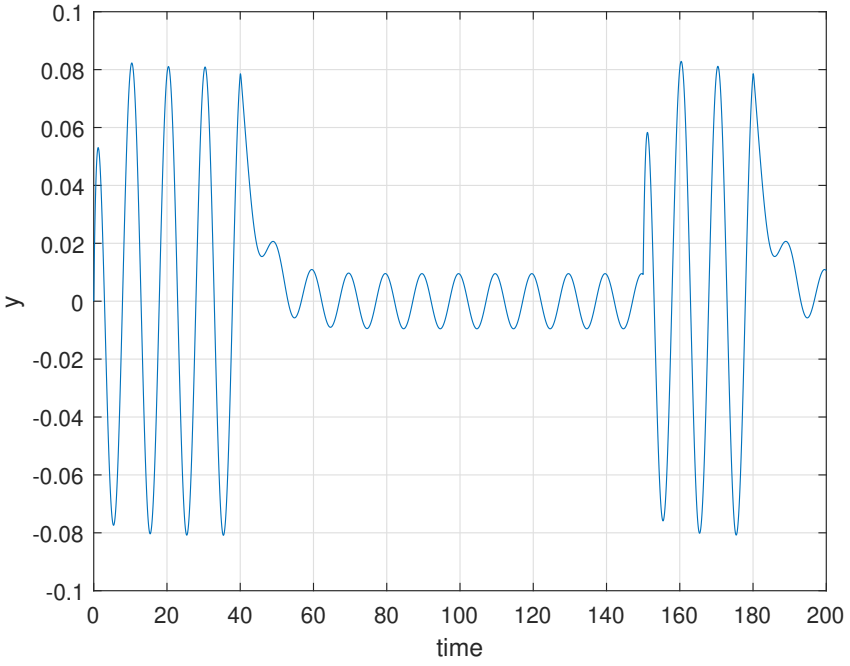

Figure B.4. Output generated when switching between controllers G_{c_local} and G_{c1}.

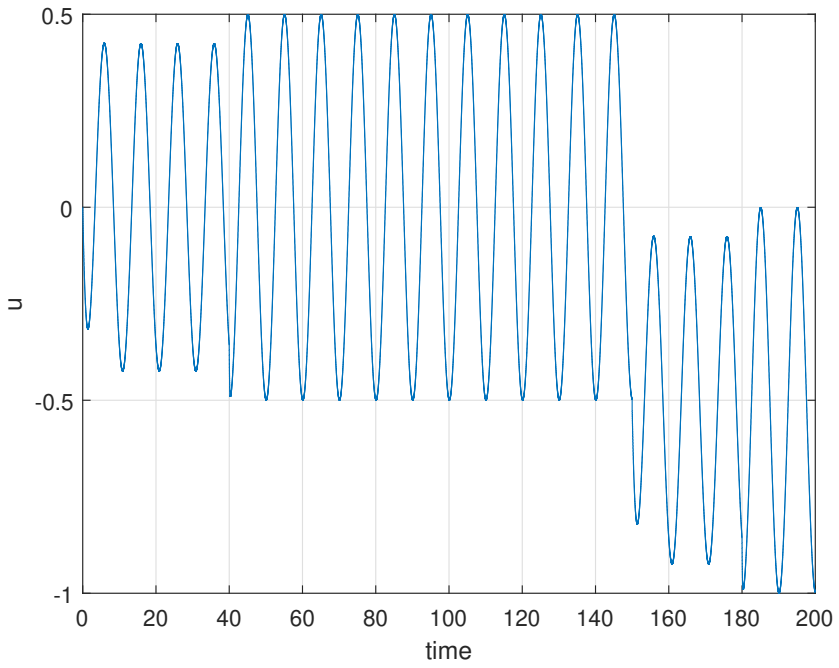

Figure B.5. Input generated when switching between controllers G_{c_local} and G_{c1}.

The logic of the selector is described as follows: The disturbance d is assumed to be measured, and is used along with the reference signal r (0 in this case) to simulate the behaviour of the two controllers G_{c_local} and G_{c1}. At the beginning of each evaluation horizon N_e, the performance measures for each controller J_{local} and J_1 are set to 0. Once the evaluation horizon is complete, the performance measures J_{local} and J_1 are calculated according to (3.1) (with $N_e = 20$ in this case). The control signal presented by each competing controller during the evaluation horizon is monitored as to whether the rate of change of the input ($^{du_i}/_{dt}$) exceeds the limit. Provided that this limit is not exceeded, control is switched over to the controller yielding the smallest performance measure J_i. When this occurs the new controller is informed, after which this controller is back initialised to output the same control move as was input to the plant at the previous time step and proceeds to take control of the plant, calculating its control moves based on the actual output of the plant. In the even that the active controller presents a control move which is in violation of the $^{du_i}/_{dt}$ constraint, control is immediately switched back to G_{c_local} for the remainder of the current as well as the following evaluation horizon in order to ensure switching does not occur within a period shorter than a single evaluation horizon. It would be possible to restart the evaluation horizon when the violation and subsequent switching takes place, but this is not done in this case as it is not necessary to illustrate the present concept.

It can be seen in Fig. B.4 that control of the plant is initially performed by G_{c_local}, after which control is switched over to G_{c1} at the 40 hour mark. The first evaluation horizon is completed at the 20 hour mark, but due to the initial transient, the control signal generated by the simulation of controller G_{c1} violates the rate of change limit and thus controller G_{c_local} remains the active controller. During the second evaluation horizon from the 20-40 hour mark, the control move generated by the simulation of controller G_{c1} does not violate the rate of change limit, and control is therefore switched over to controller G_{c1}. The improved performance is thus seen in Fig. B.4 between the 40 and 150 hour mark.

At each time step, the control move presented by the active controller is monitored to ensure that it does not exceed the allowable rate of change according to (B.7), and if it does, control of the process will be switched over to controller G_{c_local} which will not violate this condition by design. At the 150 hour mark, a step in the disturbance of 0.5 in magnitude above the sinusoidal disturbance occurs, resulting in this scenario with the control move generated by controller G_{c1} exceeding the rate of change limit. At this point the selector thus automatically switched control of the plant back over to controller G_{c_local}. This is evident in the large oscillations which occur in the output y beginning at the 150 hour mark. Controller G_{c_local} then compensates for this step in the disturbance d which is evident from the control signal u in Fig. B.5.

The next evaluation cycle takes place at the 160 hour mark. Due to the fact that controller G_{c1} has violated the rate of change constraint on the input during the preceding evaluation horizon, the plant remains under the control of G_{c_local} despite the smaller performance index produced in the simulation of controller G_{c1}. At the completion of the following evaluation period at the 180 hour mark, control is again switched over to controller G_{c1} since it yields a smaller performance index and has not violated the rate of change constraint on the input.

B.3 SURGE TANK SYSTEM

Consider the scenario of two controllers, $\mathbf{G}_{c1}$ and $\mathbf{G}_{c2}$, competing to control the surge tank process of Section 4, as well as a local fall-back controller $\mathbf{G}_{c\_local}$. The controllers are taken to have the same form as (5.4) given by:

$$\mathbf{G}_{ci} = k_i \begin{bmatrix} \frac{0.8(s+41.3)}{s} & \frac{20(s+75)}{s} \\ \frac{0.2(s+165)}{s} & \frac{-20(s+75)}{s} \end{bmatrix} \tag{B.18}$$

with gains k_i of 1000, 500 and 100 for $\mathbf{G}_{c1}$, $\mathbf{G}_{c2}$ and $\mathbf{G}_{c\_local}$ respectively.

Consider a sinusoidal disturbance of magnitude 0.1 $^{t}/_{m^3}$ and a period of 0.143 hours or 7 $^{rad}/_{sec}$ with an additional step of magnitude 0.1 $^{t}/_{m^3}$ as shown in Fig. B.6. The evaluation horizon is chosen to be 0.2 hours, and the constraints on the rate of change of both inputs is taken as 13000 $^{m^3}/_{h}/_{h}$. The local fall-back controller is designed to not violate this rate of change limit for a step change of 1 $^{t}/_{m^3}$ in the disturbance variable ρ_i. This is confirmed by the same procedure as was done in the previous section in accordance with (B.8). If the selector chooses the best controller in the same manner as the previous

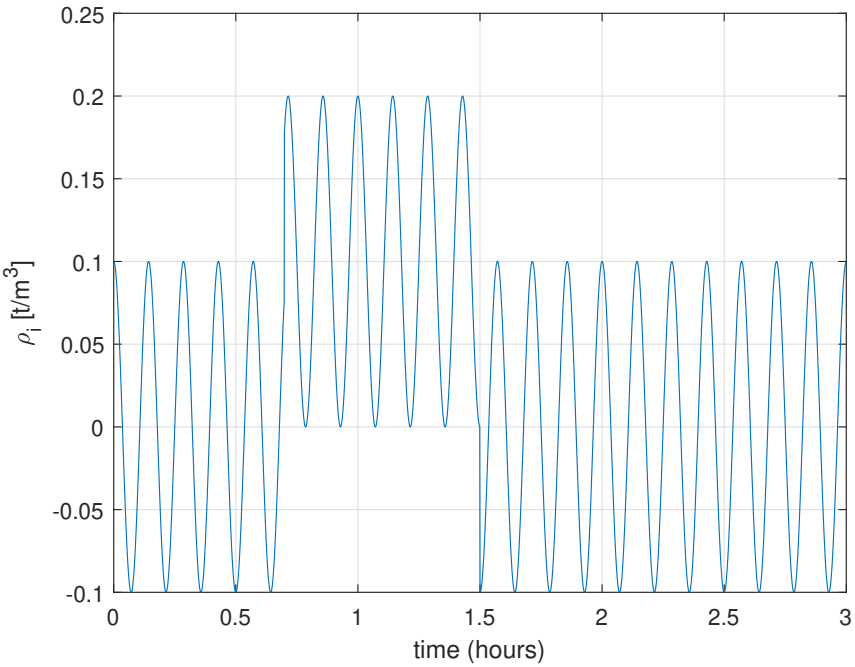

Figure B.6. Disturbance.

section according to (3.1) with

$$\mathbf{W}_e = \begin{bmatrix} 0 & 0 \\ 0 & 1 \end{bmatrix},$$

as well as taking the rate of change limitations into account, the response shown in Fig. B.7 results. This is the response of the nonlinear model with an additional 10% gain in the input water flow rate q_w. The corresponding inputs are shown in Fig. B.8.

Control of the plant begins with controller $\mathbf{G}_{c\_local}$, and it can be seen from Figs. B.7 and B.8 that the control is switched over to controller $\mathbf{G}_{c1}$ after the first evaluation period is complete at the 0.2 hour mark. When the step change of 0.1 $^{t}/_{m^3}$ occurs at 0.7 hours, $\mathbf{G}_{c1}$ is overly aggressive and violates the rate of change constraint on the input and control is switched back to $\mathbf{G}_{c\_local}$. At the subsequent end of the evaluation period at 0.8 hours, control is not switched to either controller as simulations of both $\mathbf{G}_{c1}$ and $\mathbf{G}_{c2}$ show a violation of the $^{du}/_{dt}$ constraint within that time period. Control is subsequently switched to controller $\mathbf{G}_{c1}$ at the end of the next evaluation period at 1 hour. Control remains with $\mathbf{G}_{c1}$ for the remainder of the simulation.

It should be noted that if there were no plant gain uncertainty, all controllers would keep the level at exactly 10 m^3. Due to the 10% increase in gain on the input water flow rate q_w, the tank level does change, but is brought back to set point due to the addition of integral action to the purely proportional terms in the controller resulting from taking the inverse of the plant.

Figs. B.9 and B.10 show the outputs and inputs generated by the three controllers when simulated on linear models of the plant during the competing process.

B.4 CONCLUSION

It has been shown that it is possible to improve the overall system performance by switching between controllers with the proposed platform philosophy. This has been demonstrated for a simple first order process as well as the surge tank process of Chapter 4 with measured disturbances in both cases.

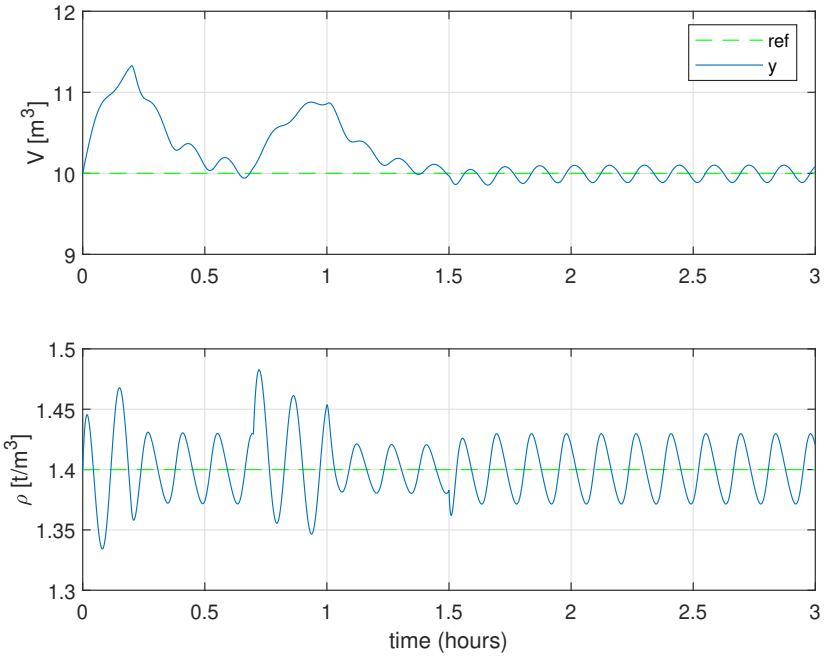

Figure B.7. Outputs of plant.

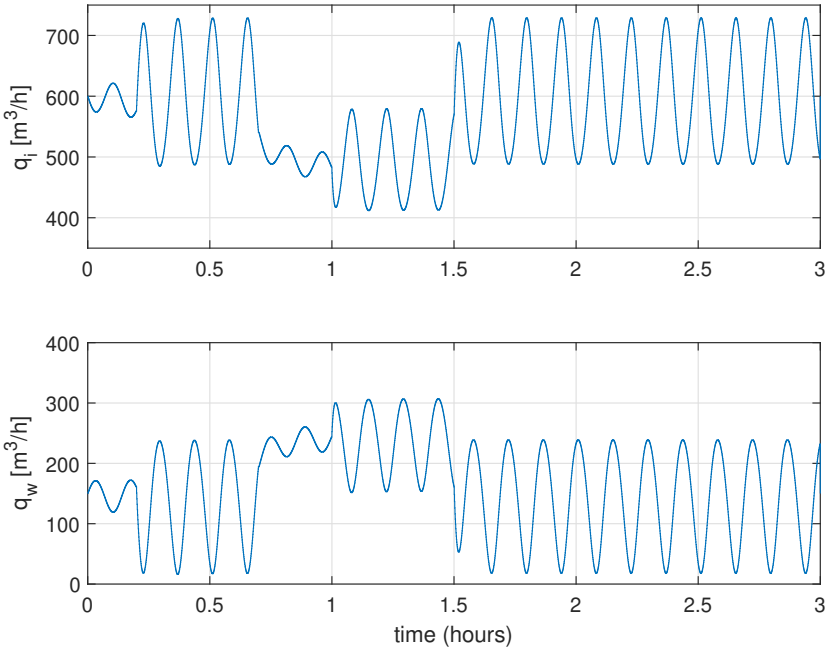

Figure B.8. Inputs to nonlinear plant.

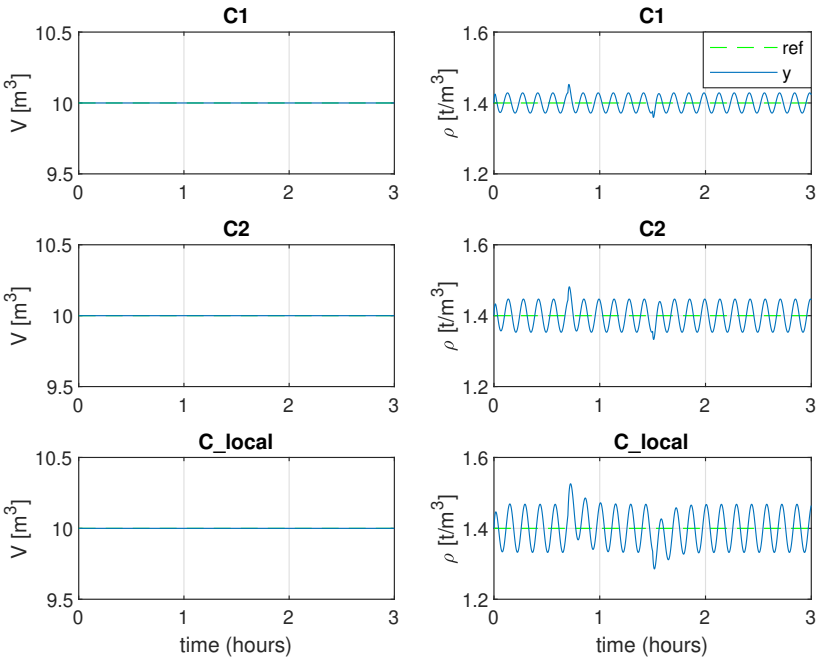

Figure B.9. Outputs of linear simulations.

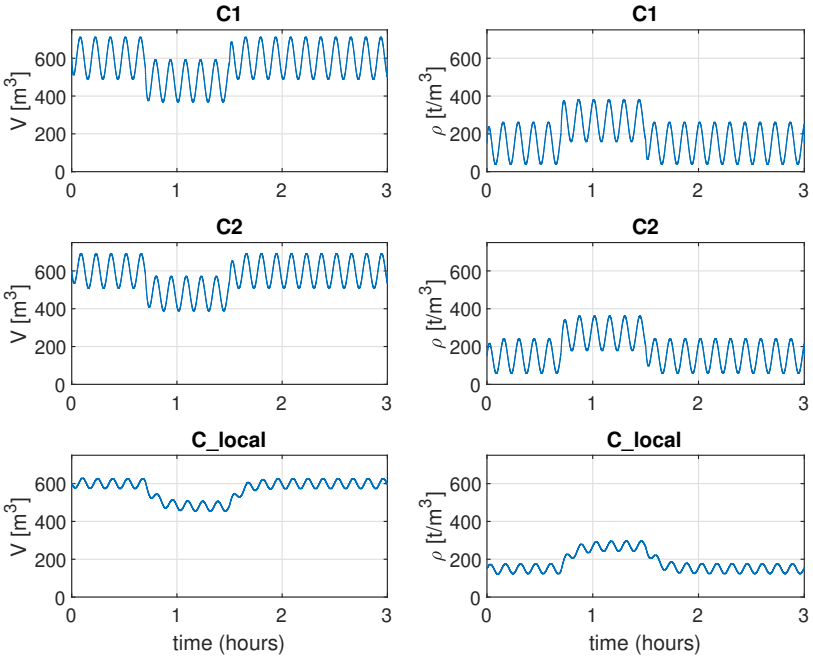

Figure B.10. Control inputs of linear simulations.

ADDENDUM C PERFORMANCE AND ROBUSTNESS TO UNCERTAINTY

C.1 OVERVIEW

This addendum presents a robust stability analysis of the four conventional feedback controllers derived in Chapter 5 for control of the surge tank process. Section C.2 presents singular value plots for each controller, Section C.3 presents the uncertainty description used in the analysis and Section C.4 shows the plots of the resulting structured singular values.

C.2 SINGULAR VALUE PLOTS

Figs. C.1 and C.2 show the singular values of the sensitivity and complementary sensitivity transfer functions **S** and **T** for all 4 feedback controllers along with the weights $\mathbf{W}_p$ and $\mathbf{W}_T$ used in the design of the $\mathcal{H}_\infty$ controller is Chapter 5 as a function of frequency. The inverse controller yields ideal control with singular values for the sensitivity and complimentary sensitivity transfer functions of the same form as shown in Fig. 2.5. The $\mathcal{H}_\infty$ controller yields similar results to the ideal controller, with the sensitivity transfer function singular values very close to the inverse of the weight $\mathbf{W}_p$ over the whole frequency range, while the complementary sensitivity transfer function decreases at a higher rate at high frequencies than the ideal case. The modified inverse controller yields slightly different results to the pure inverse controller, with one of the singular values deviating from the ideal case, while it remains below 0 dB over the entire frequency range as desired.

The maximum singular value of the complementary sensitivity transfer function does however exceed 0 dB near the bandwidth of the controller reaching 2.53 dB at $75 rad/s$ meaning sensor noise at this frequency will be amplified. The poor performance which would result from the use of a decoupled PI

controller is clearly seen from these singular value plots with both the sensitivity **S** and complementary sensitivity transfer functions **T** exceeding 0 dB over a large frequency range.

C.3 UNCERTAINTY DESCRIPTION

In this analysis, multiplicative input uncertainty will be considered where there is gain and time delay uncertainty on each input channel. Uncertainty of this form can be described as:

$$\tilde{\mathbf{G}}_p(s) = \mathbf{G}_p(s) \begin{bmatrix} k_1 e^{-\theta_1 s} & 0 \\ 0 & k_2 e^{-\theta_2 s} \end{bmatrix} \tag{C.1}$$

where

$$k_i \, \varepsilon \left[0.9, \quad 1.1\right], \quad \theta_i \, \varepsilon \left[0, \quad 0.002\right]$$

$\mathbf{G}_p(s)$ in (C.1) denotes the the nominal plant and $\tilde{\mathbf{G}}_p(s)$ denotes the uncertain plant. This equates to $\pm 10\%$ gain uncertainty as well as the possibility of 0.002 hours of time delay in each input channel. The value of 0.002 hours was chosen as this is the value of the chosen sampling time.

For a SISO transfer function element $\tilde{G}_p$, uncertainty can be represented by a complex perturbation $\Delta(s)$ as:

$$\tilde{G}_p(s) = G_p(s)(1 + \omega_A(s)\Delta(s)), \quad |\Delta(j\omega)| \leq 1, \; \forall \omega \tag{C.2}$$

where $\omega_A(s)$ is some rational transfer function. In the complex plane, the perturbation $\Delta(j\omega)$ generates a disc shaped region of radius $|\omega_A(j\omega)|$ centred at $G(j\omega)$ [27]. This provides a representation of all possible magnitudes and phase angles of $\tilde{G}(j\omega)$ in the complex plane. This is illustrated graphically in Fig. C.3 which shows the Nyquist plot of a typical nominal transfer function G and a disc shaped region whose radius is $|\omega_A(j\omega)|$ centred on the Nyquist curve.

This can be extended to the multi-variable case where there is a complex perturbation for each input channel and (C.1) can be expanded as:

$$\tilde{\mathbf{G}}_p(s) = \mathbf{G}(s)(\mathbf{I} + \mathbf{W}_A(s)\mathbf{\Delta}_A(s)), \quad ||\mathbf{\Delta}_A||_\infty \leq 1 \tag{C.3}$$

where

$$\mathbf{W}_A(s) = w_A(s) \begin{bmatrix} 1 & 0 \\ 0 & 1 \end{bmatrix}, \quad \mathbf{\Delta}_A(s) = \begin{bmatrix} \Delta^1 & 0 \\ 0 & \Delta^2 \end{bmatrix} \tag{C.4}$$

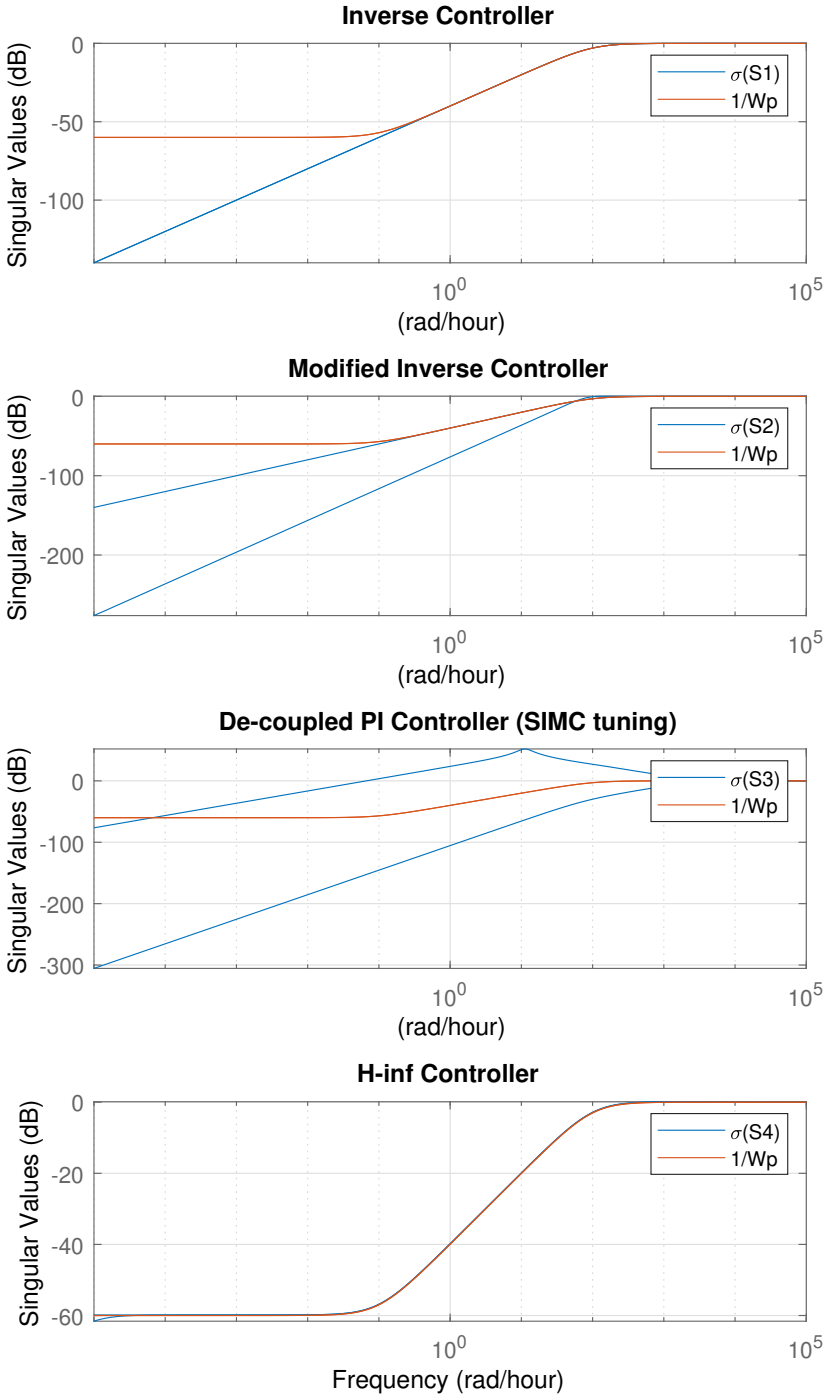

Figure C.1. Singular values of sensitivity transfer functions **S**.

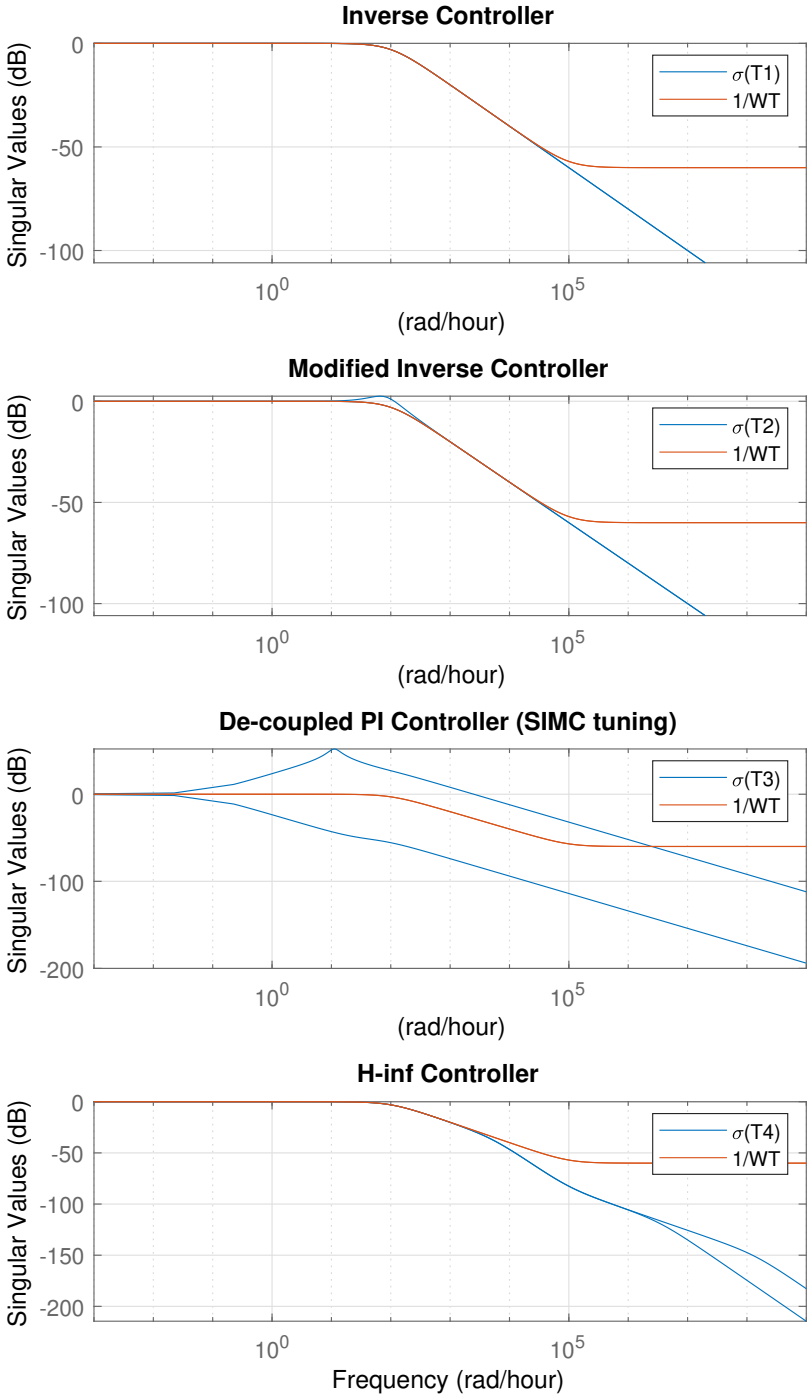

Figure C.2. Singular values of complementary sensitivity transfer functions **T**.

and where Δ^1 and Δ^2 are scalar complex perturbations as given in (C.2) with magnitudes less than one for all frequencies.

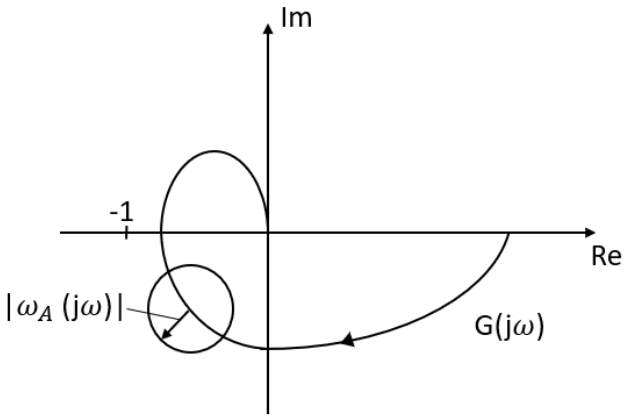

Figure C.3. Uncertainty region generated by complex perturbation.

Therefore the uncertain plant set can be described by input multiplicative uncertainty with a diagonal block matrix of three independent complex perturbations each with a magnitude less than one at all frequencies. The block diagram configuration is shown in Fig. C.4.

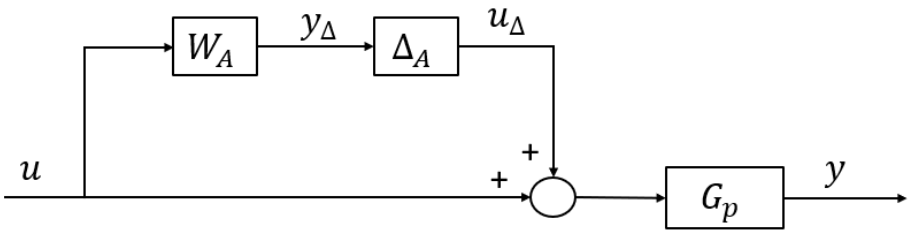

Figure C.4. Input multiplicative uncertainty

It has been shown that for multiplicative gain and time delay uncertainty, the weight ω_A can be represented as [27], [53]:

$$\omega_A = \frac{(1+\frac{r_k}{2})\theta_{max}s + r_k}{\frac{\theta_{max}}{2}+1} \cdot \frac{(\frac{\theta_{max}}{2.363})^2 s^2 + 2\cdot 0.838 \cdot \frac{\theta_{max}}{2.363}s + 1}{(\frac{\theta_{max}}{2.363})^2 s^2 + 2\cdot 0.685 \cdot \frac{\theta_{max}}{2.363}s + 1} \tag{C.5}$$

where

$$r_k = \frac{k_{max} - k_{min}}{k_{max} + k_{min}}$$

Since the range of gain and time delay uncertainty is the same for each input channel, the transfer function ω_A is the same for each input channel and is given by:

$$\omega_A = \frac{0.0021s + 0.1}{0.001s + 1} \cdot \frac{7.164e^{-7}s^2 + 0.001419s + 1}{7.164e^{-7}s^2 + 0.00116s + 1} \tag{C.6}$$

The robustness of the closed-loop system is analysed using the general $N\Delta$ structure shown in Figs. C.5 and C.6.

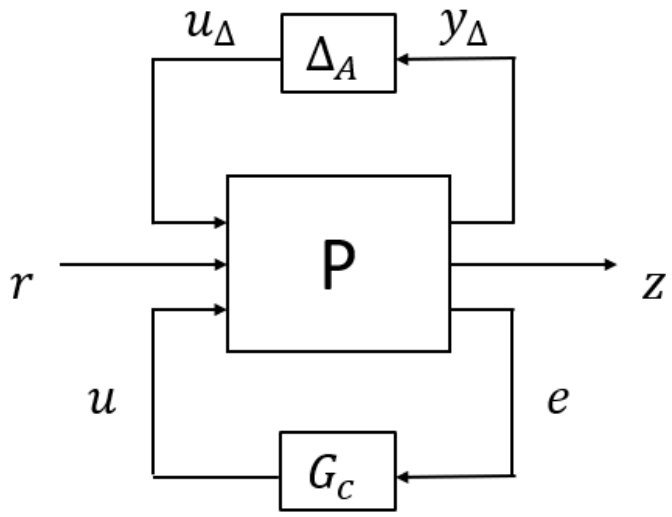

Figure C.5. General control structure.

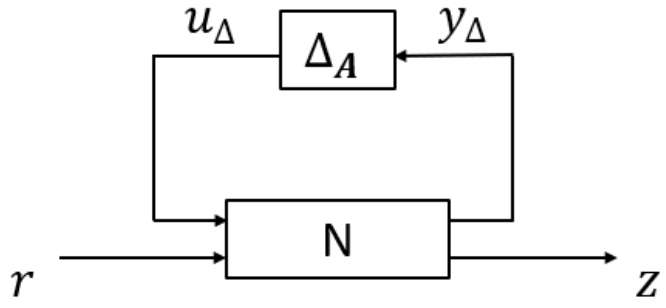

Figure C.6. $N\Delta$ structure.

This structure is formulated using the generalised plant **P** and controller in Fig. 2.6 along with the uncertainty description in Fig. C.4. The **N** structure is given as:

$$\begin{bmatrix} \mathbf{y}_\Delta \\ \mathbf{z}_1 \\ \mathbf{z}_2 \\ \mathbf{z}_3 \end{bmatrix} = \mathbf{N} \begin{bmatrix} \mathbf{u}_\Delta \\ \mathbf{r} \end{bmatrix} = \begin{bmatrix} -\mathbf{W}_I\mathbf{T}_I & \mathbf{W}_I\mathbf{G}_c\mathbf{S} \\ -\mathbf{W}_p\mathbf{S}\mathbf{G}_p & \mathbf{W}_p\mathbf{S} \\ \mathbf{W}_u & \mathbf{W}_u\mathbf{G}_c\mathbf{S} \\ \mathbf{W}_T\mathbf{G}_p & \mathbf{W}_T\mathbf{T} \end{bmatrix} \begin{bmatrix} \mathbf{u}_\Delta \\ \mathbf{r} \end{bmatrix} \tag{C.7}$$

where **S** and **T** are the sensitivity and complementary sensitivity transfer functions respectively given in (2.4) and (2.5) and $\mathbf{T}_I$ is given by:

$$\mathbf{T}_I = \mathbf{G}_c\mathbf{G}_p(\mathbf{I}+\mathbf{G}_c\mathbf{G}_p)^{-1} \tag{C.8}$$

For analysis, **N** is partitioned as:

$$\begin{bmatrix} \mathbf{y}_\Delta \\ \mathbf{z} \end{bmatrix} = \begin{bmatrix} \mathbf{N}_{11} & \mathbf{N}_{12} \\ \mathbf{N}_{21} & \mathbf{N}_{22} \end{bmatrix} \begin{bmatrix} \mathbf{u}_\Delta \\ \mathbf{r} \end{bmatrix} \tag{C.9}$$

where

$$\mathbf{N}_{11} = -\mathbf{W}_I\mathbf{T}_I \tag{C.10}$$

$$\mathbf{N}_{12} = \mathbf{W}_A\mathbf{G}_c\mathbf{S} \tag{C.11}$$

$$\mathbf{N}_{21} = \begin{bmatrix} -\mathbf{W}_p\mathbf{S}\mathbf{G}_p \\ \mathbf{W}_u \\ \mathbf{W}_T\mathbf{G}_p \end{bmatrix} \tag{C.12}$$

$$\mathbf{N}_{22} = \begin{bmatrix} \mathbf{W}_p\mathbf{S} \\ \mathbf{W}_u\mathbf{G}_c\mathbf{S} \\ \mathbf{W}_T\mathbf{T} \end{bmatrix} \tag{C.13}$$

It is evident that $\mathbf{N}_{22}$ is the same as the transfer function matrix whose $\mathcal{H}_\infty$ norm is minimised in the controller synthesis (where $\mathbf{W}_u$ was taken to be $\mathbf{0}$ in this case). Thus nominal performance in the strict sense is achieved if the three transfer function matrices **S**, $\mathbf{G}_c\mathbf{S}$ and **T** are all smaller than the inverse of their applicable weights $\mathbf{W}_p$, $\mathbf{W}_u$ and $\mathbf{W}_T$ over all frequencies. This is equivalent to the maximum singular value of $\mathbf{N}_{22}$ less than 1 over all frequencies.

$$\bar{\sigma}(\mathbf{N}_{22}) < 1, \forall \omega \tag{C.14}$$

From Figs. C.1 and C.2 it can be seen that nominal performance in this sense is only achieved by the $\mathcal{H}_\infty$ and inverse controllers. The maximum singular value of both the modified inverse and the decoupled PI controller exceed that of the inverse of the weights $\mathbf{W}_p$ and $\mathbf{W}_T$ and to a much larger extent in the case of the decoupled PI controller.

C.4 STRUCTURED SINGULAR VALUES

To determine robust stability, the $N\Delta$ structure is simplified and written as the transfer function from the reference $\mathbf{r}$ to the three outputs $\mathbf{z}_1$, $\mathbf{z}_2$ and $\mathbf{z}_3$ which gives:

$$\mathbf{z} = \mathbf{N}_{22} + \mathbf{N}_{21}\boldsymbol{\Delta}_A(\mathbf{I} - \mathbf{N}_{11}\boldsymbol{\Delta}_A)^{-1}\mathbf{N}_{12} \tag{C.15}$$

If the nominal system is stable, it follows that the only source of instability could arise from the determinant of $(\mathbf{I} - \mathbf{N}_{11}\boldsymbol{\Delta}_A)$. Robust stability has been shown to follow if and only if the Nyquist plot of $det(\mathbf{I} - \mathbf{N}_{11}\boldsymbol{\Delta}_A)$ does not circle the origin which is equivalent to [27]:

$$det(\mathbf{I} - \mathbf{N}_{11}\boldsymbol{\Delta}_A) \neq 0, \quad \forall\omega, \quad \forall\boldsymbol{\Delta} \tag{C.16}$$

When $\boldsymbol{\Delta}_A$ is a full matrix of complex perturbations with $||\boldsymbol{\Delta}_A||_\infty < 1$, this is equivalent to:

$$\bar{\sigma}(\mathbf{N}_{11}) < 1, \forall\omega \tag{C.17}$$

which states that the maximum singular value of $\mathbf{N}_{11}$ must be less than one for all frequencies [27]. It is often the case that the perturbation matrix $\boldsymbol{\Delta}_A$ has a fixed structure. For this scenario the matrix is diagonal with two perturbations as given in (C.4). When this is the case, the condition in (C.17) is overly conservative and thus robust stability may be satisfied for a given structured $\boldsymbol{\Delta}_A$ while the condition in (C.17) is violated [27]. This has led to the formulation of the structured singular value μ which is defined as follows: Given the smallest structured $\boldsymbol{\Delta}_A$ (measured as $\bar{\sigma}(\boldsymbol{\Delta}_A)$)which makes the matrix $(\mathbf{I} - \mathbf{M}\boldsymbol{\Delta}_A)$ singular, the structured singular value of the matrix $\mathbf{M}$ is defined as [27], [54]:

$$\mu_\Delta(\mathbf{M}) = \frac{1}{\bar{\sigma}(\boldsymbol{\Delta}_A)} \tag{C.18}$$

In the case where the uncertainty is unstructured and thus $\boldsymbol{\Delta}$ is a full matrix, the structured singular

value of a matrix $\mathbf{M}$ is equivalent to the maximum singular value of the matrix.

Thus for the robust stability of a controller, it is required that the structured singular value with the diagonal perturbation $\mathbf{\Delta}_A$ of $\mathbf{N}_{11}$ be less than 1 for all frequencies [27].

$$\mu_{\Delta_A}(\mathbf{N}_{11}) < 1, \forall \omega \tag{C.19}$$

Fig. C.7 shows the structured singular value as a function of frequency for all four controllers previously presented for the input multiplicative uncertainty in (C.1). It can be seen that all four controllers are robustly stable by relatively good margins. The peak values of μ are -13.9 dB, -11.6 dB, -11.4 dB and -14 dB for the inverse, modified inverse, de-coupled PI and $\mathcal{H}_\infty$ controllers respectively. Thus the $\mathcal{H}_\infty$ and inverse controllers provide the best robust stability margin while surprisingly the de-coupled PI controller with SIMC tuning has a maximum value for μ only slightly larger than that of the modified inverse controller.

C.5 CONCLUSION

It has also been shown that the four conventional feedback controllers presented in Chapter 5 are robustly stable to $\pm 10\%$ gain uncertainty and 0.002 hour time delay uncertainty on each input channel.

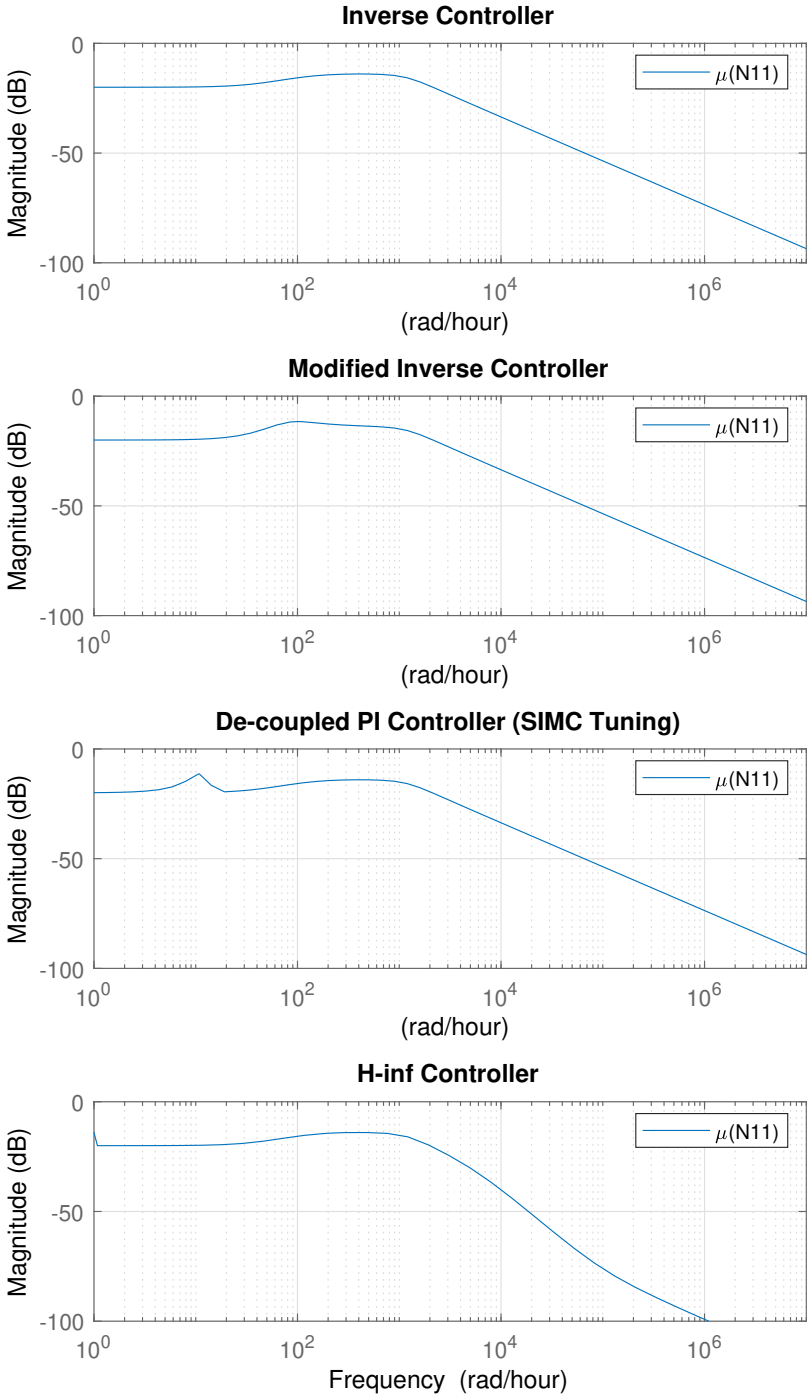

Figure C.7. Structured singular values.